Université Paris Descartes - Universidad de Chile

École doctorale Cerveau, Cognition, Comportement (Ed3C)

Sujet de la thèse

Subthreshold Ca^{2+}-dependent modulation of vesicle release dynamics and docking site occupancy at single central synapses

présentée par

Kris Blanchard Tapia

pour obtenir le grade de

Docteur en Neurosciences de l'Université Paris Descartes,

Doctor en Ciencias con Mención en Biología Molecular,

Celular y Neurociencias de la Universidad de Chile

Soutenue le 26 novembre 2018, devant le jury composé de:

Brigitte Van Zundert	Rapporteur
Ursula wyneken	Rapporteur
Cecilia Vergara	Examinateur
Stéphane Dieudonné	Examinateur
Pierre Vincent	Examinateur
Federico Trigo	Examinateur
Isabel Llano	Directeur de thèse
Juan Bacigalupo	Directeur de thèse

Université Paris Descartes - Universidad de Chile

École doctorale Cerveau, Cognition, Comportement (Ed3C)

Título de la Tesis

Subthreshold Ca^{2+}-dependent modulation of vesicle release dynamics and docking site occupancy at single central synapses

presentada por

Kris Blanchard Tapia

para obtener el grado de

Docteur en Neurosciences de l'Université Paris Descartes,

Doctor en Ciencias con Mención en Biología Molecular,

Celular y Neurociencias de la Universidad de Chile

Fecha de la defensa: 26 de noviembre de 2018. Jurado compuesto por:

Brigitte Van Zundert	Revisor
Ursula wyneken	Revisor
Cecilia Vergara	Jurado
Stéphane Dieudonné	Jurado
Pierre Vincent	Jurado
Federico Trigo	Jurado
Isabel Llano	Director de tesis
Juan Bacigalupo	Director de tesis

FACULTAD DE CIENCIAS

UNIVERSIDAD DE CHILE

INFORME DE APROBACION

TESIS DE DOCTORADO

Se informa a la Escuela de Postgrado de la Facultad de Ciencias que la Tesis de Doctorado presentada por el candidato

Kris Blanchard Tapia

Ha sido aprobada por la comisión de evaluación de la tesis como requisito para optar al grado de Doctor en Ciencias con mención en Biología Molecular Celular y Neurociencias, en el examen de Defensa de Tesis rendido el día 26 de noviembre de 2018.

Comisión de Evaluación de la Tesis:

Dra. Brigitte Van Zundert (Chile)……..

Dra. Ursula Wyneken (Chile)…….

Dra. Cecilia Vergara (Chile)…….....

Dr. Stéphane Dieudonné (Francia)……

Dr. Pierre Vincent (Francia)……....

Dr. Federico Trigo (Francia)……..

Directores de Tesis:

Dra. Isabel Llano (Francia)……...…….…….……..

Dr. Juan Bacigalupo (Chile)…..……..……...

Table of contents

I. Figures index

II. Résumé

Dans plusieurs neurones du SNC l'activité somato-dendritique infraliminaire peut se propager passivement dans l'axone et augmenter transitoirement la transmission synaptique spontanée et évoquée par le potentiel d'action de manière dépendante du Ca^{2+}. Les mécanismes sousjacents à ce type de plasticité synaptique, appelée facilitation "analogique" ou "analogo-digitale", restent largement inconnus pour la plupart des synapses centrales, principalement en raison de la difficulté à réaliser des enregistrements directs des petits boutons présynaptiques. Ici, nous utilisons de la photolyse de Ca^{2+} et de l'imagerie aux niveau des terminaisons présynaptiques individuelles des interneurones de la couche moléculaire du cervelet (ICM), combinées à des enregistrements électrophysiologiques avec la technique du patch. Nous décrivons un nouveau mécanisme de facilitation analogo-digitale qui est dépendant du Ca^{2+} infraliminaire et dans lequel la fraction et la cinétique du pool de vésicules dites “prêtes à être libérées” (readily releasable pool ou RRP en anglais), est modulée par des modifications de la probabilité d'occupation des sites d'ancrage dans des contacts synaptiques individuels. Nos résultats ajoutent une nouvelle dimension à la compréhension de la manière dont l'activité infraliminaire module le flux d'information dans les circuits neuronaux

III. Abstract

In several neurons of the CNS, subthreshold somatodendritic activity can spread passively into the axon and transiently enhance spontaneous and spike-evoked synaptic transmission in a Ca^{2+}-dependent and graded manner. Available evidence about the underlying mechanism of this type of synaptic plasticity, called "analog" or "analog to digital" facilitation (ADF), remains largely incomplete for the majority of central synapses, mainly due to the experimental inaccessibility to the small presynaptic boutons. Here we use both Ca^{2+} photolysis and imaging at individual presynaptic terminals of the rat cerebellar molecular layer interneurons (MLIs), combined with whole-cell paired recordings from synaptically connected MLIs, to report a novel subthreshold Ca^{2+}-dependent mechanism for ADF whereby the fraction and the kinetics of the pool of vesicles available for immediate release, the readily releasable pool (RRP), are modulated by changing the docking site occupancy probability in single synaptic contacts. Our results add a new dimension in the understanding of how subthreshold activity modulates information flow in neuronal circuits.

IV. Mots clés; Keywords:

Analog signaling, Analog-to-digital, Docking Sites, GABAergic interneurons, Readily Releasable Pool, Single synaptic contacts, Synaptic plasticity.

V. List of abbreviations

1. NT: neurotransmitter

2. AP: Action potential

3. SSD: subthreshold somatic depolarization

4. ADF: Analog-to-digital facilitation

5. MLI: Molecular layer interneuron

6. VDCC: Voltage-dependent calcium channels

7. PKC: Protein kinase C

8. NMDA: N-methyl-D-aspartate

9. DAG: Diacylglycerol

10. RRP: Readily releasable pool

11. pNR: Probability of neurotransmitter release

12. PSC: Postsynaptic current

13. p: Probability of a single quantum to be released

14. IS: intracellular solution

15. OGB-1: Oregon Green BAPTA-1

16. DMNP: DM-Nitrophen

A mi amada esposa, quien con su amor y coraje me recuerda día a día el real sentido del éxito.

A mí amada hija, por darme la oportunidad de experimentar una fuerza tan poderosa, y por alegrar mi mundo con su inocencia y belleza.

VI. Acknowledgment

First of all, I would like to thank Federico, Alain and Isabel for accepting me into the lab. It's been amazing to work in Paris doing beautiful experiments. Thank you, Fede, for giving me the chance to explore and to think freely, and also for putting up with my stubbornness; I have learned a lot from you. Thank you, Isabel for your support and guidance. Thank you, Alain, for your support and advice; it's a pleasure to discuss results with you. A special thanks to Professor Juan Bacigalupo for your support, advice and trust over the years, none of these would have been possible without your help and mentorship; I have no words to express my gratitude.

I would like to thank to the members of the thesis committee: Dra. Brigitte Van Zundert, Dra. Ursula Wyneken, Dr. Stéphane Dieudonné, Dr. Pierre Vincent, Dra. Magdalena Sanhueza, and Dra. Cecilia Vergara. I really appreciate your help, advice and support.

Thank you to all the past and present members of the Cell Physiology Lab, it is been a real pleasure to work in the lab.

Thank you to David and Celine for being so nice to me in spite of my poor English and French. Thank you to Philippe and Boris, it was a pleasure to share the working space with you. Thank you to Brandon for always smiling and your

willingness to help. Thank you to Michael for being such a nice guy, it was great to work next to you the last year. Thank you, Thibault, for helping me every time I had a question related to science or the French language. A super special thank you to Jorge, Gerardo, Taka, Camila, Lupe, Javier, Merouann, Bastian, Laura Castro, Laura Gomez, Enrico and Maria, you are totally awesome!!! I am very happy to have met you. Thanks to Patrick, Linda and Chantal for being so kind and helpful.

Thank you to all my Parisian-Chilean friends; it's been a real pleasure to share part of my life with you. A special thank you to "los terribles voisins" Vale and Enrique, for your friendship and support.

Thank you to my parents for your love and the enormous effort you have put into my education. Thanks to my big brother Israel for walking with me through life and for your unconditional love. Thanks to my little sisters Nathalie and Ambar for your love and support, you are amazing. Thanks to all my friends for the advices and amazing conversations.

Thanks to my mother-in-law Lita for your love and support. A super mega thank to my beloved wife for all your love, patience, kindness and bravery, you are wonderful. It is been amazing to share my life with you. Finally, I would like to thank to my baby Violeta, you are everything to me now, thank you for making me a better person.

1 Introduction

1.1 Subthreshold somatic depolarization enhances neurotransmitter release in cerebellar molecular layer interneurons and other central synapses

It is well known that the probability of neurotransmitter (NT) release depends on the recent history of synaptic activity, which can influence residual calcium (Ca^{2+}) and modulate the amount of NT released when an action potential (AP) arrives to the presynaptic terminal (short-term synaptic plasticity). Traditionally, AP-dependent transmission has been considered as the only fast way of communication between the somatodendritic compartment and the presynaptic terminals (Shu et al., 2006). However, a growing body of evidence suggests that the neuronal activity on which short-term synaptic plasticity depends, not only involves intracellular Ca^{2+} changes as a result of the "all-or-nothing" (or “digital”) nature of the AP, but also involves the subthreshold, AP-independent or “analog” synaptic activity that produces changes in membrane potential without reaching the AP threshold. On invertebrate preparations it was demonstrated long ago that the application of subthreshold presynaptic depolarization can increase the amount of NT released to the synaptic cleft (Shimahara and Tauc, 1975; Nicholls and Wallace, 1978). In mammals, this feature was demonstrated more recently by

recording synaptic activity in pairs of connected neurons (Shu et al., 2006; Alle and Geiger, 2006). Direct recordings from hippocampal mossy fiber boutons in slices have revealed that subthreshold somatic depolarization (SSD) can passively spread hundreds of microns into the axon and modulate the process of NT release at the mossy fiber bouton–CA3 pyramidal neuron synapse (Alle and Geiger, 2006). In the Calyx of Held (where direct pre- and postsynaptic recordings is achievable), it has been shown that subthreshold depolarization of the presynaptic terminal is capable of potentiating NT release by a mechanism that involves both, an increase in the basal Ca^{2+} levels (Awatramani et al., 2005) and an increase in the AP-dependent Ca^{2+} influx as a consequence of a change in the AP shape (Hori and Takahashi, 2009). In cortical neurons, it has been proposed that changes in the AP shape may be mediating the potentiation induced by the application of SSD (Shu et al., 2006). However, no changes have been found in the axonal Ca^{2+} levels (neither basal nor AP-evoked) during this so-called "analogue signaling" in hippocampal mossy fibers (Scott et al., 2008). Given the discrepancies, it has been proposed that different forms of analog (or analog-to-digital[1]) facilitation (ADF), that are Ca^{2+}-dependent or Ca^{2+}-independent, can co-exist in different synapses and with different contributions (Scott et al., 2008).

1. Considering that the effect of SSD is evidenced in the "digital" AP-dependent neurotransmitter release.

Little is known about the molecular mechanisms underlying this form of synaptic plasticity; however, important advances were recently made in this direction using cerebellar molecular layer interneurons (MLIs) as a model (Bouhours, et al., 2011). In these cells, SSD pulses are electrotonically spread to the presynaptic terminals, where they produce an enhancement of NT release through a signaling pathway involving the activation of the P/Q type, voltage-dependent Ca^{2+} channels (VDCC), followed by an increase in the basal Ca^{2+} levels and a local activation of protein kinase C (PKC) (Bouhours, et al., 2011); the target of PKC that mediates this effect is unknown. Additionally, for the same preparation it has been also proposed that the SSD-evoked Ca^{2+} influx facilitates the AP-evoked Ca^{2+} entry and enhances NT release (Christie et al., 2011). Interestingly, in the same study was reported that 4 out of 10 MLI-MLI recorded pairs showed a depression instead of a facilitation when the SSD pulse was preceded by the application of a high frequency train of action potentials. More recently, some controversy has arisen because the group of Christie did not see any SSD-mediated facilitation in MLIs in PKC knockout animals. Instead, they attributed the presence of analog signaling to a broadening of the AP due to the rapid inactivation of the Kv_3 type of potassium channels in the presynaptic terminals, which modifies the currents accounting for the AP waveform, directly enhancing the spike-evoked Ca^{2+} influx independently of PKC

(Rowan and Christie, 2017). Previous studies showed that both, the application of NMDA and the application of SSD in cerebellar MLIs can significantly increase the frequency of miniature GABAergic events (Glitsch and Marty, 1999), thus suggesting that physiological subthreshold activity can efficiently modulate the axonal function. Additionally, the application of SSD also produces an increase in the frequency of the so-called "preminis" (Trigo et al., 2010), which correspond to synaptic events that emerge from the autocrine activation of the presynaptic GABAergic receptors in the axon of MLIs. It was recently shown that these preminis can have an impact on the interneuron excitability, because the voltage changes that they produce are transmitted to the soma antidromically (de San Martin JZ et al., 2015). Furthermore, since preminis are prominent during the formation of the molecular layer (P11-15), it is thought that they could guide the formation of the neuronal circuits in growing GABAergic neurons through an increase in the release probability of newly formed synaptic contacts by a positive feedback mechanism.

During the last decade, a growing body of evidence suggests that many of the neurons in the nervous system can express ionotropic receptors in the axonal terminals that can modify the membrane potential locally. For example, in several preparations in which the SSD-mediated facilitation effect has been studied, the

presynaptic terminal expresses $GABA_A$ or glycine receptors [calyx of Held (Turecek and Trussell, 2001); mossy fibers (Ruiz et al., 2003; Alle and Geiger, 2007); MLIs (Pouzat and Marty, 1999; Trigo et al., 2007)]. In addition, unlike the somatodendritic compartment, where the activation of these receptors is inhibitory (or mixed inhibitory/excitatory), their activation in the axonal compartment is excitatory, leading to membrane depolarization, increase in the axonal Ca^{2+} levels and increase in NT release (Trigo et al., 2008). Consequently, it has been proposed that the activation of these presynaptic receptors and the SSD-mediated facilitation could share a common signaling pathway.

In summary, the analog-to-digital signaling, by which subthreshold synaptic activity reaches the presynaptic terminals and modules the AP-evoked process of NT release, has deep implications in the way the NS encodes and processes information. Indeed, in a "digital" synapse NT release follows the all-or-nothing nature of the AP, hence being a binary process that either does ("1") or does not ("0") happen, while in an analog synapse the dynamic range in which information can be transferred is very large (Rama, Zbili, Debanne, 2015). Thus, a hybrid type of synaptic transmission where subthreshold activity modulates the following AP-dependent release will largely increase the amount of information that can be transmitted in neural circuits. Furthermore, if we consider that many neurons in the

mammalian brain possess axons with lengths of a few hundred microns, it became clear that the extent of SSD penetration can result in that a high proportion of presynaptic terminals are modulated; for example, the space time constant (distance at which the change in the membrane potential has experienced a decrease of 63%) in hippocampal neurons where ADF has been described is approximately 430 μm (Alle and Geiger, 2006).

It would be very helpful, to determine the synaptic processes controlling NT release in central synapses, to describe the specific synaptic parameters that are being modulated during ADF, their differences between individual synaptic contacts of the same neuron, and from different neuronal types at different developmental stages.

1.2 Possible role of protein kinase C in the subthreshold somatic depolarization-mediated facilitation of neurotransmitter release

Protein kinase C is a family of kinases that are implicated in controlling the function of others proteins by the phosphorylation of their hydroxyl group of Ser/Thr amino acid residues. The conventional isoforms of PKC (PKCα, PKCβI/βII, and PKCγ) are expressed in several tissues (including the brain) and require the binding of the lipid second messenger diacylglycerol (DAG) and Ca^{2+} for their full activation (Hirokazu Hirai, 2017). The effects of the activation of the conventional isoforms of PKC by DAG (through its C_1 binding domain) or directly by Ca^{2+} (through its C_2 domain) have been implicated in many studies with the induction of synaptic enhancement/augmentation (Francis et al., 2002, Majewski and Iannazzo, 1998, Stevens and Sullivan, 1998). There is also evidence that PKC plays a critical role in the phenomenon of post-tetanic potentiation[2], which results from a high-frequency or "tetanic" stimulation of 30-50 or 100 Hz (commonly, 50 Hz for 5 seconds). (Alle et al., 2001, Beierlein et al., 2007, Brager et al., 2003; Fioravante et al., 2011; Korogod et al., 2007; Lee et al., 2008; Wierda et al., 2007). Because post-tetanic potentiation as well other types of short-term synaptic plasticity (including depression) are elicited by different temporal patterns of presynaptic activity, it has been hypothesized that they may contribute to the

2. The short-term synaptic plasticity is often separated into three categories according to their temporal scales: facilitation (which lasts for tens of milliseconds), augmentation (lasts for seconds) and potentiation (also called post-tetanic potentiation), that lasts for minutes. It is thought that all depend in one way or another on the residual presynaptic Ca^{2+} levels acting in different targets.

phenomenon of temporal filtering by facilitating or impeding the transmission of different patterns of activity (Fortune and Gary, 2000). Additionally, post-tetanic potentiation is thought to correspond to one of the mechanisms that significantly contribute to the formation of short-term memory, synaptic filtering and information processing in the nervous system (Abbott and Regehr, 2004; Klug et al., 2012; Silva et al., 1996).

Many forms of regulation of neurotransmitter release are mediated through an increase in the size of the readily releasable pool (RRP) (fraction of vesicles in the active zone available for immediate release upon strong stimulation) and/or by an increase in the probability of NT release (pNR) (Pan and Zucker, 2009, Regehr et al., 2009, Zucker and Regehr, 2002).

In a recent study in the calyx of Held (Chu et al., 2014) it was demonstrated that, depending on the developmental stage of the animal, the activation of different conventional PKC isoforms is capable of mediating post-tetanic potentiation either by an increase in pNR or through an increase in the RRP; however, the PKC substrate that could be mediating these processes is unknown.

From a functional perspective, knowing which of the two mechanisms (changes in pNR or the RRP size) is governing the properties of NT release in different

synapses is very important, since they have very different outcomes in response to the application of high frequency stimulation trains (Pan and Zucker, 2009; Thanawala and Regehr, 2013): an increase in RRP proportionally increases the amplitude of the synaptic responses (an effect similar to increasing the number of postsynaptic receptors), while an increase in pNR has also the effect of increasing the use-dependent depression of the response. In this way under tetanic stimulation, the total amount of NT released is doubled if the RRP is doubled, while it essentially remains unchanged if pNR doubles (Chu et al., 2014).

Proteins of the release machinery (SNAP25, MUNC18-1, GAP-43, and synaptotagmin-1) and some voltage-dependent ion channels (K^+ and Ca^{2+}) have been identified as putative presynaptic substrates of PKC, whose phosphorylation could be involved in the phenomenon of synaptic plasticity. However, with the notable exception of MUNC-18, evidence for a role of the rest of the proteins in the PKC-mediated potentiation is either incomplete or has been ruled out (Parfitt and Madison, 1993; Finley et al., 2003; Hulo et al., 2002; Nagy et al., 2006). MUNC18-1 is an essential component of the vesicle fusion complex and is indispensable in the process of NT release (Verhage et al., 2000; Zilly et al., 2006). Interestingly, MUNC18-1 presents multiple sites of phosphorylation by PKC (Barclay et al., 2003; Fujita et al., 1996); phosphorylation of these sites has been

previously implicated in vesicle replenishment after intense stimulation (Nili et al., 2006) and in the control of RRP size in GABAergic and glutamatergic synapses (Toonen et al., 2006). Additionally, it is known that MUNC18-1 is rapidly phosphorylated by PKC under depolarizing conditions (Craig et al., 2003; de Vries et al., 2000). All these observations make the MUNC18-1 protein the most likely candidate to mediate the effects of PKC activation during subthreshold somatic depolarizations.

1.3 Synapse-specific differences in the number of docking sites and their occupancy probability as key parameters in the subthreshold somatic depolarization-mediated synaptic facilitation

Central mammalian synapses differ substantially among each other in several key parameters like quantal size (postsynaptic response to the release of NT from a single vesicle), pNR and short-term synaptic plasticity. One of the most basic parameters within the set of synaptic heterogeneities is the size. It is known that differences in synaptic size can reach up to an order of magnitude, and that the dimensions of the presynaptic active zones and the postsynaptic densities, as well as the number of synaptic vesicles and the number of postsynaptic receptors, vary in direct proportion with the synaptic size (Harris and Stevens, 1988, Schikorski and Stevens, 1997, Nusser et al., 1997). Recently, it was demonstrated in the Calyx of Held (by local electrophysiological recordings in the presynaptic terminal, Sheng et al., 2012) and in hippocampal glutamatergic synapses (by optical quantal analysis, Holderith et al., 2012; see later section 1.5: Approaches for the study of single synaptic contacts in brain slices) that the number of Ca^{2+} channels and the corresponding pNR increases linearly with the size of the active zone.

In a recent publication using MLIs of the cerebellum as a model, the differences between presynaptic parameters (such as the number of docking sites and release

probability) and postsynaptic parameters (such as the amplitude and kinetics of the synaptic currents) were explored at the level of single synaptic contacts. This was carried out using an approach that allows studying individual contacts by simultaneously recording the pre- and postsynaptic activity in pairs of connected neurons in slices of rat cerebellum (Pulido et al., 2015), based on the fact that a significant percentage of the MLI-MLI connections consist of single synaptic contact with a single active zone and a single postsynaptic density (Nusser et al., 1997; Kondo and Marty, 1998).

Pulido et al. (2015) used a simple binomial model (briefly explained in Figure 1-1) to propose that the differences observed between individual synaptic contacts could emerge as a consequence of differences in the number of docking sites (NDS), which would increase in direct proportion with the synaptic size. They also suggested that the application of depolarizing subthreshold pulses could significantly modify the docking site occupancy, which would have a direct impact on the synaptic performance during high-frequency stimulation (40 Hz). In this way, variations in the synaptic size might account for the differences that were reported in both presynaptic (release probability) and postsynaptic parameters such as the peak amplitude and the kinetics of the postsynaptic current (PSC). This neuronal property could be particularly important in synapses with a marked

saturation of postsynaptic receptors such as in GABAergic synapses between MLIs (~70%), since in these synapses an increase in the amount of released NT would not generate a substantial change in the amplitude of the PSCs, unless both an increase in the amount of NT released as well as an increase in the number of postsynaptic receptors occurs in a coordinated way. Thus, in the long-term, a fixed synaptic size would markedly decrease the efficiency of the transmission process.

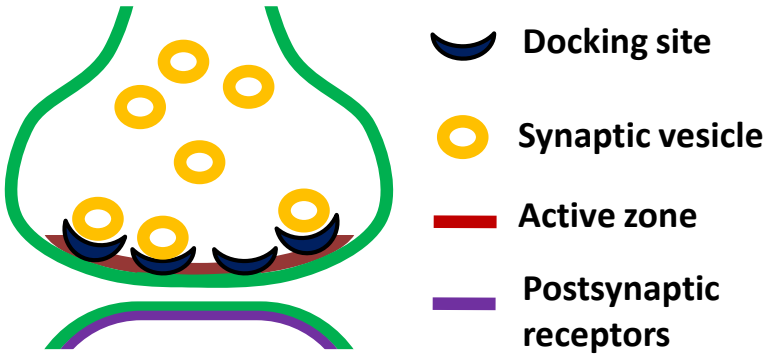

Figure 1-1. Vesicular release model for a single synaptic contact between cerebellar MLIs.
The figure illustrates the active zone, the docking sites, the docked vesicles (RRP), the recycling vesicle pool (which fill the empty docking sites after release) and the postsynaptic receptors of a single synaptic contact. This central synapse, unlike the typical models of synaptic transmission (the calyx of Held, the amphibian neuromuscular junction, or the squid giant synapse), has a single active zone associated with a single postsynaptic density. In this model of Pulido et al., (2015), NT release is described according to the following assumptions: a synapse contains "N" independent docking sites, each of which has a probability (δ) of being occupied by a vesicle. At the same time, a docked vesicle has a probability (p) of fusing with the plasma membrane and releasing its content to the synaptic cleft. After the exocytosis, each empty docking site will be refilled according to a replacement constant rate "R".

1.4 The importance of studying the mechanisms of modulation of synaptic transmission at the level of single synaptic contacts

One of the ultimate goals of neuroscience is the detailed understanding of the processes by which humans and other animals with a nervous system are capable of sensing and processing the environmental information in order to perform an action that allows an adequate adaptation to a particular situation. Virtually all the evidence accumulated to this day support the idea that all this amazing capacity of the nervous system depends on the ability to generate and propagate electrical signals between its essential neuronal components during the process of synaptic transmission.

The importance of the electrical activity for the physiology of the nervous system was highlighted more than two centuries ago by the Italian physicist and anatomist Luigi Galvani (Piccolino, 1998), and since then the research has mainly focused on understanding the cellular and molecular bases by which this electrical activity allows the transmission of information in a fast and efficient way between excitable cells[3], and how this activity relates to animal behavior. Consistent with this idea, most of the information that we have today about the physiological aspects of synaptic transmission has been obtained by electrophysiological approaches. Although this approximation has a series of remarkable advantages

3. Those cells that present some type of electrical signaling as a result of a differential gene expression pattern that allows them to express ion channels through which they are able to generate and propagate an electrical signal: neurons, muscle cells, glia, endocrine pancreatic cells, endocrine pituitary cells, adrenal medulla cells, gametes and some endothelial cells.

(e.g., high temporal resolution of the synaptic current), electrophysiological recordings have proved insufficient to study the functional properties of synaptic transmission at the level of individual synaptic contacts. This is mainly because most electrophysiological recordings usually reflect the averaged electrical activity of many different synapses that are activated in a determined time interval. This is very relevant if we consider that mammalian central synapses differ widely in morphological and functional aspects, even within the same family of synapses, where the pre- and postsynaptic cells belong to the same neuronal type (Branco and Staras, 2009).

On the other hand, the experimental preparations that have been commonly used for the study of synaptic physiology correspond to "special" types of synapses that do not represent the vast majority of the central synapses. These are: the amphibian neuromuscular junction, the squid giant synapse, and the mammalian Calyx of Held. These synapses have been very useful as models; however, they markedly differ in several important aspects with the great majority of the central synapses; for example, central synapses are usually smaller (up to orders of magnitude) and possess well-defined synaptic contacts that are morphologically and functionally differentiable from each other (Schikorski and Stevens, 1997, Nusser et al., 1997). As mentioned before, one important parameter of the synapse is the size, especially

if we consider that a decisive and often limiting aspect in the study of central synapses is the relationship between the amplitude of the response evoked by an AP and the quantal response. Unlike the amphibian neuromuscular junction, the squid giant synapse or the Calyx of Held, where the quantal responses produce only modest fluctuations in the AP-evoked response, in the central synapses the quantal and AP-evoked responses can be similar in magnitude, hence the influence of a single quantum in the AP-evoked response becomes much more significant.

Although the probability of a single quantum to be released (p) does not differ markedly between central synapses and the traditional models of synaptic transmission, these last synapses have a quite distinctive feature that makes them very special: they present a very low probability of failures in the transmission process, thus ensuring that NT is released every time that an AP arrives to the presynaptic terminal. In the amphibian neuromuscular junction and the squid giant synapse, a low failure rate confers to the animal the ability to reliably move away from potential life-threatening dangers, while the Calyx of Held confers the ability to efficiently locate the source of a sound. These exceptional features are a direct consequence of the high number of actives zones (hundreds) in the presynaptic terminal, which allow them to have both a high probability of an AP generating NT release (synaptic reliability), and also a high average postsynaptic response

(synaptic efficacy). Contrary to this, a typical central synapse in the brain has a single active zone in the presynaptic terminal and presents a high rate of failures, which translates directly into a low synaptic reliability and efficacy in the process of synaptic transmission. Although this may be seen as a disadvantage, in evolutionary terms this feature plays a fundamental role: it allows the neurotransmitter release process to be modulated within a wide dynamic range, which is extremely important for the phenomenon of synaptic plasticity and in consequence for the processes of memory and learning (Kandel, Schwartz, and Jessell, 2000). A comparison between the sizes of the traditional synaptic models and a typical central synapse is presented in Fig.1-2.

Considering the arguments presented so far, it should be evident that studying synaptic transmission and its mechanisms of modulation, as for example the SSD-mediated facilitation in more representative models of synaptic transmission and at the level of individual synapses is crucial. Nevertheless, it is also clear that the experimental interrogation of a single and small synapse that is immersed in the complexity of brain tissue is an extremely difficult task. It is absolutely necessary to overcome this barrier in order to understand the details of the mechanisms that could be governing the different aspects of synaptic physiology and that may

account for the differences that have been observed among different synapses, for example, the differences in Ca^{2+} dependency during the SSD-mediated facilitation.

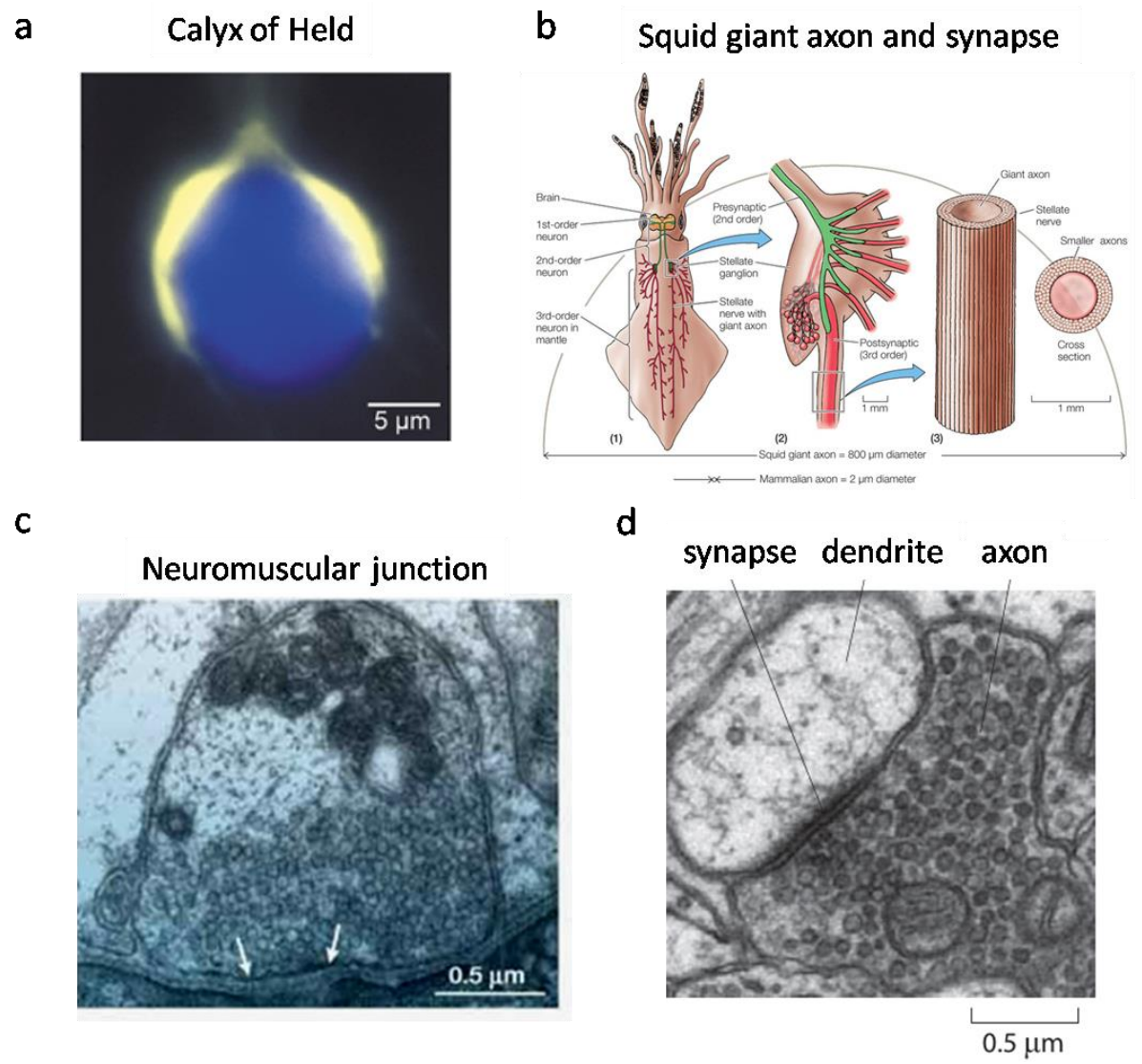

Figure 1-2. Traditional synapses used as synaptic transmission models and a typical central synapse. **(a)** Image of the calyx of Held and its large presynaptic terminal in the mammalian brain stem. The calyx was filled with Lucifer Yellow. The presynaptic terminal and the postsynaptic cell body are presented in pseudocolors, yellow and blue, respectively (adapted from Meinrenken, Borst, and Sakmann 2003). **(b)** Giant synapses in the squid nervous system. The squid brain possesses "first-order" giant neurons (left) whose activation excites second-order giant neurons (middle) that make connections with the stellate ganglia at the squid mantle. The giant axons of several third-order giant neurons (~1 mm in diameter; right) radiate from the ganglia to the mantle muscles and cause contraction (Animal Physiology, Fourth edition, box extension 12.3 Giant Axons). **(c)** Electron micrograph of a cross-section through the nerve terminal of the frog neuromuscular junction where the actives zones are indicated by the white arrows (adapted from S. O. Rizzoli and W. J. Betz, 2005). **(d)** Electron micrograph of a central synapse in the brain (image by Linnaea Ostroff and adapted from Cell Biology by the Numbers by Ron Milo, Rob Phillips).

1.5 Approaches for the study of single synaptic contacts in brain slices

Given the extreme difficulty of studying NT release at the level of single synaptic contacts, the problem has usually been solved by the use of cellular cultures. In these preparations the accessibility to the small and well-defined cellular structures makes relatively easy to induce the exocytosis of NT by direct electrical stimulation of the presynaptic terminals, to visualize the release events by performing imaging experiments and to perform recordings of synaptic current from single synaptic contacts (Liu and Tsien, 1995, Ryan et al., 1997, Forti et al., 1997). However, the relevance of these results is uncertain, since it is highly probable that the synaptic function is altered in this type of preparations. A more physiological approach, although more difficult, is to search for pairs of synaptically connected neurons in brain slices, since in some cases a single synaptic contact is established between them (Gulyás et al., 1993, Kondo and Marty, 1998).

One approach that has been extensively used is the technique called “minimal synaptic stimulation of single synapses”, where extracellular electrical stimulation attempts to trigger release from a single presynaptic fiber, for example, in CA3 to CA1 connections in the hippocampus (Stevens and Wang, 1995). However, with this methodology it becomes very difficult to control of the extracellular

stimulation well enough to ensure that a single presynaptic fiber is being stimulated.

The exocytosis-inducing effect of the α-latrotoxin has previously been used to study synaptic transmission between cerebellar MLIs at single synaptic contacts (Auger and Marty, 1997). This toxin, when applied in low doses, is able to stochastically activate one synaptic site in periods of about one minute, resulting in a burst of quantal signals arising from a single contact. This method has been used to study the number, the unitary conductance and the opening probability of the postsynaptic channels in GABAergic synapses (Auger et al., 1997) and to study the replenishment of vesicle and the degree of desensitization of AMPA receptors in glutamatergic synapses (Crowley et al., 2007). However, the main disadvantage of this approach is that it does not allow identifying the sites that are activated and is difficult to control the duration and intensity of the presynaptic stimulus.

On the other hand, at the level of individual glutamatergic synapses the so-called "quantal optical analysis" method has been used to study synaptic vesicular release; the method relies in visualizing the Ca^{2+} rises produced by the opening of NMDA receptors on the postsynaptic dendritic spines (Yuste et al., 1999; Oertner et al., 2002). This approach has provided convincing information in favor of

multivesicular release in synapses where previous results obtained by using the minimal synaptic stimulation approach had been interpreted in favor of the one-site-one-vesicle hypothesis[4]. These Ca^{2+} imaging experiments, while providing relatively high spatial resolution of synaptic events, do not reliably reflect the current through the postsynaptic receptors, and lack the temporal resolution required to analyze in detail the effects of receptor activation (as can be obtained by measuring the synaptic currents).

The ideal approach to study synapses at the level of individual synaptic contacts with high spatial and temporal resolution should be capable of detecting individual synaptic release events.

A method that allows studying single synaptic contacts between cerebellar MLIs without the disadvantages of the previous methodologies was recently developed. It combines the photorelease of Ca^{2+} from a photosensitive "cage" in the presynaptic terminal and the simultaneous measurement of postsynaptic currents by dual pre-and postsynaptic whole-cell recordings. This methodology has already been used successfully to estimate the size of the RRP at individual synaptic contacts in the same preparation used in the present study (Trigo et al., 2012).

4. Hypothesis that propose that although a synaptic contact can contain several docked vesicles in the active zones, only one of them fuses with the plasma membrane and releases its content as consequence of the arrival of an action potential to the terminal.

2 Thesis project proposal

The discovery of the dual nature of the rapid communication between the soma and the presynaptic terminals (through the generation of APs and by analog-to-digital signaling) has profound implications in our understanding of the mechanisms by which the brain processes information: the analog signaling phenomenon can significantly modify the synaptic output that determines the functioning of cellular circuits, either through an increase in the amount of information transmitted by a particular neuron or by modulating the synaptic activity in groups of neurons subjected to fluctuations of membrane potential, such as those produced by oscillatory activity (Alle and Geiger, 2008).

Although today we know that this type of signaling is capable of modulating NT release in both excitatory and inhibitory synapses, we still have much to discover about the mechanisms by which this modulatory effect is set; for example, it is still unknown whether the Ca^{2+}-dependency of this phenomenon is a particular feature of some experimental preparations or whether it is a general mechanism in central synapses. On the other hand, we do not know what are the parameters associated with the vesicular cycle that could be modified during SSD-mediated facilitation and if they exhibit or not variations among individual synaptic contacts within the same neuron.

In cerebellar MLIs, a SSD-dependent increase in both asynchronous release (during SSD) and AP-evoked release (after SSD) has been reported (Glitsch and Marty, 2009; Trigo et al., 2012; Bouhours, et al., 2011; Christie et al., 2011). It has also been suggested that the strength of the effect on AP-evoked NT release could depend on the availability of fusion-competent vesicles to release their content upon the arrival of an AP (Christie et al., 2011).

The evidence presented so far suggests that the analog signaling phenomenon in MLIs of the cerebellum could act through a mechanism that involves a subthreshold Ca^{2+}-dependent modification of the dynamics of the occupation of the docking sites; this mechanism may depend on the activation of PKC and the downstream phosphorylation of some of the proteins of the release machinery, like MUNC18-1. This would generate changes in the amount of NT that is released both asynchronously as well as evoked by a suprathreshold increase in Ca^{2+} levels, which in turn would generate changes in the reliability and/or efficacy of the synaptic transmission.

In this thesis work, we studied the relationship between the ADF phenomenon and the synaptic parameters accounting for NT release (like peak amplitude, charge and synaptic latency of postsynaptic currents). Additionally, we studied how

possible changes on these parameters are associated with the occupancy probability of docking sites, and the size of the RRP at single synaptic contacts of cerebellar MLIs. In order to do this, we used a methodology that combines optical and electrophysiological techniques (see methods) that provides the temporal and spatial resolution required to perform direct measurements of the synaptic activity at the single synaptic level.

3 Hypothesis

The subthreshold Ca^{2+} rises reached during analog-to-digital facilitation in cerebellar MLIs can effectively modulate GABA release by a mechanism that involves an increase in the occupancy probability of docking sites, which translates directly into an increase in the RRP size and an enhancement of the synaptic reliability/efficacy in single synaptic contacts.

4 General objective

To explore the effects of the direct manipulation of presynaptic subthreshold Ca^{2+} levels on the synaptic parameters controling the features of the postsynaptic response, and their possible differences between individual GABAergic MLI-MLI synapses of the rat cerebellum.

5 Specific objectives

1. To study the nature of the RRP at the single synaptic level and its possible modulation by subthreshold Ca^{2+} rises.

2. To directly determine the number of docking sites (NDS), their occupancy probability (δ) and its putative modulation by subthreshold Ca^{2+} changes.

3. To explore the effects of modulating subthreshold Ca^{2+} influx on the features of PSC by the application of presynaptic SSD in pairs of synaptically connected MLIs.

6 Methods

6.1 General methods used in this work

In this thesis work we studied quantal release in single synaptic contacts between MLIs of the rat cerebellar cortex. Individual synaptic connections were interrogated by measuring quantal events evoked postsynaptically by presynaptic Ca^{2+} uncaging with a localized laser spot and after establishing a recording from a synaptically connected pair of MLIs. Direct control of Ca^{2+} levels in the sub- and suprathreshold range was made by varying the laser intensity. The presynaptic cell was recorded with an intracellular solution (IS) containing a high millimolar concentration of the Ca^{2+} cage DM-nitrophen and the fluorescent dye Alexa 594 to allow identification. In some experiments, the Ca^{2+} indicator Oregon Green BAPTA-1 (OGB-1) was included in the IS to monitor the laser-evoked Ca^{2+} changes. The postsynaptic cell was recorded using a KCl-based IS to obtain large quantal sizes. Alexa 488 was included to distinguish the postsynaptic MLI from the presynaptic MLI. An additional set of experiments were performed using purely electrophysiological interrogation of synaptic contacts in pairs of connected MLIs, where subthreshold somatic depolarizing steps were delivered to modulate synaptic transmission. Figure 6-1 shows the principal components of the setup for simultaneous dual patch-clamp recording and photolysis experiments.

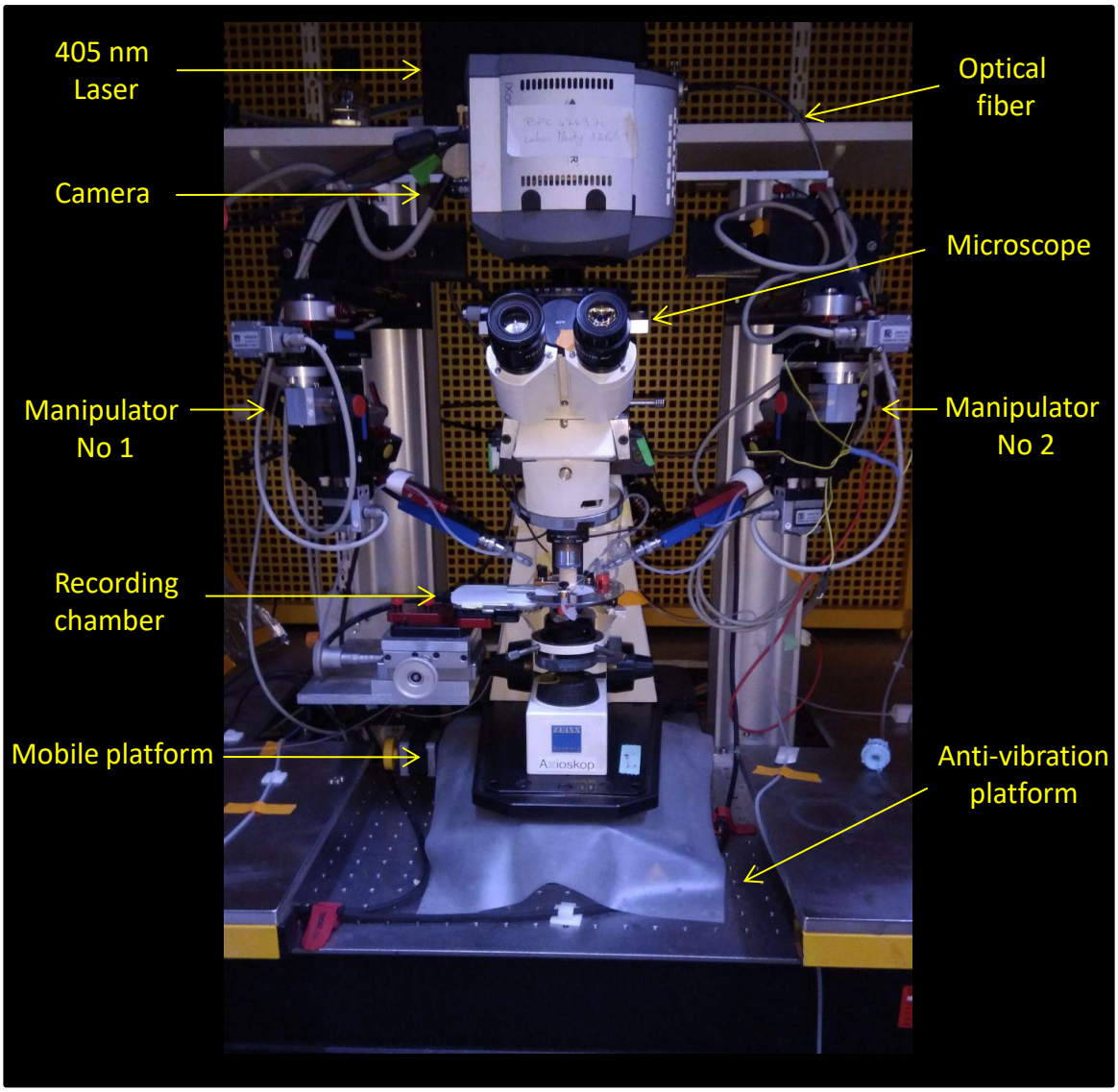

Figure 6-1. Main components of the electrophysiological setup for simultaneous dual whole-cell patch-clamp recordings and photolysis experiments.

6.2 Preparation of cerebellar slices

Sagittal cerebellar slices from young (11–17 days old) Sprague–Dawley rats were obtained according to the established procedures used in the Brain Physiology Lab (Llano et al., 1991). Rats were killed by direct decapitation in accordance with institutional guidelines for ethical procedures. The cerebellar vermis was carefully dissected (see Figure 6-2) and placed in ice-cold bicarbonate-buffered solution (BBS; see composition below) that was constantly gassed with a mixture of 5% (vol/vol) CO_2 and 95% O_2.

The meninges that were still attached to the surface of the vermis were carefully removed by using tweezers under a stereomicroscope in order to facilitate the slicing procedure. 200 μm thick slices were cut with a vibroslicer (VT1200S; Leica) in ice-cold BBS and then placed in an incubating chamber at 34°C for 45 min, to recover from the slicing damage. Thereafter, they were kept at room temperature until use. The slices were transferred to the recording chamber and used during a period of up to 8 h after the decapitation procedure. The composition of the BBS for cutting, storing slices and recording was (in mM): 115 NaCl, 2.5 KCl, 1.3 NaH_2PO_4, 26 $NaHCO_3$, 25 glucose, 5 Na-Pyruvate, 2 $CaCl_2$, and 1 $MgCl_2$, with an osmolality of 300 mOsm/kg, and pH 7.4 when gassed with 5% (vol/vol) CO_2 and 95 O_2.

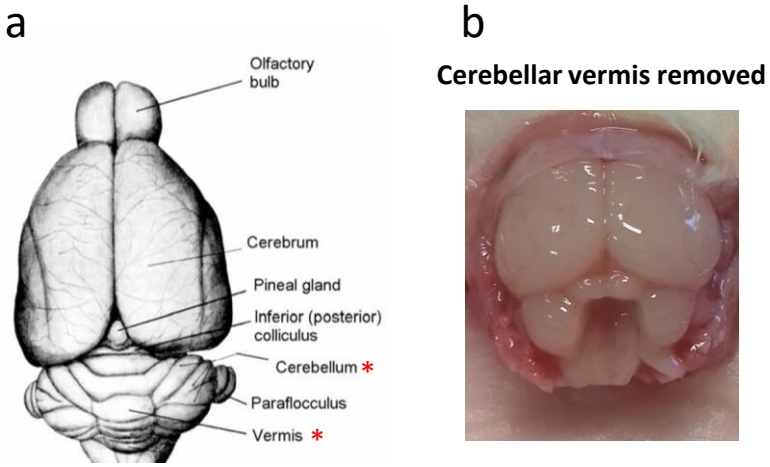

Figure 6-2. Dorsal and caudal view of the rat brain.
(a) Illustration of the dorsal aspect of the brain. Red asterisks denote the structures relevant for this work: the cerebellum and the cerebellar vermis (https://instruct.uwo.ca/anatomy/530/ratpix.pdf). **(b)** Picture showing the caudal view of the head of a rat where the vermis has been removed.

6.3 Electrophysiology

6.3.1 Electrophysiology for uncaging experiments in pairs of molecular layer interneurons

Molecular layer interneurons were selected based on their location in the molecular layer and the soma size, ranging from 6 to 8 μm. MLIs were voltage-clamped with the whole-cell patch-clamp technique using a double EPC-10 USB amplifier (HEKA Elektronik). In these experiments we used a high [Cl^-] in the postsynaptic IS in order to optimize the amplitude of PSCs and readily detect individual fusion events. The composition of the postsynaptic IS was as follows (in mM): 150 KCl, 1 EGTA, 10 Hepes, 0.1 $CaCl_2$, 4.6 $MgCl_2$, 4 Na_2ATP, 0.4 NaGTP, and 0.08 Alexa

488, with an osmolality of 300 mOsm/kg, and pH 7.3. The composition of the presynaptic IS was as follows (in mM): 95 K-Gluconate, 5.6 KCl, 50 Hepes, 0.5 $MgCl_2$, 4.2 $CaCl_2$, 5 Na_2ATP, 0.2 NaGTP, 5.2 KOH, 5 1-(2-nitro-4,5-dimethoxyphenyl)-N,N,N′,N′-tetrakis[(oxycarbonyl)methyl]-1,2-ethanediamine (DM-nitrophen), 0.08 Alexa 594, and 10 GABA, with an osmolality of 300 mOsm/kg, and pH 7.3. GABA was included in the IS to prevent rundown of the PSCs by the emptying of synaptic vesicles, as reported previously by Bouhours et al., 2011. The experiments were performed at room temperature (20–22 °C) and the recording chamber was continuously perfused at a rate of 1–2 ml/min with gassed BBS. Holding potentials were −60 mV for both presynaptic and postsynaptic neurons and the reported values for Vm were corrected for the calculated liquid junction potential of 13.8 mV and 1.4 mV, giving final Vm values of -73.8 mV and -61.4 mV for the presynaptic and postsynaptic cells, respectively. Patch electrodes (micropipettes) were pulled from borosilicate glass to a tip resistance of ~ 4.5 MΩ when filled with the postsynaptic IS. Series resistance was in the range of 10–35 MΩ and was not compensated. Cells were discarded when the series resistance value was larger than 35 MΩ or if it varied more than 20%. Synaptic connectivity was tested by delivering short depolarizing voltage steps of 1 ms to 0 mV to the presynaptic cell. Immediately after the connectivity test was

successful (as ascertained by the presence of postsynaptic currents), TTX (0.2 µM final concentration) was included in the bath solution throughout the entire experiment in order to minimize contamination from AP dependent neurotransmitter release. Recordings from both pre- and postsynaptic cells were acquired at a sampling rate of 50 kHz and low-pass filtered at 2.9 KHz. Most data were obtained from cells located in the proximal 1/3 part of the molecular layer (basket cells). However, interneurons located in the outer 2/3 of the molecular layer (stellate cells) were also included.

6.3.2 Pure electrophysiological recordings in pairs of molecular layer interneurons

Molecular layer interneurons were selected following morphological criteria and voltage-clamped with the whole-cell patch-clamp technique. The composition of the IS for the pre and postsynaptic cells was as follows (in mM): 145 KCl, 10 GABA, 0.02 EGTA, 10 HEPES, 0.1 $CaCl_2$, 4.6 $MgCl_2$, 4 Na_2ATP, 0.4 NaGTP, with an osmolality of 300 mOsm/kg, and pH of 7.3. Synaptic connectivity between the two cells was tested by delivering depolarizing voltage steps of 1 ms to 0 mV to each of them (they were dialyzed with the same IS, thus connectivity could be detected in both directions). Holding potential was set at −75 mV for both presynaptic and postsynaptic MLIs. The subthreshold somatic depolarization

protocol used in these experiments consisted of a 2 s pulse from -75 mV of holding potential (Vm= -76.4 mV after correcting by the junction potential) to a value just below the spike threshold (usually -50 mV, corresponding to -51.4 of Vm). The spike-evoked PSC accounting for the properties of presynaptic GABA release was evoked by applying a short depolarizing step of 1 ms to 0 or 10 mV to the presynaptic cell. Series resistance was in the range 10–35 MΩ and was 50 % compensated. Cells were discarded when the series resistance value was larger than 35 MΩ or if it varied more than 20%. Recordings in both pre and postsynaptic cells were acquired at a sampling rate of 50 kHz and low-pass filtered at 2.9 KHz.

6.4 Fluorescence imaging and synaptic contact identification

The localization of putative individual synaptic contacts was made by alternating the excitation of the fluorescent dyes Alexa 594 and Alexa 488 that were included in the presynaptic and postsynaptic IS, respectively (see composition above). In the juvenile MLIs used in this work, the presynaptic axon and the postsynaptic somatodendritic compartment are readily distinguished by their characteristic ramification pattern and neurite thickness. The functional identification of a putative individual synaptic contact was made by photoreleasing Ca^{2+} from the photosensitive Ca^{2+}chelator DM-nitrophen (Kaplan and Ellis-Davies, 1988; see below on Methods: Photolysis of DM-Nitrophen). Epifluorescence excitation was

obtained from a light emitting diode (LED) system (Optoled; Cairn Research) equipped with 2 LEDs resulting in outputs at 470/40 nm and 572/35 nm wavelength by using excitation filters (Chroma Technology). The emitted fluorescence was collected after emission filters of 520/40 nm and 630/60 nm (Chroma Technology) and directed to an EM CCD camera (Ixon, 512 × 512 pixels; Andor Technology). Reconstruction of the morphology was made by taking single full frames pictures with excitation of Alexa 488 or Alexa 594 and varying the focal depth. ImageJ (National Institutes of Health; https://imagej.nih.gov/ij/) was used to make the stacks (at 1μm increments) and the composite images. Figure 6-3 shows and example for the reconstruction of a pair of connected MLIs and the localization of the interrogated synaptic contact.

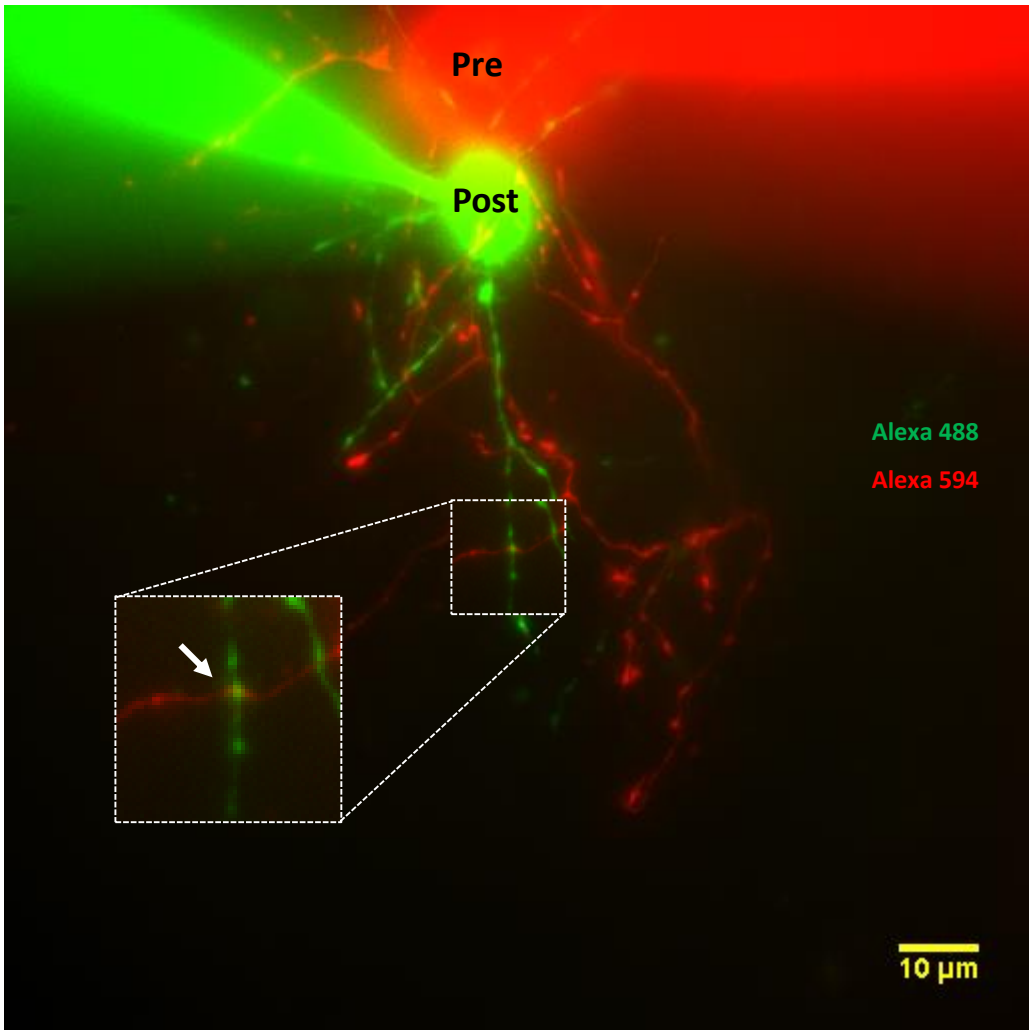

Figure 6-3. Fluorescence image and synaptic site localization of a synaptically connected pair of MLIs.
The image corresponds to the composite of the individual z-projections of the stacks taken at 594 nm and 488 nm of excitation. Cells are presented with pseudocolors: presynaptic in red, postsynaptic in green. The arrow indicates the site chosen for uncaging.

6.5 Photolysis of DM-Nitrophen

Photolysis of DM-nitrophen (Kaplan and Ellis-Davies, 1988) was implemented with a 405 nm wavelength diode laser (DeepStar 405; Omicron). The light was focused through a 63× Zeiss objective as a ~5 μm diameter spot in the focal plane of the objective and viewed with an electron multiplying charge-coupled device (EM CCD) camera at 0.25 μm per pixel (Ixon, 512 × 512 pixels; Andor Technology). The position and the approximate size of the laser spot was checked every experimental day by looking at the fluorescence of HPTS (8-Hydroxypyrene-1,3,6-Trisulfonic Acid; 100 μM), which is excited by the 405 nm laser light. Upon photolysis, the affinity of DM-nitrophen for Ca^{2+} decreases around 6,000,000-fold and its K_d increases from 5 nM to 3 mM, resulting in a pulse of free Ca^{2+}. Lyophilized DM-nitrophen (Synaptic Systems) was dissolved in KOH solution in a 1:4 DM-nitrophen/K^+ proportion (50 mM of final concentration) and stored at -20°C. The potassium salt was then added to the IS the same day of the experiment. For the control protocols of uncaging used in this work, a single laser pulse that releases the RRP was applied in single varicosities. For the test protocol, the same RRP-releasing pulse was preceded by a train of five low intensity pulses at 10 Hz and separated by 200 ms or 2 s from the RRP-releasing pulse. The ranges of energies for the subthreshold train and the suprathreshold pulse was 0.0085-

0.098 µJ and 0.1–0.4 µJ, respectively. These energies were set during individual experiments and varied for each synapse. The energies for the train of subthreshold laser pulses was set to reach the maximal level that does not produce a postsynaptic response within the first 5 ms after triggering the laser. The RRP-releasing nature of the suprathreshold pulse was confirmed by the lack of response to a second pulse of the same energy that was delivered 30 ms later (Figure 6-4). During photolysis of DM-nitrophen, two net OH^- ions are formed for each Ca^{2+} ion released. In order to minimize the alkalinization on photolysis, 50 mM Hepes was included in the IS (see composition above). At this concentration of Hepes a change of ~ 0.37 pH units is still expected. Nevertheless, in similar experimental conditions, this pH change had no effect on synaptic transmission (Trigo et al., 2012).

The number of repetitions that can be performed under these experimental conditions is limited. The minimum and maximal number of repetitions obtained in this work was 10 and 46, respectively. This restriction is not a consequence of photodamage produced by the 405 nm laser because it does not happen when other cage compounds like glutamate or GABA are photolised in the extracellular milieu (Trigo et al., 2009b) using the exact same technique. It may be caused by oxidizing

byproducts of photolysis (nitrosoacetophenone; Kaplan and Ellis-Davies, 1988), but the exact mechanism of this phenomenon remains to be explored.

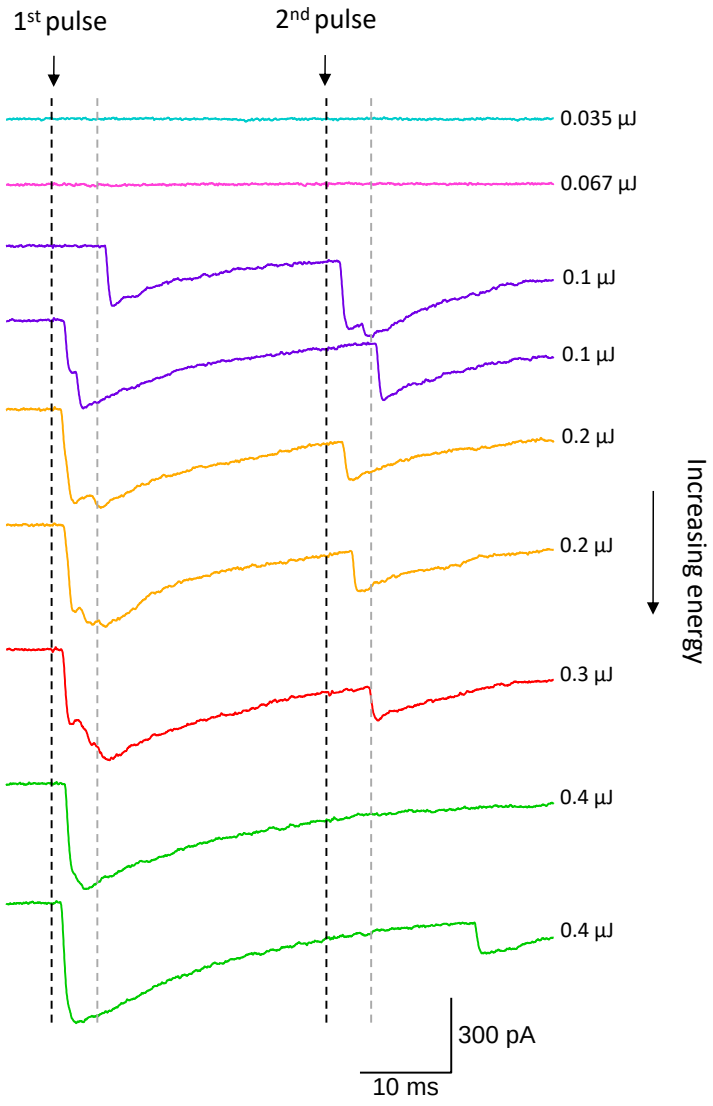

Figure 6-4. RRP release by Ca^{2+} uncaging from the cage compound DM-nitrophen (DMNP). The traces correspond to a group of PSCs evoked by the photorelease of Ca^{2+} at different laser energies. Laser timing is indicated by the black dashed lines. First and second pulses were separated by 30 ms; the grey dashed lines correspond to the end of the 5 ms interval after triggering the laser. Any postsynaptic event that has a first latency within this range was considered as part of the RRP. From the figure it is possible to observe that there was no second response for laser energies of 0.4 µJ (last 2 traces in green), thus we concluded that at this energy the RRP was fully released by the first laser pulse.

6.6 Calcium imaging

For Ca^{2+} imaging experiments, 200 µM of the high-affinity indicator (K_d=170 nM) Oregon Green BAPTA-1 (OGB-1) (Invitrogen) was added to the presynaptic IS (see composition above) to monitor changes of Ca^{2+} upon photolysis of DMNP. The axonal compartment of the recorded cell was identified by using Alexa 594 and the selected varicosity for uncaging was imaged after letting the dye diffuse for at least 10 min after break-in. A subregion of the CCD comprising sixteen 4 × 4 binned pixels, giving a resolution of 1 µm, was imaged in 2.11 ms exposure at 259.7 Hz. Fluorescence was corrected for background, determined in pixels at the periphery of the subregion. The traces shown in this work are averaged responses from individual varicosities in which averaging was done from at least 5 repetitions. The experiments were performed in the same experimental set-up as detailed for the uncaging work (see above). Imaging data was analyzed with IGOR Pro (Wavemetrics) using a routine written in the laboratory by Brandon M. Stell and Jorge Ramirez. The fluorescence signals are reported as $\Delta F/F_0$ corresponding to changes in background subtracted fluorescence with respect to the values before stimulation (ΔF: $F - F_0$), normalized to the pre-stimulus values (F_0). For the analysis of the kinetics of the axonal Ca^{2+} signal, exponential functions were fitted to the recovery phases of the responses.

6.7 Determination of the readily releasable pool at a single synaptic contacts

The onset kinetics of all the detected events was analyzed for a time window of 100 ms after the laser pulse and histograms of synaptic latency were constructed. Single exponential fit of the histograms were used to determine the event distribution and to set a criteria to estimate whether a fusion event belonged to the RRP. A time corresponding to 4 time constant (4τ =10 ms) in the histogram of all events (in the 100 ms time window), at which 98% of the events have occurred, was defined to associate an event with the laser pulse. Considering this limit, normal and cumulative histograms of the first latencies were constructed to determine the superior limit to associate a first event with the laser pulse. A time limit corresponding to t = 5 ms (at which almost 100 % of the first events have occurred) was defined as the superior limit to associate a first event with the laser pulse. Hence, in this work any event (or series of events) was considered as part of the RRP if it had latency values up to 10 ms and first latency values were below than or equal to 5 ms. Peak amplitude, synaptic charge (from 0-150 ms), rate of failures, first and all latencies and time to peak values were calculated for all the PSCs responses associated with the release of the RRP. These synaptic parameters were calculated for each of the individual and interleaved PSCs in control and test

conditions. The comparison between conditions was made considering the average values per experiment. The statistical results are given as mean ± SEM; n is the number of independent experiments.

As it was evidenced in Figure 6-4, the postsynaptic response to local presynaptic Ca^{2+} uncaging typically results in a multiphasic pattern of PSCs where several inflexions points can be detected in the curve. These inflexions represent the semi-asynchronous release of the NT from several synaptic vesicles in the presynaptic terminal, thus allowing a direct estimation of the number of vesicles composing the RRP. However, the precision in the counting of individual fusion events depends on the level of desynchronization achieved. Figure 6-5 shows examples of PSCs where the differences (in terms of the synchronicity of fusion events) between physiological (AP-evoked) and laser-evoked responses can be observed. The optimal situation for a precise estimation of the RRP by using laser stimulation is when a high level of desynchronization of fusion events is achieved; unfortunately, this was not commonly observed. Nevertheless, the typical postsynaptic response to laser stimulation, which generates a partial level of desynchronization of the fusion events, provides valuable information that can be used to extract the synaptic parameters controlling NT release (Figure 6-5b) and also to estimate the number and the dynamics of individual fusion events in the presynaptic terminal.

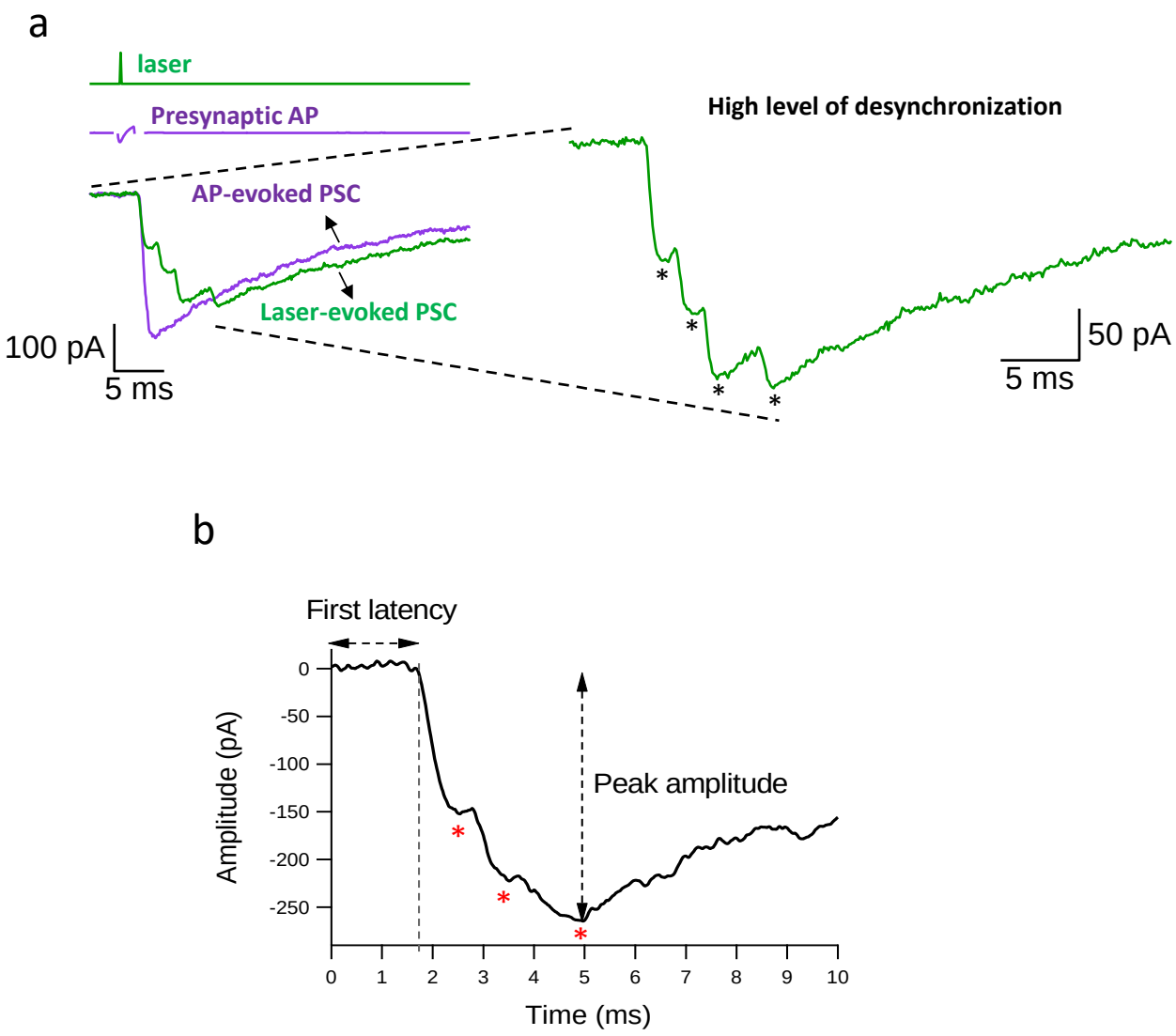

Figure 6-5. Comparison between the optimal situation where a high level of desynchronization of single fusion events is obtained vs. the typical postsynaptic response evoked by presynaptic Ca^{2+} uncaging at single synaptic contacts.

(a) The photolysis of DMNP triggers the asynchronous release of 4 vesicles (green traces). A magnified view is presented in the right panel. The black asterisks represent individual fusion events. An example of the physiological AP-evoked PSC (purple traces), where a high level of synchronization is observed, was included for reference. **(b)** Laser-evoked postsynaptic response where a semi-asynchronous release of several synaptic vesicles is observed. In this case a progressive decrease in the amplitude of individual peaks is evidenced and presumably reflects the saturation of postsynaptic receptors. In this case the asterisks represent single inflexions of the curve, not necessarily single fusion events.

6.8 Counting single fusion events and estimating docking site occupancy probability

The counting of individual fusion events was done in a first instance by detecting the number of inflexions in the PSC. Nevertheless, because typically the laser-evoked Ca^{2+} transients can only produce a partial desynchronization of the fusion process, this inspection is expected to fail in detecting some closely spaced fusion events; hence, this approach results in an underestimation of the number of vesicles in the RRP because it does not consider the differences observed in the amplitude of individual peaks. To overcome this limitation, we used the amplitude of single fusion events to correct our first estimation by adding quantal information. Single quantal responses are typically seen during the laser stimulation repetitions in any particular experiment either as a single and isolated event (for example at low laser energies, as in the first sweeps in Figure 6-4) or as the first inflexion that has the smallest size in the composed PSC. Figure 6-6 shows and example where the detected number of inflexions in the rising phase of the PSC does not account for the differences in the peak amplitude: there are some responses with the same number of inflexions but with obvious differences in the peak amplitude, for example, the first and last PSC (both present a single inflexion in the PSC,

however, the last response is several times larger than the first one, thus they hardly reflect the same number of fusion events).

We used both the number of inflexion and the quantal amplitude to estimate the number of fusion events for each laser-evoked PSC. This approach gives a better estimate of the number of released quanta in the time period where more synchronicity occurs, which usually corresponds to the first detected valley, and where the lower level of saturation takes place.

By using these criteria, we estimate the average value of the RRP (RRP_{avg}), the number of docking sites in the presynaptic terminals (NDS), which correspond to the maximal observed value for the RRP across repetitions (Trigo et al., 2012) and the docking site occupancy probability (δ). These parameters were calculated for each presynaptic terminal tested in this work, and according to the following equations.

1) $\mathrm{RRPavg} = \frac{\sum_1^n \mathrm{RRPn}}{n}$; where "n" corresponds to the number of sweeps per experiment.

2) $\delta = \frac{\mathrm{RRPavg}}{\mathrm{NDS}}$; where NDS corresponds to the number of docking sites.

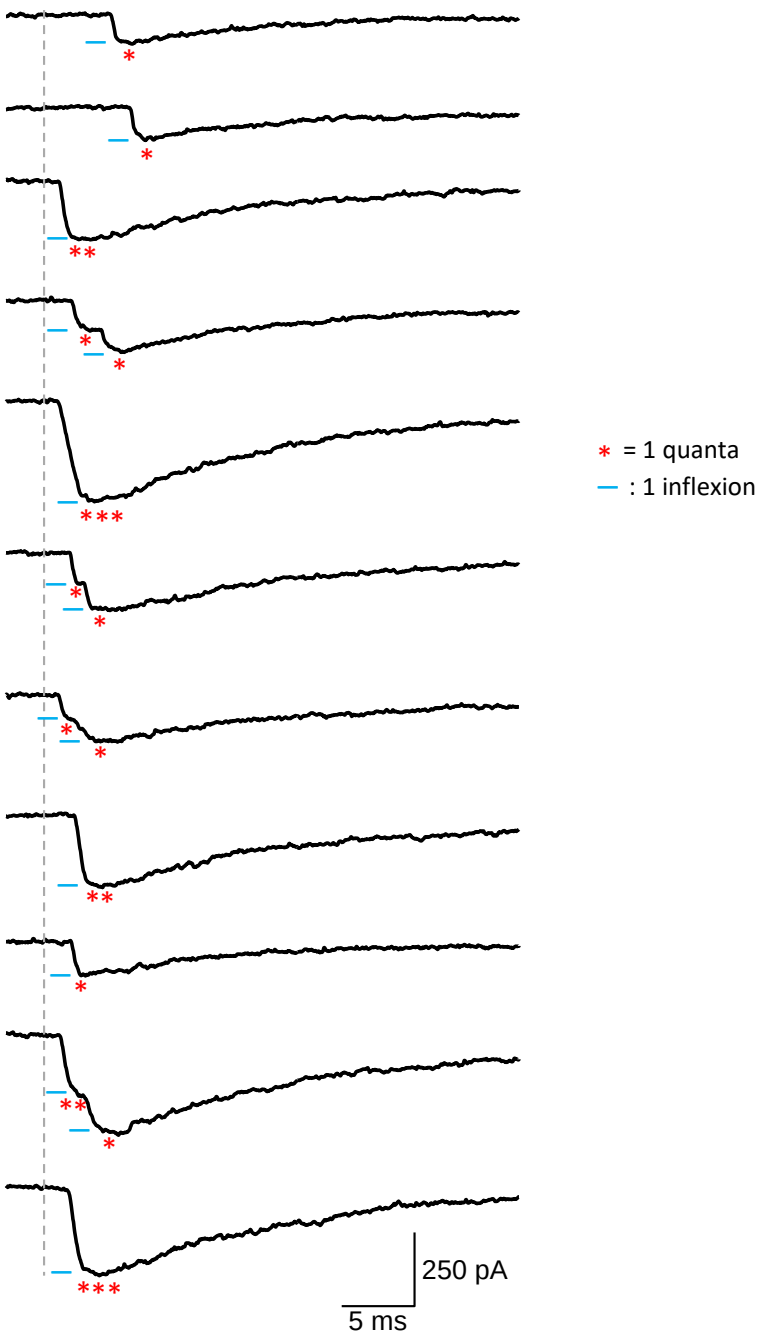

Figure 6-6. Quantal analysis and estimation of the RRP for each sweep.
The image describes the counting methodology used in this work, and corresponds to a selected group of traces (from a total number of 38 repetitions). The detected inflexions in the curve are denoted by the sky-blue lines. The number of estimated quantum is denoted by the red asterisk. It is possible to observe that traces with the same number of inflexions can have very different peak amplitudes, thus the number of inflexion is not a good indicator of the number of fused vesicles (compare first and last traces). Hence, we used both the number of inflexion and the quantal amplitude to estimate the number of vesicles in the RRP for each repetition.

6.9 Data Analysis

All the analysis in this work was made on IGOR Pro (Wavemetrics). The detection of postsynaptic events was made automatically by using Taro Tools (Taro Ishikawa) for IGOR Pro. To accurately measure the first synaptic latency of the laser-evoked events, the automatic detection was inspected by using cursors and corrected by using an amplitude threshold of 5 pA after the baseline adjustment of the trace. Synaptic charge was calculated for the next 150 ms after the laser was triggered. Statistical results are given as means ± SEM; n denotes the number of independent experiments, and p indicates the result of Student's T-Test for two dependent (paired) or two independent means, and the results from Pearson (R) correlation coefficient value; ns $p > 0.05$, * $p \leq 0.05$, ** $p \leq 0.01$, *** $p \leq 0.001$. Differences were considered significant at $p < 0.05$.

7 Results

7.1 Calcium photolysis and release of the readily releasable pool at single synaptic contacts

In the present work, we study the RRP of synaptic vesicles in single presynaptic terminals of rat cerebellar MLIs. This was accomplished by combining Ca^{2+} photolysis with electrophysiological whole-cell voltage-clamp paired recordings from synaptically connected MLIs, as described previously by Trigo et al., 2012.

A representative experiment is illustrated in Figure 7-1. We first established a paired recording from two MLIs and tested synaptic connectivity by inducing unclamped APs in the presynaptic neuron. Immediately after the connectivity test was successful (as ascertained by the presence of postsynaptic currents), TTX (0.2 µM) was included in the bath solution throughout the entire experiment in order to minimize contamination from AP-dependent NT release. Next, we localized putative individual synaptic contacts by alternating excitation of the fluorescent dyes Alexa 594 and Alexa 488 (both at 80 µM) present in the pre and postsynaptic cells, respectively. This allowed us distinguish between the presynaptic axon and the postsynaptic somatodendritic compartment. The identification of an individual synaptic contact was made by producing a high, ultrafast, uniform and spatially constrained Ca^{2+} transient in single presynaptic varicosities through laser induced

photo-release from the caged-Ca^{2+} chelator DM-nitrophen (Kaplan and Ellis-Davies, 1988), included in the presynaptic IS. In order to target single synapses, we constrained the laser spot by adjusting its diameter to a size around 5 µm, which is slightly bigger than presynaptic terminals (Trigo et al., 2009). A schematic representation of the experimental approach is illustrated in Figure 7-1a (see Methods for further details).

After the identification of a single synaptic contact, the intensity of the laser stimulation was adjusted to the minimal value required to induce the fusion of the entire pool of vesicles available for immediate release, the RRP (Regehr, 2012), most likely corresponding to the pool of vesicles in the docked state (Trigo et al., 2012). The emptying of the RRP was confirmed by the lack of response to a second pulse of the same energy that was applied 30 ms later (see Figure 6-4 in Methods, for further details).

The features of the AP-and laser-evoked PSCs from a representative experiment are illustrated in Figure 7-1b. Unlike the canonical spike-induced PSCs, which typically correspond to the release of GABA from several synaptic contacts (Figure 7-1b, gray traces), the laser-evoked PSCs (Figure 7-1b, blue traces) show a "burst-like" multiphasic pattern that represents the multivesicular and semi-

asynchronous release of the RRP from a single synaptic contact, thus allowing quantal analysis of the RRP by estimating the number of individual vesicle fusion events (red asterisks in the example of Figure 7-1; see histogram of Figure 7-1c). See Methods for further details regarding the counting of released vesicles.

When comparing the properties of the AP- and the laser-evoked PSCs, a slight but significant tendency to obtain larger mean values for the peak amplitude of the laser-evoked PSCs was observed (peak amplitude ratio (laser/AP)=1.59 ± 0.29, p=0.0327; n=16). Furthermore, the variability of the peak amplitude, quantified as the coefficient of variation (CV), was significantly lower for the laser-evoked responses, which is typical for synaptic responses arising from a single synaptic contact (Auger and Marty, 2000; Trigo et al., 2012), (for the same data set, CV:0.42 ± 0.04 vs. 0.24 ± 0.02, p=0.0006, for AP and laser-evoked PSCs, respectively; see Figure 7-1b-upper histogram for the representative experiment).

When comparing the latencies of the postsynaptic events, an increase in both the mean value and the CV was observed in the laser-evoked responses (see Figure 7-1b, bottom histogram). This can be interpreted in two ways: late events may correspond to some vesicles of the RRP that were not released by the Ca^{2+} levels reached after the arrival of an AP or they may correspond to replenishment of the

docking sites from which release occurred (latency: 1.65 ± 0.14 ms vs. 2.56 ± 0.21 ms, p=0.0008; ratio (laser/AP)=1.69 ± 0.16, p=0.0002; and CV: 0.28 ± 0.04 vs. 0.57 ± 0.04, p=0.000004, for AP and laser-evoked PSCs, respectively). The latency and peak amplitude values for the AP-evoked and the laser-evoked PSCs analyzed in this work are presented in Table 1 (which can be found on the appendix).

For a given presynaptic terminal and across all the synapses tested here, the number of vesicles in the RRP varied from sweep to sweep but exhibited a fixed maximal value, which we interpreted as the number of docking sites in a particular presynaptic active zone (Trigo et al., 2012). For example, the synaptic terminal analyzed in Figure 7-1 has 4 docking sites and displays RRP values ranging from 2 to 4 vesicles, with a modal value of 3 (see histogram of Figure 7-1c). A schematic representation of this presynaptic terminal is illustrated in Figure 7-1e.

Because MLI-MLI synapses display postsynaptic receptor saturation following multivesicular release (Kondo and Marty, 1998; Auger et al., 1998; Pulido et al., 2015), the relation between GABA release and the PSC can be complex. As illustrated in Figure 7-1d, the laser-evoked PSC exhibits sublinear amplitude summation when PSC peak amplitudes are plotted against the number of vesicles in the RRP. For the representative experiment of Figure 7-1, the release of two or

three vesicles, corresponding to 50% and 75% of the maximal value of the RRP that was observed (and which reflects the number of docking sites), generates a receptor occupancy level of 70% and 94%, respectively. These results suggest that postsynaptic receptor saturation should be taken into consideration when using maximal amplitudes of PSCs as a reliable indicator of the RRP size in terms of number of vesicles.

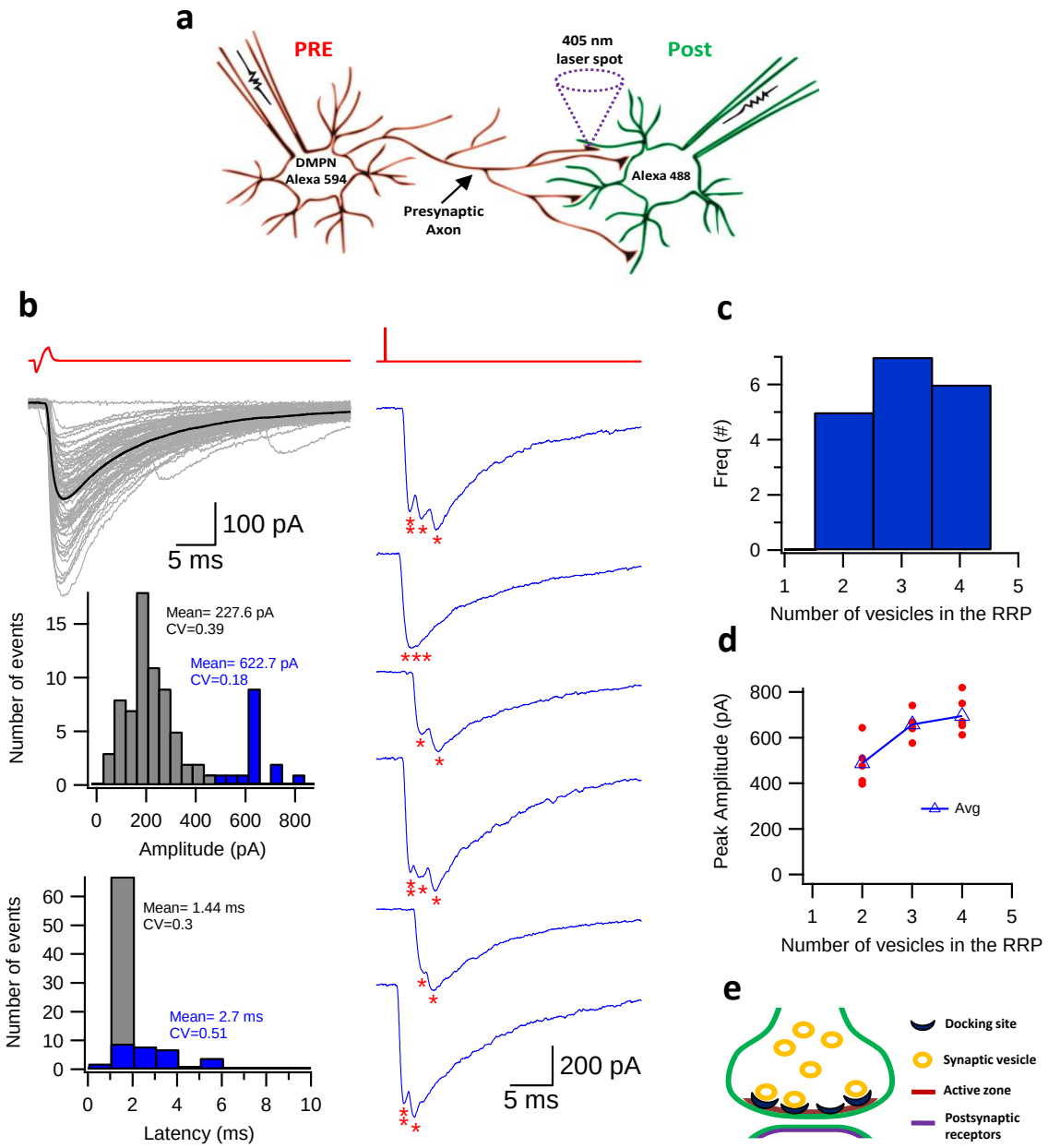

Figure 7-1. Direct control of GABA release at single synaptic contacts by photo-release of caged Ca^{2+}. **(a)** Schematic representation of the experimental approach. The pre- and postsynaptic cells were loaded with the fluorescent dyes Alexa 594 and Alexa 488, respectively, to allow neuron identification and discrimination between pre- and postsynaptic neurites. The presynaptic cell also contains the photosensitive Ca^{2+} cage DMNP. Presynaptic Ca^{2+} uncaging was achieved by delivering a brief (100-200 µs) and spatially confined laser pulse (~5 µm of diameter; 405 nm λ) in one of several synaptic contacts. **(b)** AP- (gray, left) and laser-evoked (blue, right) PSCs. Laser-evoked single fusion events are indicated by the red asterisks. PSC peak amplitude and latency histograms are shown for both stimuli. **(c)** Histogram of the number of vesicles in the RRP. **(d)** Relationship between number of vesicles in the RRP and PSC peak amplitude. **(e)** Schematic representation of the presynaptic terminal. The synaptic vesicles bind to the docking sites (black) previous to the exocytosis. The RRP is represented by the number of docked vesicles, which varies from trial to trial. Postsynaptic receptors are represented in purple.

In order to accurately categorize a fusion event as belonging to the RRP, and to set a criteria for a precise and reliable estimation of this important parameter, we determined the onset kinetics of all the detected events in a time window of 100 ms after the laser pulse (t=0 ms) for a total number of 31 individual synapses. Figure 7-2 shows the latency histograms at low (upper) and high (bottom) time resolutions both for all latencies (left) and for the first event latencies (first latencies, right). From the exponential fit of the histogram of all latencies in Figure 7-2a (upper panel, left), it is expected that for a $t=4\tau = 4*(2.5)$ ms=10 ms, 98% of the events had already occurred. For this work we have hence considered as belonging to the RRP all the laser-evoked events in a time window between the laser pulse (t=0 ms) and 10 ms (Figure 7-2a, bottom). Additionally, from the first latencies histograms it is possible to observe that for this time window (0-10 ms), almost the totality of the events occur within the first 5 ms (Figure 7-2b, bottom), hence, we have considered only belonging to the laser-evoked RRP the events having latencies in a time window from 0 to 10 ms and with first latency values below than or equal to 5 ms. All together the results presented in this section show our ability to release and measure the RRP at the single synaptic level.

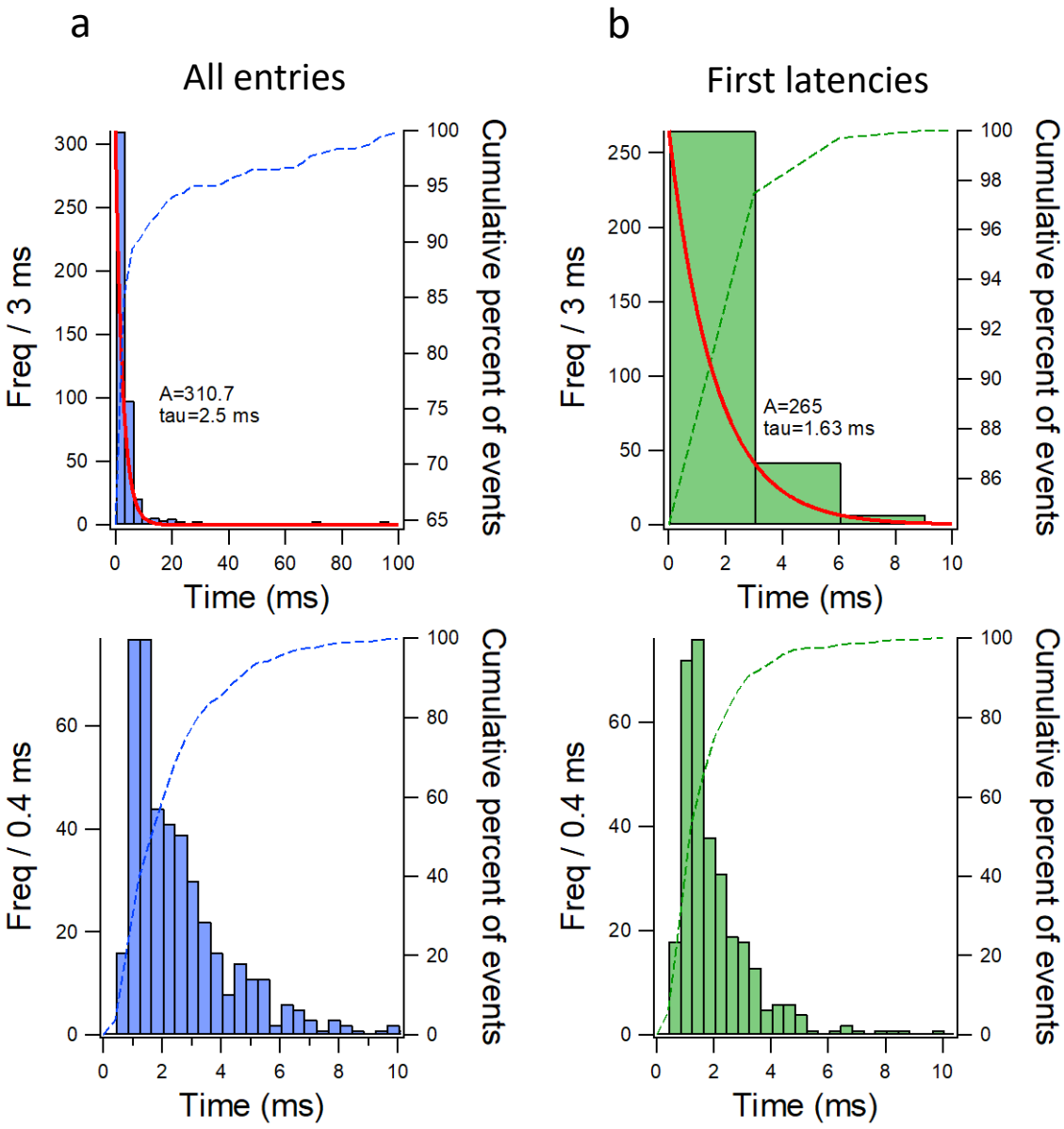

Figure 7-2. Latency histograms of the laser-evoked PSCs.
Histograms of PSC latencies for 31 synaptic contacts displayed at intermediate (Top; 3-ms bins; Freq, frequency) and high (bottom; 0.4-ms bins) time resolutions, for **(a)** all entries, and **(b)** first events. The triggering time of the laser pulse correspond to t=0 ms. The laser energy range was: 0.1–0.4 μJ. The intervals were fitted with a single exponential function (red curves superimposed on the histograms; upper panels) with decay constants of 2.5 ms and 1.63 ms, corresponding to all and first latencies, respectively. The cumulative percent of events is superimposed on each bar histogram (dashed curves).

7.2 Subthreshold calcium rises modulates the readily releasable pool size and its kinetics at single synaptic contacts

As mentioned in the introduction, the phenomena called analog-to-digital facilitation (ADF), by which the application of a subthreshold depolarization in the soma of MLIs produces an increase in the amount of GABA released per AP, has been previously described by different laboratories (Bouhours et al., 2011; J.M Christie et al., 2011; Rowan and Christie, 2017). However, the underlying mechanism of this type of synaptic plasticity is poorly understood and highly controversial.

It has been proposed that this type of facilitation is mediated by a signaling pathway involving a depolarization evoked subthreshold Ca^{2+} influx through voltage-dependent calcium channels (VDCC) followed by Protein kinase C (PKC) activation (Bouhours et al., 2011). Nevertheless, a recent work has shown that a subthreshold somatic depolarization can rapidly inactivate the Kv_3 channels in the presynaptic terminals, resulting in AP broadening and enhanced spike-evoked Ca^{2+} influx that does not depend on subthreshold Ca^{2+} rises or PKC activation (Rowan and Christie, 2017), but it depends on the inactivation of a K^+ conductance.

In the present work we took advantage of the methodology described so far, where one can effectively control and measure vesicle release without the complexity

introduced by the coupling between the somatic and the axonal compartments. We tested the hypothesis that the subthreshold Ca^{2+} increases (like the ones that are reached during ADF in MLIs) can effectively modulate GABA release by a mechanism that involves an increase in the occupancy probability of docking sites in single active zones, which translates directly into an increase in the RRP size.

In order to test this idea, we performed Ca^{2+} uncaging experiments in single synapses, where a direct and reliable control of both sub- and suprathreshold Ca^{2+} levels can be produced (see methods for further details). In the first set of experiments, we applied two different and interleaved laser stimulation protocols. The control protocol consisted of a single suprathreshold laser pulse that released the RRP; the test protocol consisted of the same suprathreshold pulse preceded by a low intensity train of 5 subthreshold laser pulses at 10 Hz (200 ms delay) that generates an increase in the basal Ca^{2+} level (see later section 7.4: Ca^{2+} imaging at single synaptic contacts). For each experiment, the subthreshold laser energy was set to reach the maximal intensity that does not produce a postsynaptic response, while for the suprathreshold RRP-releasing laser pulse the energy was set to reach the minimal value that does not produce a postsynaptic response when a second pulse of the same energy was applied 30 ms later (see Methods for further details).

Figure 7-3 shows the experimental approach where the laser protocols and the PSCs are illustrated in black and red, for control and test conditions, respectively. A clear alignment between the PSCs and the laser onset is observed (Figure 7-3a). Additionally, it is possible to observe that the frequency of miniature GABAergic events before and after the suprathreshold laser pulse was relatively low (see Figure 7-3a, and the summary histograms of events for 21 individual synaptic contacts in the panels of Figure 7-3b).

The subthreshold laser energies were set to avoid the trigger of the vesicle fusion process, nevertheless there is a possibility that the elevations of Ca^{2+} levels during the application of the train can increase the probability of neurotransmitter release, enhancing the frequency of miniature GABAergic events and modifying in consequence the number of available docked vesicles in the RRP previous to its experimental interrogation by the suprathreshold pulse. The results presented in the histograms (middle and bottom) of Figure 7-3b show that there was no significant change in the frequency of GABAergic miniature events between control and test conditions during the time window between the start of the train and the start of the suprathreshold pulse (-600 to 0 ms). This confirms our ability to control the Ca^{2+} dependent triggering of the vesicle fusion process.

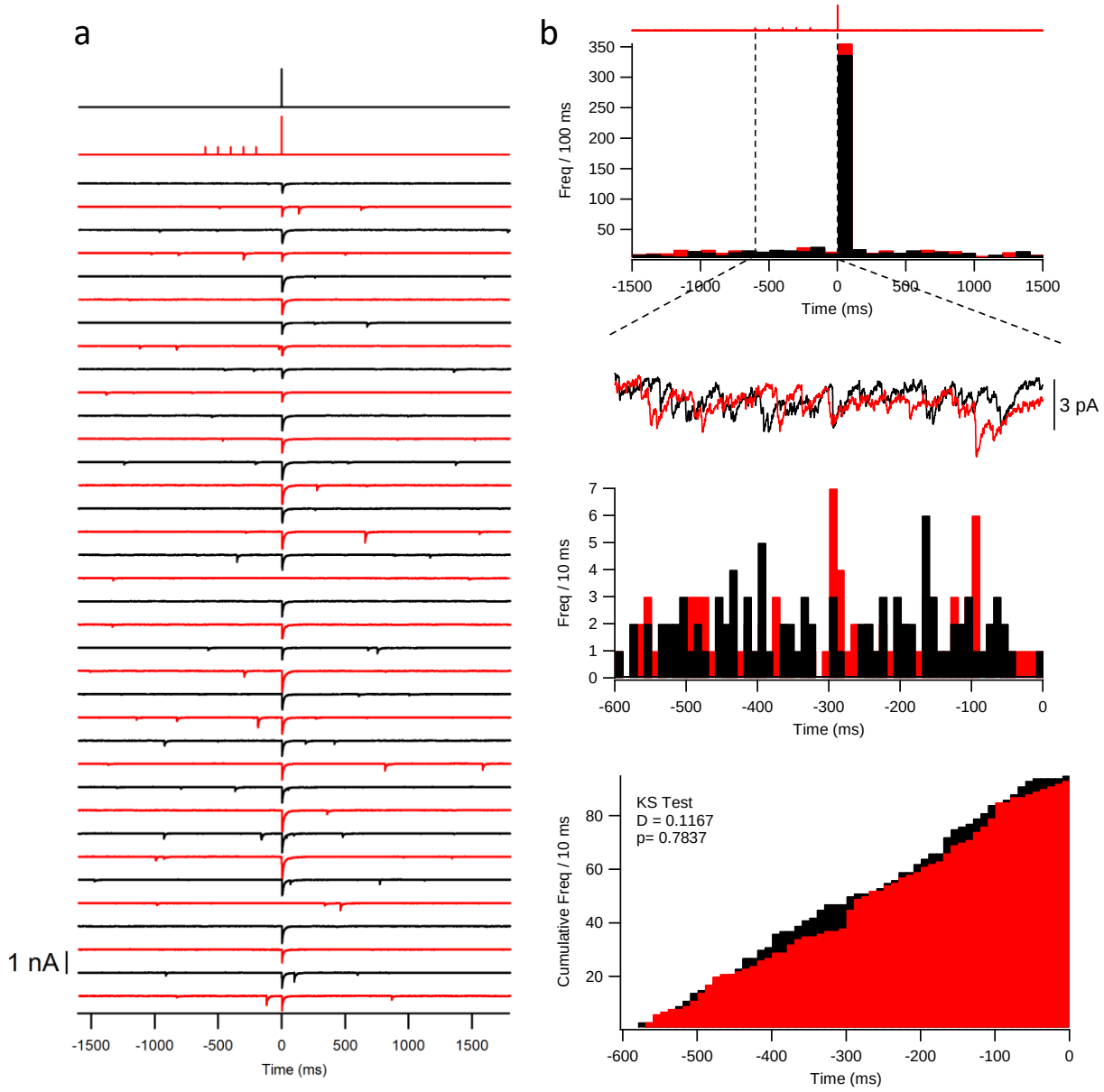

Figure 7-3. Experimental approach to evaluate the effect of subthreshold Ca^{2+} transients on asynchronous and evoked synaptic transmission at single synaptic contacts.
(a) Representative experiment illustrating the experimental approach. The control protocol consisted of a single suprathreshold laser pulse that releases the RRP; the test protocol consisted of the same suprathreshold pulse preceded by a low intensity train of five subthreshold laser pulses at 1 Hz (200 ms delay); TTX (0.2 µM) was included in the bath solution to avoid contamination from AP-dependent release. A low frequency of miniature events and a clear alignment of PSCs with the laser were observed. **(b)** Histograms of laser-evoked PSCs at low (Top; 100 ms bins; Freq, frequency) and intermediate (middle and bottom; 10ms bins) time resolution for the time window comprehended between the start of the subthreshold train and the start of the suprathreshold laser pulse (-600 ms to 0 ms; n=21). Middle panel also shows the averaged PSC traces for control (black) and test (red). The cumulative distribution of asynchronous (miniature) events is presented in the bottom panel; KS test, Kolmogorov-Smirnov test**.**

In order to obtain a precise and reliable measurement of the amount of GABA released in control and test conditions (and considering the presence of postsynaptic $GABA_A$ receptor saturation in the laser-evoked postsynaptic response), we decided to measure the following synaptic parameters of the PSC to have a better idea of the timing and amount of NT released by the suprathreshold laser pulse; peak amplitude, synaptic charge, rate of failures, first and all latencies (in the burst of multivesicular release) and time to peak. The results are presented in Table 2 and Table 3 and illustrated in Figure 7-4 and Figure 7-5.

The results show that when the relation between control and test condition for individual experiments is considered, a small but significant increase in both peak amplitude and synaptic charge (including failures) arises. This indicates that the amount of GABA released after applying the conditioning protocol is significantly larger than the interleaved control amplitudes without the train (peak amplitude ratio (test/control)=1.11 ± 0.04, p=0.0088; synaptic charge ratio (test/control)=1.18 ± 0.06, p=0.0061, Figure 7-4a and Figure 7-4c, respectively). Additionally, we evaluated whether the effect of subthreshold Ca^{2+} rises can modify the dispersion of these parameters in single synapses. To do this we calculated the CV of the peak amplitude and synaptic charge for each condition in single experiments. The results show a significant decrease in the CV for synaptic charge but not for peak

amplitude (see Table 2), indicating that the application of the conditioning protocol can also modify the degree of variation in the amount of GABA released (which accounts for the total charge crossing the postsynaptic membrane) (peak amplitude CV: 0.58 ± 0.06 vs. 0.51 ± 0.06, p=0.0576; synaptic charge CV: 0.65 ± 0.06 vs. 0.57 ± 0.06, p=0.0495 for control and test conditions, respectively).

The fact that the effect on synaptic charge was larger than the effect on peak amplitude (ratio test/control= 1.11 ± 0.04 vs. 1.18 ± 0.06, for peak amplitude and synaptic charge, respectively) is in agreement with what is expected if we consider that the integral of the curve (charge=current * time) is much more informative than the peak amplitude of PSCs, especially for synapses displaying postsynaptic receptor saturation. Thus, the synaptic charge is a better indicator of the amount of neurotransmitter that is released in a particular condition, as had been already shown by Pulido et al., 2015. The results shown so far for both peak amplitude and synaptic charge show that the amount of neurotransmitter released after applying the conditioning protocol is larger than that obtained in control conditions, thus indicating that subthreshold Ca^{2+} rises can increase the number of docked vesicles that constitute the RRP in single presynaptic terminals.

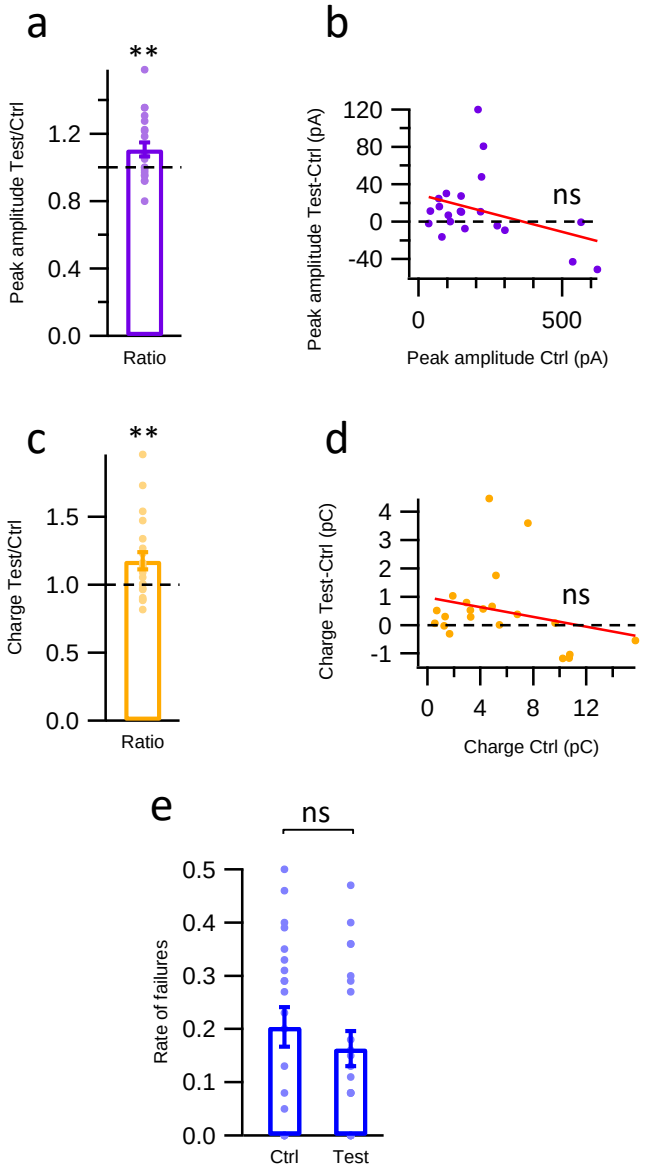

Figure 7-4. Peak amplitude, synaptic charge and rate of failures for control and test conditions.
(a) Amplitude ratio between test and control conditions. **(b)** Difference between test and control peak amplitudes as a function of the initial peak amplitude in control. **(c)** Charge ratio between test and control conditions. **(d)** Difference between test and control current charges as a function of the initial charge in control. **(e)** Summary data for the rate of failures in both conditions. Mean values ± SEM, one tail T-Test for two dependent means, and Pearson correlation coefficient P value; ns $P > 0.05$, * $P \leq 0.05$, ** $P \leq 0.01$, *** $P \leq 0.001$. n=21.

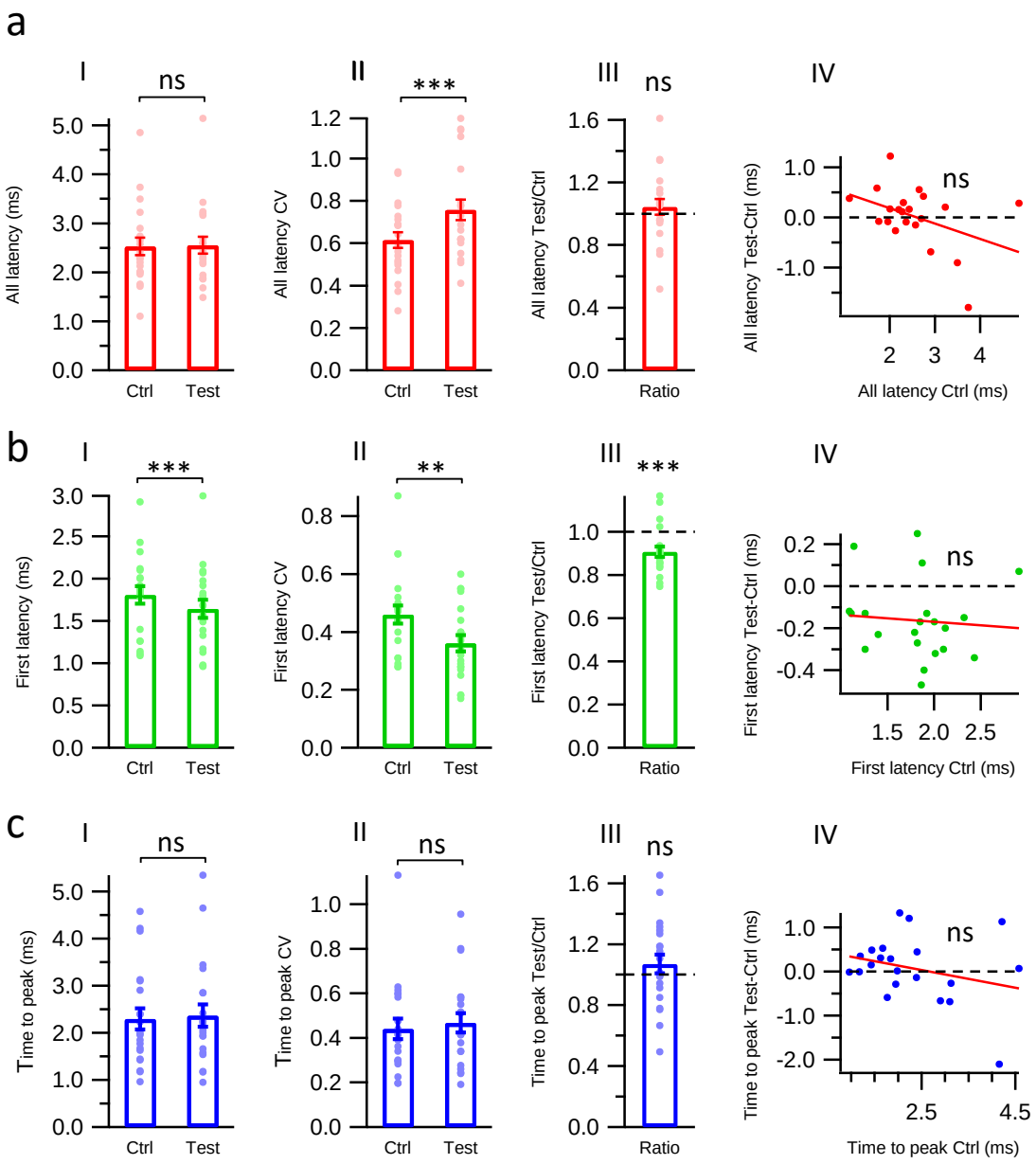

Figure 7-5. All latencies, first latencies and time to peak for control and test conditions. Summary data for mean values, coefficient of variation, ratio (test/control) and relationship between the "strength" of the effect and the initial value in control condition (I, II, III and IV, respectively) for **(a)** all latencies, **(b)** first latency, and **(c)** time to peak. Mean values ± SEM, one tail T-Test for two dependent means, and Pearson correlation coefficient P value; ns $P > 0.05$, * $P \leq 0.05$, ** $P \leq 0.01$, *** $P \leq 0.001$. n= 21.

Interestingly, when looking for possible differences between individual synapses, the results for peak amplitude and synaptic charge might suggest a negative correlation between the "strength" of the effect and the initial value in control the condition (p values from Pearson (R) calculator: p=0.3799 and p=0.1803, for peak amplitude and synaptic charge, respectively; see Figure 7-4b and Figure 7-4c, respectively). This would indicate that the synapses displaying larger postsynaptic currents tend to be less sensitive to the facilitating effect generated by increasing the subthreshold Ca^{2+} levels in the presynaptic compartment. Even more, for synapses displaying larger peak amplitude and synaptic charge values, the application of the conditioning train tends to produce the opposite effect, decreasing the amount of GABA released in test condition, and hence producing a depression of the synaptic response. These results might suggest a possible correlation between the localization and/or the size of the synapse (of which the features of PSCs depend) and the strength of the facilitating effect. Furthermore, may be possible that the type of synaptic plasticity obtained by the elevation of subthreshold Ca^{2+} levels (facilitation/depression) also depends on these parameters.

Next and regarding the analysis of the rate of failures in both conditions, if the hypothesis proposed in this work is correct, one would expect to obtain a lower number of failures in test condition as a direct consequence of an increased

docking site occupancy probability, which will translate directly into an enhanced number of vesicles composing the RRP.

First, the results show a considerable number of failures in both conditions (See Table 2). This indicates that, under our experimental conditions, the presynaptic terminal goes through phases where there are no docked vesicles in the active zone to be released (meaning RRP=0). Our results further suggest that the failures that are often observed when the system is interrogated by using other methods, like electrophysiological paired recordings, can be a consequence of a combination of factors, like the presence of empty docking sites and failures in reaching the suprathreshold Ca^{2+} levels required for triggering the fusion of a docked vesicle, like for example as a consequence of AP propagation failures.

Concerning the differences in the rate of failures in control and test conditions, the results show a not significant decrease ($p=0.0654$) in the number of failures after applying the conditioning train (control failure rate: 0.20 ± 0.04 vs. 0.16 ± 0.03, for control and test conditions, respectively, see Figure 7-4e). This result suggests that the increased levels of subthreshold Ca^{2+} obtained by the application of the conditioning train of subthreshold laser pulses do not modify the average rate of failures between control and test conditions.

Next and regarding the possible differences in the release kinetics of the RRP, the results showed no significant difference in the averaged latency of all the events in the burst of multivesicular release after the application of the conditioning train (synaptic latency: 2.53 ± 0.18 ms vs. 2.55 ± 0.17 ms, p=0.4298 for control and test condition, respectively; ratio (test/control)=1.04 ± 0.05, p=0.1997; Figure 7-5a-I and Figure 5a-III). This result suggests that the conditioning treatment does not modify the average kinetics of the pool of fusion events that account for the RRP. Nevertheless, a significant increase in the CV was observed in the test condition Figure 7-5a-II), probably as a consequence of the enhanced number of vesicles that account for the effect in the peak amplitude and synaptic charge, which possibly introduce a source of variability in the timing of fusion events, increasing in that way the heterogeneity of synaptic latencies (CV: 0.61 ± 0.04ms vs. 0.76 ± 0.05, p=0.0072, for control and test condition, respectively; n=21).

Although the averaged latency of all the events in the multivesicular burst of RRP release did not change with the conditioning treatment, a significant decrease in both the average latency and CV was observed for the first events in the burst of multivesicular release (synaptic latency: 1.81 ± 0.10 ms vs. 1.64 ± 0.11 ms, p=0.0003; ratio (test/control)=0.91 ± 0.02, p=0.0005; CV: 0.46 ± 0.03 vs. 0.36 ± 0.03, p=0.0027, for control and test condition, respectively; Figure 7-5b, panels I,

II and III). These results suggest that presynaptic subthreshold Ca^{2+} rises can modulate the temporal precision of GABA at the time it is first detected by $GABA_A$ receptor in the postsynaptic compartment, by speeding-up GABA release and decreasing the CV of first latencies.

Considering that the results so far show an increase in the number of vesicles in the RRP and a decrease in the first latencies of PSCs as a consequence of subthreshold Ca^{2+} rises, we next evaluated whether this increment in the number of docked vesicles can modify the timing at which the peak amplitude is reached with respect to the first latency, because a larger number of vesicles being released in a semi-asynchronous manner should in theory take longer to reach the maximal concentration of GABA that is detected by the postsynaptic receptors. For this purpose, we measured the time to peak for each experiment by making the subtraction between the time at which peak amplitude was reached (peak time) and the first latency. The results of Table 3 and Figure 7-5c showed no significant difference between control and test condition (time to peak: 2.29 ± 0.23 vs. 2.37 ± 0.24, p=0.3309; ratio (test/control) =1.07 ± 0.06, p=0.1380; CV:0.44 ± 0.05 vs. 0.47 ± 0.04, p=0.2998, for control and test condition, respectively; Figure 7-5c, panels I, II and III).This suggests that while there is a larger amount of GABA being released in test condition, the release seems to occur in a more synchronized

way, probably as a consequence of an increment in the probability of a docked vesicle to undergo exocytosis (as can be suggested by the decrease in the first latency), thus the time at which the peak of synaptic current is reached does not change.

Additionally, and for all of these temporal parameters the results show no significant correlation between the strength of the effect and the values obtained in control condition (Fig.5 a-IV, b-IV, c-IV; p value from Pearson (R) calculator: p=0.0649, p=0.7173, and p=0.2189, for all latencies, first latencies and time to peak, respectively).

7.3 Time dependency of the effects of subthreshold calcium rises on synaptic transmission

Considering that the previously described effect of SSD on synaptic transmission has been categorized as a facilitation type of synaptic plasticity (lasting for dozens to hundreds of ms), we decided to explore the time dependence of the effect of subthreshold Ca^{2+} rises on the synaptic parameters that we have described so far. In order to do this, we increased the delay between the end of the subthreshold train and the RRP-releasing suprathreshold pulse from 200 ms to 2 s. The results obtained for this second pool of experiments are presented in Tables 4 and 5, and illustrated in Figure 7-6, Figure 7-7 and Figure 7-8.

The results show that when the suprathreshold laser pulse was applied a long time (2 s) after the end of the subthreshold train, there was no change in the amount of GABA released (measured using peak amplitude and synaptic charge values) and in the failure rate (peak amplitude ratio (test/control)=0.93 ± 0.04, p=0.0684; synaptic charge ratio (test/control)=0.95 ± 0.05, p=0.1599; rate of failures: 0.14 ± 0.05 vs. 0.20 ± 0.06, p=0.1249; n=9; see Table 4 and Figure 7-6). Nevertheless, the observed tendency towards a depressing effect of the conditioning train applied 2 s before the suprathreshold laser pulse is probably due to an enhanced frequency of miniature events prior to RRP interrogation with the suprathreshold laser pulse. To

test this idea, we next measured the frequency of GABAergic miniature events between control and test conditions during the time window comprehended from the start of the train of subthreshold laser pulses and the start of the suprathreshold RRP-releasing laser pulse (-2400 to 0 ms). The results (Figure 7-7) show that there was a significant increase in the frequency of miniature events after applying the conditioning train, thus confirming the partial emptying of the RRP previous to its experimental interrogation (see the cumulative histogram of Figure 7-7c).

Additionally, there was no significant change for all the resting parameters evaluated in the previous set of experiments (peak amplitude CV: 0.46 ± 0.08 vs. 0.58 ± 0.10, p=0.1000; synaptic charge CV: 0.59 ± 0.08 vs. 0.68 ± 0.10, p=0.0991; all latency: 2.33 ± 0.21 vs. 2.35 ± 0.19, p=0.4442; all latency ratio (test/control)=1.03 ± 0.07, p=0.3232; all latency CV: 0.50 ± 0.06 vs. 0.53 ± 0.05, p=0.3028; first latency: 1.82 ± 0.17 ms vs. 1.74 ± 0.16 ms, p=0.2108; first latency ratio (test/control)=0.97 ± 0.05, p=0.2673; first latency CV: 0.39 ± 0.04 vs. 0.38 ± 0.05, p=0.3557; time to peak: 1.82 ± 0.25 ms vs. 1.94 ± 0.19 ms, p=0.2585; time to peak CV: 0.50 ± 0.06 vs. 0.47 ± 0.06, p=0.3654; time to peak ratio (test/control)=1.13 ± 0.07, p=0.0567, for control and test condition, respectively). Nevertheless, there was a negative correlation between the strength of the effect and the control value for this new set of experiments, and interestingly the

correlation is significant for both the peak amplitude and synaptic charge analysis, suggesting that the strength of the effect (depression for this case) might depends on the location/or the size of the synapse (p value from Pearson (R) calculator: p=0.0321 and p=0.0346, for peak amplitude and synaptic charge, Figure 7-6b and Figure 7-6d, respectively).

These results additionally suggest that the mechanism(s) that account for the effect in the kinetic parameters that were observed in the previous set of experiments are vesicle-dependent, acting in a relatively short time scale and not lasting beyond the release of the "newly" docked vesicle(s). So once the vesicle(s) is released, the effect on the first latency is gone. All these results suggest that the facilitating effect of subthreshold Ca^{2+} rises on synaptic transmission acts in the same time scale that the previously reported subthreshold somatic depolarization-induced facilitation, in the milliseconds range. Our results further suggest that the net effect on synaptic transmission (facilitation/depression) will depend on both the time at which the RRP is interrogated and the size or location of the synapse with respect to the postsynaptic neuron.

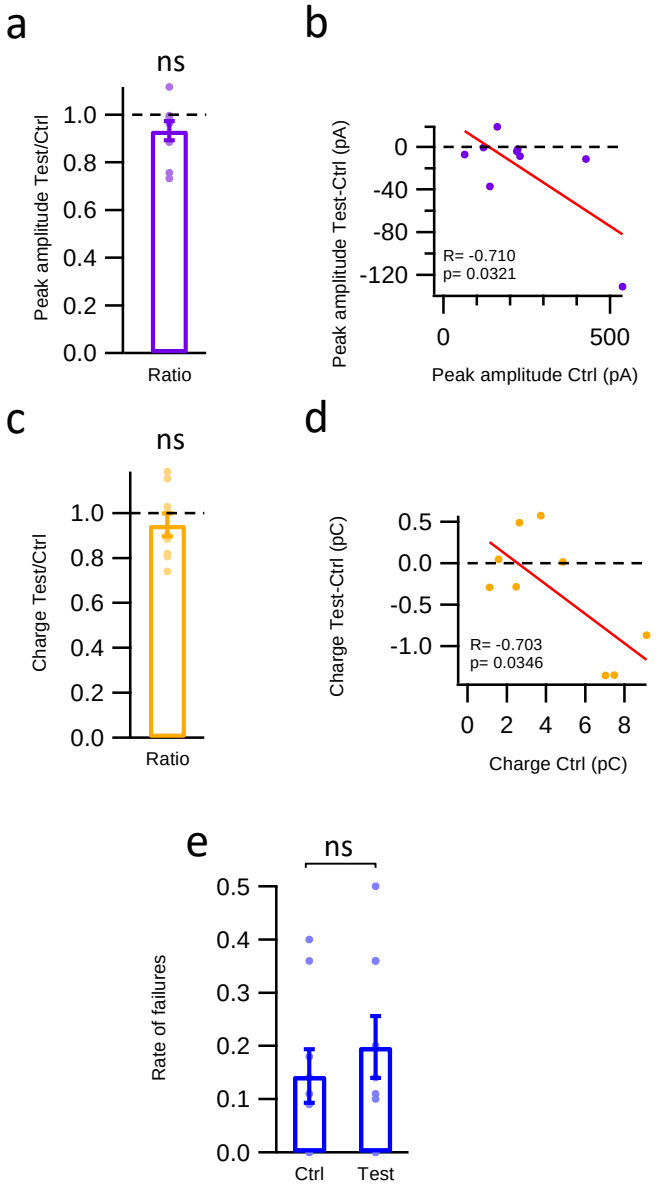

Figure 7-6. Peak amplitude, synaptic charge and rate of failure for control and test conditions for 2 second delay.
Summary data for ratios (test/control) and the relationship between the strength of the effect and the initial value in control condition: **(a)** and **(b)** peak amplitude; **(c)** and **(d)** synaptic charge**. (e)** Summary data for the rate of failures in both conditions. Mean values ± SEM, one tail T-Test for two dependent means and Pearson correlation coefficient P value; ns $P > 0.05$, * $P \leq 0.05$, ** $P \leq 0.01$, *** $P \leq 0.001$. n=9.

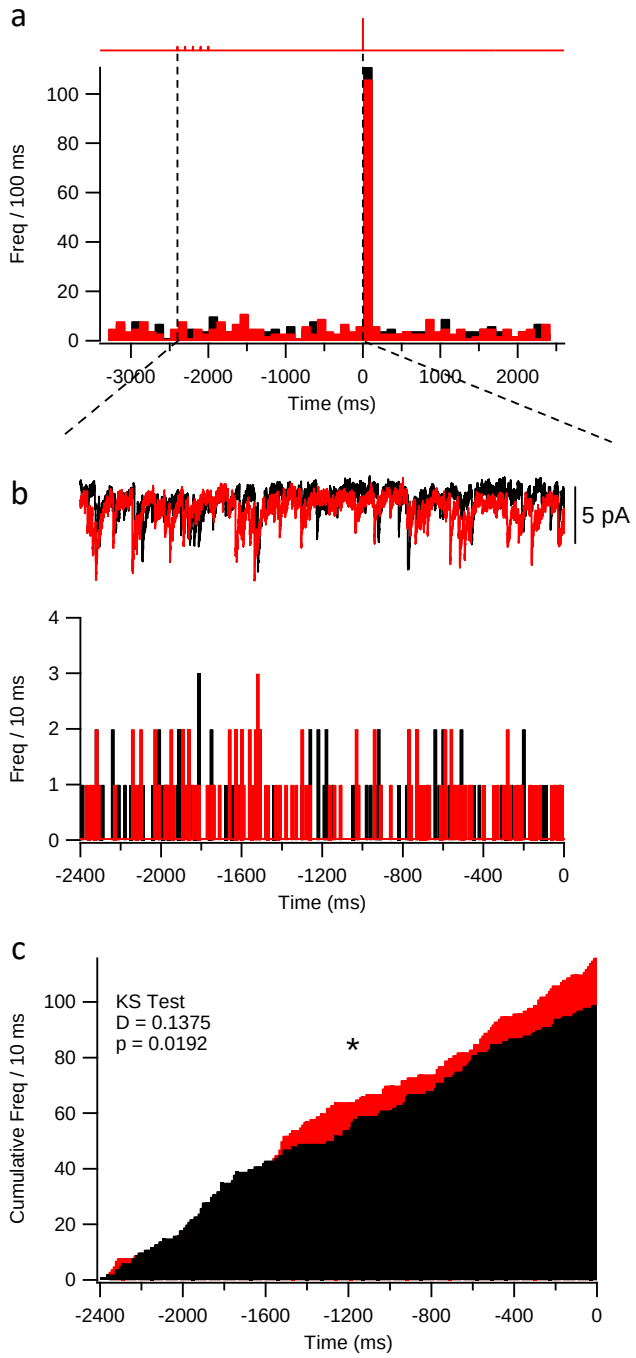

Figure 7-7. Comparison of miniature GABAergic event frequency between control and test conditions for the 2 second delay.

(a) Histogram of miniature laser-evoked PSCs at low time resolution (100 ms bins; Freq, frequency). **(b)** Averaged PSC traces for control (black) and test (red) condition (upper; n=9) and histogram of miniature laser-evoked PSCs at intermediate (10 ms bins) time resolution for the time window comprehended between the start of the subthreshold train and the star of the suprathreshold laser pulse (-2400 to 0 ms; bottom). **(c)** Cumulative histograms of the events in the same time window. KS test, Kolmogorov-Smirnov test. P value; ns $P > 0.05$, * $P \leq 0.05$, ** $P \leq 0.01$, *** $P \leq 0.001$. n=9.

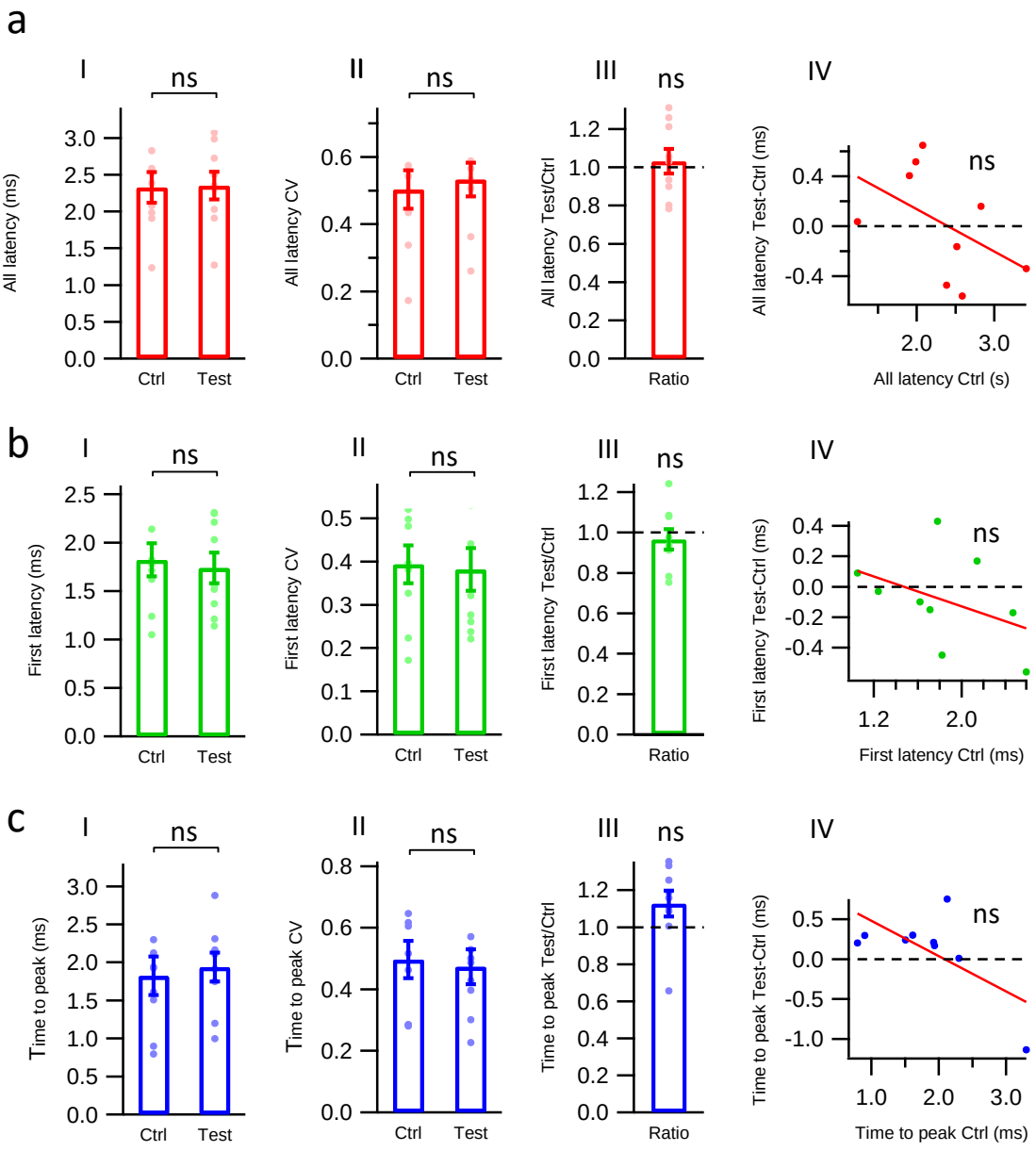

Figure 7-8. All latencies, first latencies and time to peak for control and test conditions for 2 second delay.

Summary data for mean values, coefficient of variation, ratio (test/control) and relationship between the strength of the effect and the initial value in control condition (I, II, III and IV, respectively) for **(a)** all latencies, **(b)** first latency**,** and **(c)** time to peak. Mean values ± SEM, one tail T-Test for two dependent means and Pearson correlation coefficient P value; ns $P > 0.05$, * $P \leq 0.05$, ** $P \leq 0.01$, *** $P \leq 0.001$. n=9.

7.4 Calcium imaging at single synaptic contacts

It is well known that during normal synaptic release, the magnitude of synaptic strength, which depends on the number of vesicles that fuse with the plasma membrane, relies on the local and short-lived Ca^{2+} increase in the surroundings of the docking sites, near open Ca^{2+} channels (Regehr, 2012). These Ca^{2+} rises (10-30 µM, Meinrenken, Borst, and Sakmann 2003) occurs in small and localized sites in the presynaptic terminal called "microdomains" (tens of nanometers in length) and exhibit both rapid rise and decay kinetic (tens of microseconds; see Smith & Augustine, 1988; Augustine & Neher, 1992). During the type of artificial laser-evoked synaptic transmission performed in this work, the vesicle fusion process relies on the "global" and long-lasting Ca^{2+} increase of the entire volume of the presynaptic terminal, which is high enough to induce the fusion of all the docked and release-competent vesicles.

We evaluated the features of the sub-and suprathreshold laser-evoked Ca^{2+} rises in single presynaptic terminals by using the kinetic properties of the high-affinity Ca^{2+} indicator OGB-1, in a pool of experiments where the indicator was included in the presynaptic IS. Using the saturation properties of OGB-1, we estimated the Ca^{2+} level reached during the conditioning test protocol in single varicosities. To this end, a train of 50 subthreshold laser pulses at 10 Hz (see Figure 7-9-b) was

applied. The fluorescence changes recorded with such protocol indicate that the K_d of OGB-1 (170 nM) is reached at the 7th pulse. This result demonstrates our ability to effectively control the basal Ca^{2+} levels in single presynaptic terminals of MLIs. Additionally, they indicate that when applying the train of 5 laser pulses utilized in the previous set of experiments (see above), the global Ca^{2+} concentration in the terminal stays in the nanomolar range).

We also evaluated whether the application of the conditioning protocol can modify the suprathreshold Ca^{2+} transient that accounts for the release of the RRP. The results from Figure 7-9-c shows that the fluorescent signal evoked by the conditioning protocol did not return to the baseline before applying the suprathreshold pulse, thus indicating a slight enhancement in the level of basal Ca^{2+} previous to the interrogation of the RRP (left inset). Regarding the kinetics of the suprathreshold Ca^{2+} transients, the results showed no statistical differences between the time constants τ_1 and τ_2 and the amplitude A_1 and A_2 values from the double exponential fit that describe the recovery phase (A_1= 0.4887 ± 0.0847, τ_1=0.0579 s ± 0.0091, A_2= 0.1867 ± 0.0402, τ_2=0.4895 s ± 0.0268 and A_1=0.2607 ± 0.0329, τ_1= 0.1225 s ± 0.07005, A_2= 0.4203 ± 0.1362, τ_2=0.5829 s ± 0.3029, for control and test condition, respectively; n=3, Figure 7-9-d). However, an average

increase in the recovery phase can be seen in the figure, probably as a consequence of a summation effect between the sub-and the suprathreshold Ca^{2+} transients.

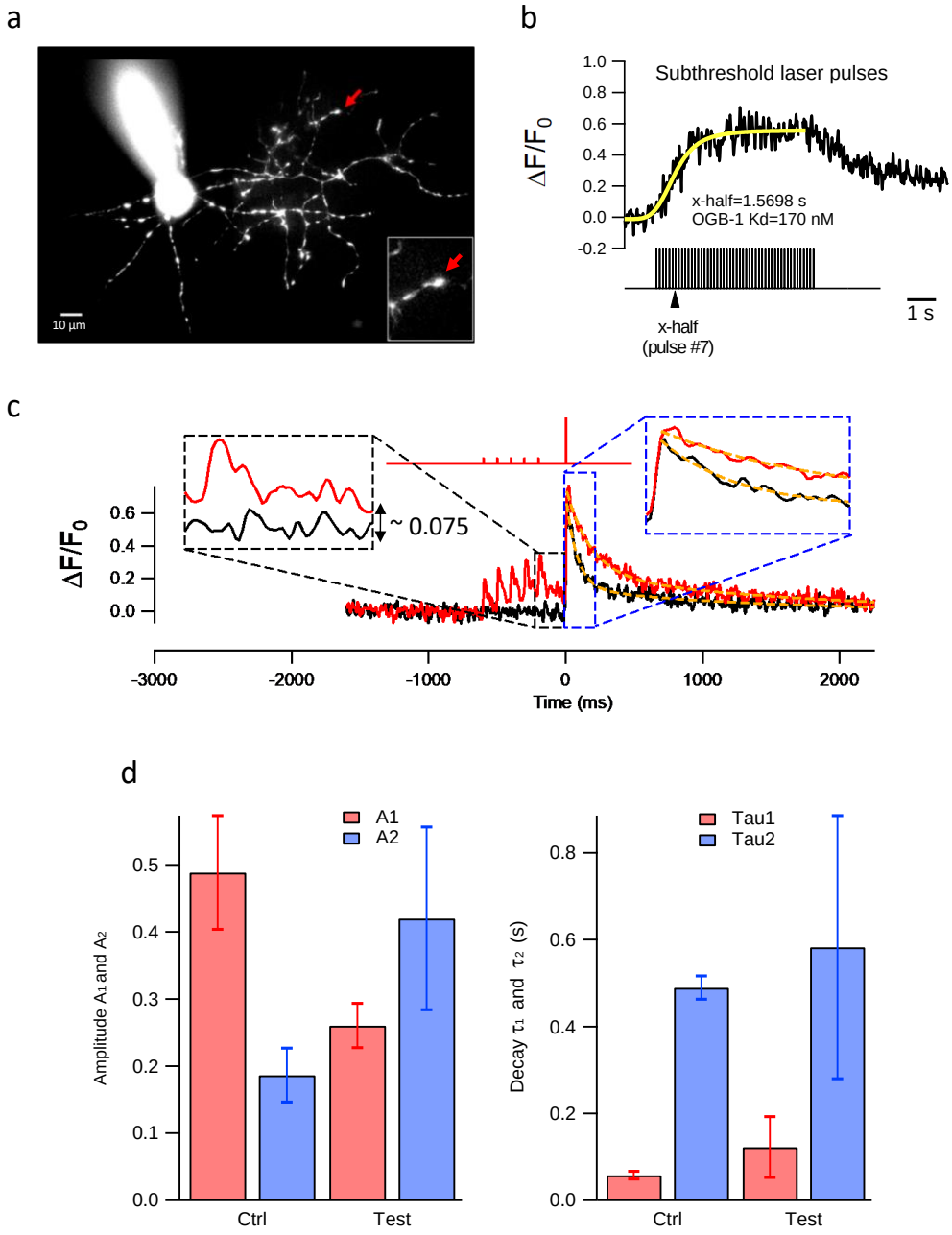

Figure 7-9. Modulation of Ca^{2+} levels in the sub- and suprathreshold range.
(a) Epifluorescence image of a representative MLI filled via patch pipette with DMNP, Alexa 594 and OGB-1. The inset shows a zoom of the varicosity where DMNP was photolized. **(b)** Fluorescence records ($\Delta F/F_0$) of Ca^{2+} transients triggered by the application of a train of 50 low-energy laser pulses. The yellow line corresponds to the fitting of the data with a Hill equation (yellow line); the x-half value corresponds to pulse # 7. This result indicates that at pulse # 7 the [Ca^{2+}] is inferior to 170 nM (subthreshold level, no NT release). **(c)** Fluorescence ($\Delta F/F_0$) signal of Ca^{2+} transients for control (black) and test (red) conditions. In test condition, a train of 5 subthreshold laser pulses (range=0.0085-0.0245uJ) was applied 600 ms before the high energy pulse stimulation (range=01-04 uJ). **(d)** Amplitudes (A_1, A_2) and decay time constants (τ_1,τ_2) obtained from the double exponential fit of the suprathreshold Ca^{2+} transient.

7.5 Docking site occupancy probability accounts for the subthreshold calcium-dependent modulation of GABA release in single synaptic contacts

For any given experiment the RRP varies from trial to trial but exhibits a fixed maximal value (RRP_{max}) that most likely represents the number of docking sites in the presynaptic terminal (Trigo et al., 2012; Pulido et al., 2015).

With the intention to perform a detailed analysis of the mechanism(s) by which the subthreshold Ca^{2+} rises modulates GABA release in MLIs, we performed vesicular release statistics by counting individual fusion events in control and test condition for both 200 ms and the 2 second delay. By doing this it is possible to obtain a reliable estimation of the RRP and the docking site occupancy probability in single presynaptic terminals.

We counted individual fusion events by both counting the number of inflexions in the PSC of each trace and by comparing their amplitudes with the value obtained for the release of a single quantum. This method allowed us to obtain a better estimation of the number of vesicles in the RRP to allow detecting possible differences between control and test condition (see methods for further details).

During vesicular release, each docking site undergoes a cycle starting from an occupied state, followed by exocytosis and the docking of a new synaptic vesicle. Considering this, we took advantage of the methodology described so far to calculate the following parameters: 1) Average value of RRP (RRP_{avg}), corresponding to the mean value obtained from the sequence of repetitions in each condition. 2) The number of docking site (NDS), corresponding to the maximal value of the RRP observed in the sequence and 3) the docking site occupancy probability (δ), corresponding to the ratio between RRP_{avg} and the NDS (see equations 1 and 2, bellow). A representative experiment is presented in Figure 7-10.

1) $\mathrm{RRPavg} = \frac{\sum_1^n \mathrm{RRPn}}{\mathrm{n}}$; where "n"corresponds to the number of trials per experiment.

2) $\delta = \frac{\mathrm{RRPavg}}{\mathrm{NDS}}$; where NDS corresponds to the number of docking sites.

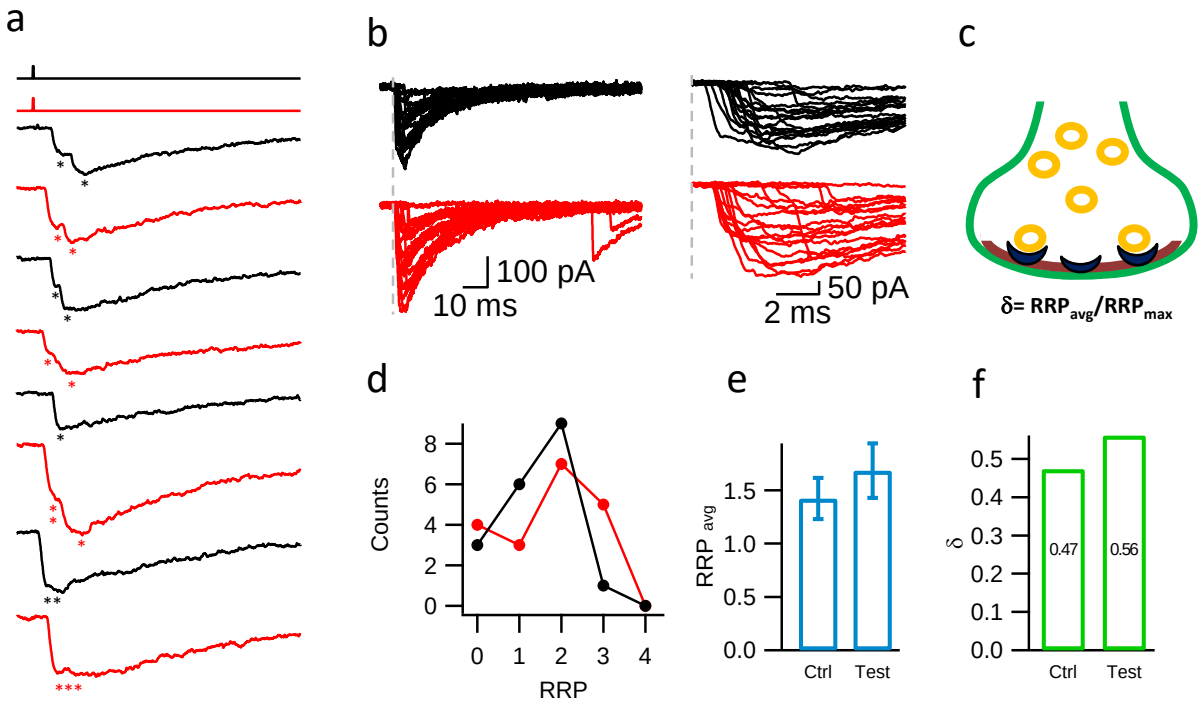

Figure 7-10. Representative experiment showing the approach for quantal analysis of the RRP in single synaptic contacts.
(a) Example of the PSCs obtained from the application of the control and test protocols (black and red, respectively). The estimated number of vesicles is indicated by the asterisks. **(b)** Superimposition of all the traces obtained for control and test condition (19 repetitions each). The dashed grey lines corresponds to the laser onset (t=0 ms). A clear enhancement in the peak amplitude of PSCs is observed for the test condition. Right panel shows an amplified view where the effect on the first synaptic latency is also evidenced. **(c)** Schematic representation of the synaptic terminal interrogated during the experiment. **(d)** RRP histogram for both conditions **(e)** Summary data for the average value of the RRP and **(f)** the docking sites occupancy probability for control and test condition.

The distribution of docking sites among all the synaptic terminals evaluated in this section was: 3.3%, 16.7%, 50%, 26.67% and 3.3% for 1,2,3,4 and 5 docking sites, respectively. Table 6 shows the summary of distribution of the number of docking sites for the two pools of experiments presented in this section. The results for the number of docking sites, RRP_{avg} and docking sites occupancy probability are

presented in Tables 7 and 8 for 200 ms and 2 second delays, respectively, and illustrated in Figure 7-11.

When comparing both RRP_{avg} and docking site occupancy probability between control and test conditions in 200 ms delay, a clear and significant increase in both parameters was observed (RRP_{avg}: 1.70 ± 0.18 vs. 1.86 ± 0.16, p=0.0148; docking site occupancy: 0.53 ± 0.04 vs. 0.58 ± 0.03, p=0.0106, for control and test condition, respectively; Figure 7-11a and Figure 7-11b). These results suggest that subthreshold Ca^{2+} rises can control the strength of synaptic transmission by modulating the dynamics of docking site occupancy in single synapses. For the 2 second delay pool, as expected from the previous analysis of peak amplitude and synaptic charge, the results show a not significant average decrease in the value of the RRP_{avg} and docking site occupancy probability (RRP_{avg}: 1.83 ± 0.27 vs. 1.74 ± 0.27, p=0.0845; docking site occupancy: 0.6 ± 0.05 vs. 0.56 ± 0.04, p=0.0586, for control and test condition, respectively).

Interestingly, for the 200 ms and 2 s delays it is possible to observe that there was a slight negative correlation between the strength of the facilitating effect on both the RRP_{avg} and the docking site occupancy probability and their initial values in control conditions (only significant for the docking site occupancy probability in

200 ms delay; see Figure 7-11. Quantal analysis of RRP release in control and test conditions for 200 ms and 2 s delay.). Furthermore, these results suggest that the synapses displaying RRP values larger than 2 vesicles and docking site occupancy probabilities larger than 0.5, tend to exhibit depression instead of facilitation as a consequence of the conditioning treatment.

In order to test whether the synapse-specific initial values of RRP_{avg} and docking site occupancy probability can account for real differences in the outcome after the conditioning protocol (facilitation vs. depression), we decided to compare the differences between the "extreme points" along the distribution of the absolute difference values (test-ctrl) for RRP_{avg} and δ values of Figure 7-11c,d and Figure 7-11g,h for 200 ms and 2 s delay, respectively. The results (Figure 7-12) show a significant difference for both RRP_{avg} and docking site occupancy probability when comparing the largest and the smallest differences (test-control) for 200 ms and 2 s delay, (5 and 3 extreme points, respectively) [RP_{avg} (test-ctrl): 0.60 ± 0.10 vs. -0.22 ± 0.07, p= 0.00007; δ (test-ctrl): 0.18 ± 0.03 vs. -0.06 ± 0.02, p=0.00016, for 200 ms delay] and [RP_{avg} (test-ctrl): 0.076 ± 0.076 vs. -0.241 ± 0.087, p= 0.02591; δ (test-ctrl): 0.025 ± 0.025 vs. -0.102 ± 0.017, p=0.00692, for 2 s delay]. These results confirm that different synapses can exhibit opposite behaviors

(facilitation/depression) to the same conditioning stimulus, depending on their initial state in terms of RRP size and docking site occupancy probability.

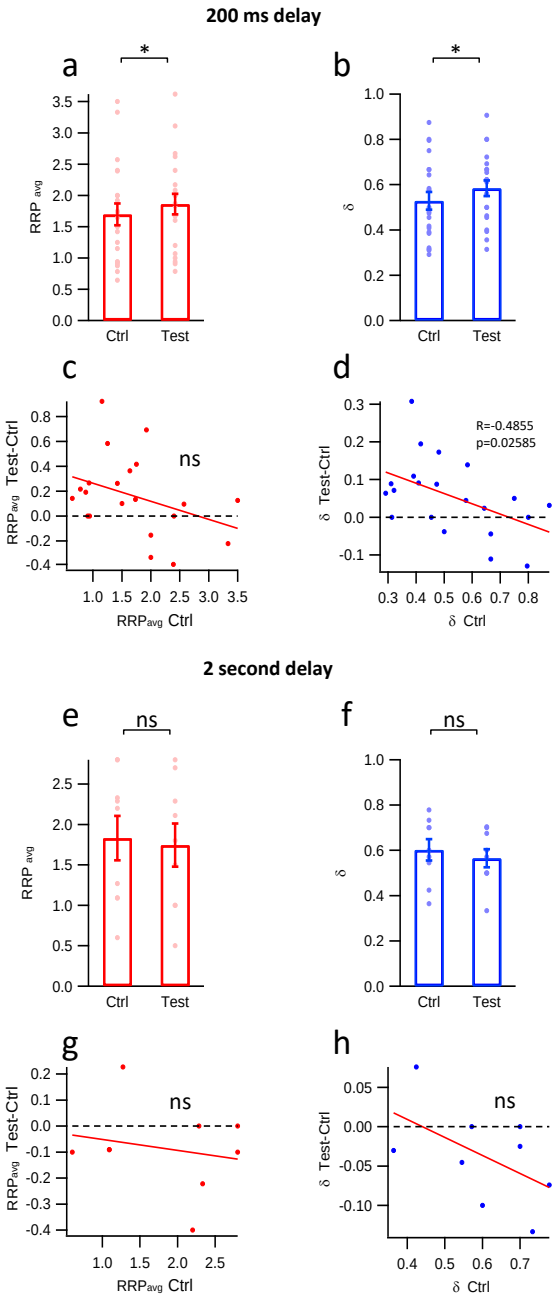

Figure 7-11. Quantal analysis of RRP release in control and test conditions for 200 ms and 2 s delay. **(a)** Summary data for RRPavg. **(b)** Summary data for δ. **(c)** Relation between the strength of the effect on the RRPavg and the initial value in control condition. **(d)** Relation between the strength of the effect on the docking site occupancy and the initial value in control condition. **(e)** Summary data for RRPavg for 2 second delay. **(f)** Summary data for docking site occupancy probability for 2 second delay. **(g)** Relation between the strength of the effect on the RRPavg and the initial value in control condition for 2 second delay. **(h)** Relation between the strength of the effect on the docking site occupancy and the initial value in control condition for 2 second delay. Mean values ± SEM, one tail T-Test for two dependent means; ns $P > 0.05$, * $P \leq 0.05$, ** $P \leq 0.01$, *** $P \leq 0.001$

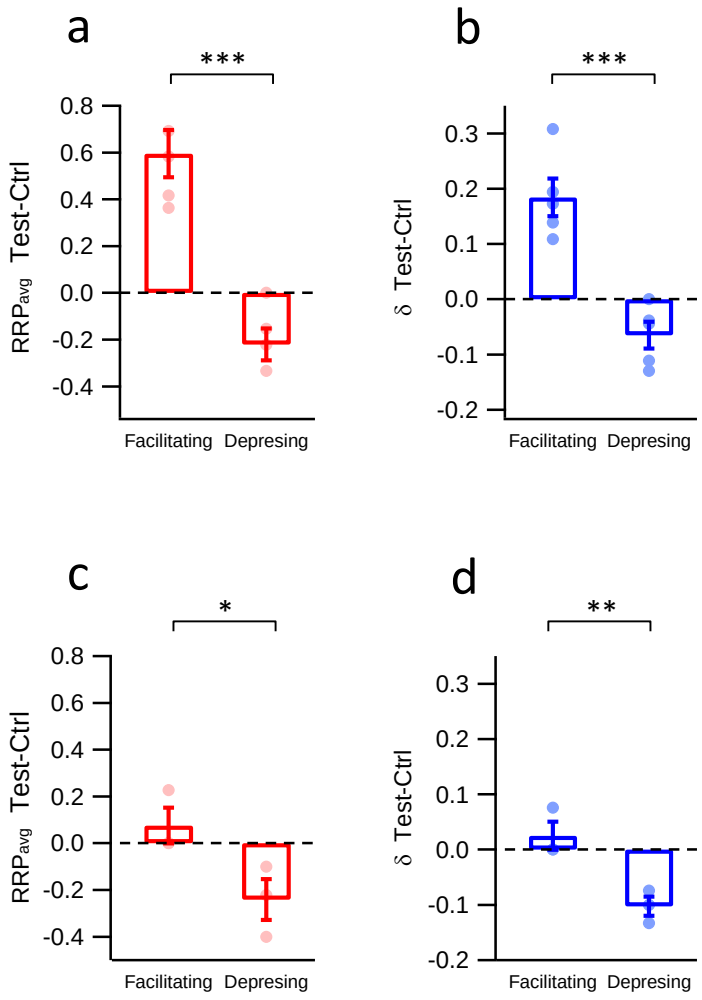

Figure 7-12. Differences between the "extreme points" along the distribution of the (test-ctrl) values for RRPavg and docking site occupancy probability.
Upper panels: comparison between the 5 largest and smallest values for **(a)** RRPavg and **(b)** docking site occupancy probability for 200 ms delay. Bottom panels: comparison between the 3 largest and smallest values for **(c)** RRPavg and **(d)** docking site occupancy probability for 2s delay. Mean values ± SEM, one tail T-Test for two independent means; ns $P > 0.05$, * $P \leq 0.05$, ** $P \leq 0.01$, *** $P \leq 0.001$.

7.6 Depolarization-induced changes in presynaptic calcium modulates vesicular release dynamics

So far in this work we have explored the role of subthreshold Ca^{2+} rises on synaptic transmission by using a non-physiological approach to modulate Ca^{2+} levels in single presynaptic terminals. Our next step was to confirm our findings in a more physiological context. To this purpose we performed whole-cell recordings from pairs of MLIs and produced a subthreshold Ca^{2+} rise by applying subthreshold somatic depolarization in the presynaptic neuron, as it has been previously described for by Bouhours et al., 2011, J.M Christie et al., 2011 and Rowan and Christie, 2017.

Considering the differences in the duration of the subthreshold SSD protocols that can be found in these studies, where AP broadening (Rowan and Christie, 2017; 100 ms of SSD), facilitated spike-evoked Ca^{2+} entry (Christie et al., 2011: 300 ms of SSD) and Ca^{2+}-dependent PKC activation (Bouhours et al., 2011; 10 s of SSD) have been proposed to mediate the phenomenon of analog to digital facilitation in MLIs (see introduction), we hypothesized that two independent mechanisms with different kinetics may be contributing to this form of synaptic plasticity: a) One that depends only on AP broadening, that does not require subthreshold Ca^{2+} rises (during the SSD) or large depolarization steps (seconds).

b) Another one in which subthreshold Ca^{2+} rises are essential, and a signaling pathway is probably involved.

It has been shown previously that the onset of Ca^{2+} rises when applying a 10 s subthreshold somatic depolarization from -60 mV to -40 mV is around 1.5 s (Bouhours et al., 2011). So, we decided to use a protocol with a depolarization step from -75 mV up to a value just below the spike threshold (usually -50 mV) and long enough to see the contribution of both mechanisms (2 seconds of SSD). We hypothesized that if both mechanisms coexist, one way to dissect them is to consider that a signaling pathway requires one single step to trigger the cascade (an increase in Ca^{2+} levels in this case), and then the cascade will continue even if the Ca^{2+} returned to its basal level.

We decided to use a stimulation protocol where the presynaptic spike is triggered at 3 different times from the end of the SSD: a) 0 ms (no delay), b) 200 ms and c) 2 s. The three delays (test condition) were applied in an interleaved manner within the same experiment and each of them has its own control where no SSD was applied. The results are illustrated Figure 7-13 and presented in Table 9, Table 10 and Table 11 for peak amplitude of both PSC and autoreceptor current “ARC”, (which corresponds to the current obtained by activation of the presynaptic

$GABA_A$ receptors in the axon, see introduction) and synaptic latency, respectively. A scheme of the protocol used is presented in Figure 7-13a.

Figure 7-13b shows a representative experiment (for 200 ms delay) where the test condition is presented in both purple and red for presynaptic (upper) and postsynaptic (bottom) traces, respectively. The upper inset of Figure 7-13b shows a magnified view of the ARC where no difference between control and test condition is evidenced. The bottom inset of Figure 7-13b shows a magnified view of the PSC, where a clear increase of the PSC amplitude can be observed. The summary plots for the ratios of PSC peak amplitude, autoreceptor current peak amplitude and synaptic latency are presented in Figure 7-13c, d and e, respectively.

Although an average increase in PSC amplitude can be seen after the application of the SSD at no delay condition, the effect is larger and only significant at 200 ms delay. This result suggests that there is a summation process that requires time, probably as a consequence of a signaling pathway or another relatively slow mechanism(s) that is contributing to the net effect. In addition, and as it was expected from our previous results by using Ca^{2+} uncaging, no significant effect was observed for a 2 s delay.

Interestingly, in relation with the autoreceptor current it is possible to see that in this case the larger and only significant effect was obtained when there is no delay between the end of the SSD and the presynaptic AP, and the effect is gone for 200 ms and 2 s delays. This suggests that the effect of SSD on GABA release depends on the specific type of $GABA_A$ receptors, affecting the pre- and postsynaptic cells in different ways, probably due to the type and number of synapses that PSC and ARC reports.

Erratum: The results from this last section should be taken carefully because there was a mistake in the composition of the internal solution, which resulted in a high concentration of free Ca^{2+} (~ 80 µM).

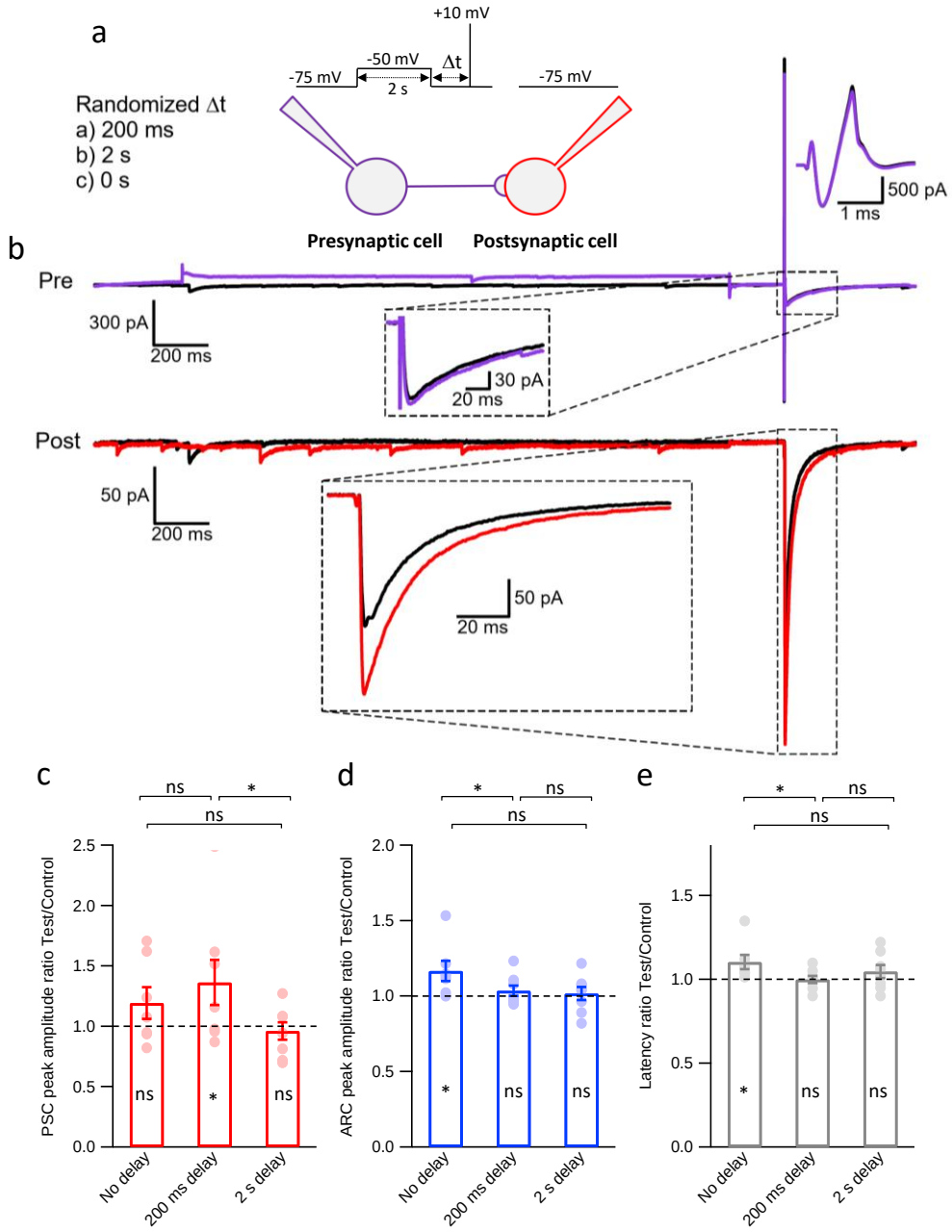

Figure 7-13. Presynaptic subthreshold somatic depolarization enhances AP-evoked release in MLIs.
(a) Schematic representation of the protocols. In control condition the presynaptic MLI was clamped at -75 mV and a 0.1 ms pulse to 10 mV that triggers an unclamped action potential was applied. In test condition the holding potential was held at -50 mV for 2 seconds previous to the AP, which was triggered 200 ms (n=8), 0 ms (no delay, n=7) or 2 s (n=8) later. The order was randomized across experiments. **(b)** Presynaptic and postsynaptic traces from a representative experiment. Control condition is shown in black and test condition is shown in purple and red for both ARC and PSC, respectively. **(c)**, **(d)** and **(e)** Summary plots for the ratios of PSC peak amplitude, ARC peak amplitude and synaptic latency, respectively, for the 3 different tested delays. One tail T-Test for two dependent means was used for the analysis of ratios while Mann-Whitney U Test was used to compare the ratios between different delays; ns $P > 0.05$, * $P \leq 0.05$, ** $P \leq 0.01$, *** $P \leq 0.001$.

8 Discussion

In this study we found that local subthreshold Ca^{2+} rises at single presynaptic terminals of young rat cerebellar MLIs enhances GABA release by a mechanism that is likely to involve an increase in the occupancy probability of docking sites, which directly translates into an increase in the number of vesicles available for immediate release under high Ca^{2+} conditions (RRP). We also show that subthreshold Ca^{2+} rises can decrease the latency of the first fusion events, thus enhancing the temporal precision at which released GABA is first detected by the postsynaptic receptors. The strength of these effects appears to depend on both the initial number of docking sites and their initial occupancy level: when the delay between the conditioning and the suprathreshold stimuli was 2 seconds, there was an enhancement of the asynchronous release that had decreased the initial occupancy level of docking sites previous to its interrogation by the suprathreshold pulse, hence weakening the facilitating effect or instead, even producing a depression in some synapses. Furthermore, synapses exhibiting larger presynaptic terminals (in terms of number of docking sites) tend to produce depression rather than facilitation. This occurs probably as a consequence of an elevated sensitivity to subthreshold Ca^{2+} rises, which causes a decrease in the occupancy level of docking sites as well. Our results suggest that subthreshold Ca^{2+} rises resulting

from physiological processes like analog-to-digital signaling or periods of high suprathreshold activity leading to high levels of residual Ca^{2+} can efficiently change the occupancy of docking sites at single synaptic contacts and thereby modulate the synaptic output in a synapse-specific manner.

8.1 Approaches for release and measurement of the readily releasable pool in single synaptic contacts

(i) RRP release: In this work we used an approach to study small synaptic contacts that relies on the local photorelease of Ca^{2+} in single axonal presynaptic varicosities of MLIs in slices. The spatial restriction of the Ca^{2+} signals that are produced by this method has been previously demonstrated to be sufficient to avoid triggering the unspecific release of neurotransmitter from neighboring synaptic terminals (Trigo et al., 2012). Additionally, it has been previously demonstrated that in the postsynaptic side GABAergic synapses are sparse and compact, thus ensuring that GABA release from a single terminal reaches a single postsynaptic density (Nusser, Cull-Candy and Farrant, 1997). The main features of the results presented here are in agreement with the hallmarks that have been previously used to identify synaptic release originating from single synaptic contacts: low variability of peak amplitude and occlusion between events that occur closely in time (Auger and Marty, 2000; Trigo et al., 2012; Pulido et al.,

2015; see Figure 7-1). This strongly suggests that the synaptic signals presented here originate from single synaptic contacts. Our approach presents the advantage that photorelease permits an accurate and flexible control of Ca^{2+} levels which can trigger vesicular release with submillisecond precision from unambiguously identified synaptic contacts. This allows the measurement of kinetic parameters without the inherent error of having unknown delays due to the propagation of the AP (Kondo and Marty, 1998). Additionally, our approach can generate a high enough level of desynchronization of individual fusion events to perform quantal analysis of the RRP. The main disadvantage of our approach is that is does not allow a high number of repetitions, probably as a consequence of oxidizing byproducts from the photolysis reaction (Kaplan and Ellis-Davies, 1988), precluding a more efficient statistical analysis.

(ii) RRP measurement: Here we used two approaches with different resolutions to estimate RRP from single synaptic contacts; both of them rely on the features of PSCs as a proxy of presynaptic GABA release. The first one consisted in using the values of peak amplitude, synaptic charge and latency as indicators of the amount and timing of GABA release. The second approach consisted in combining the counting of individual inflexions in the multiphasic rising phase of laser-evoked PSCs with both their amplitude (local peaks) and the quantal size for each synapse.

This allows to obtain a reliable estimate of the number of vesicles that fused with the plasma membrane upon Ca^{2+} photorelease. Because we can control the amount of photoreleased Ca^{2+}, this approach can be used to deplete the terminal and directly estimate the number of vesicles composing the RRP. The major challenge to accurately measure the RRP by using more physiological approaches (like prolonged trains of presynaptic APs) is to release the RRP while accounting for the replenishment contribution (Kaeser and Regehr, 2017). Here we avoided this problematic issue by releasing the RRP in a time window which is significantly shorter (within 10 ms; see Fig. 7-2) than the reported value for the replenishment time constant (1.7 s under resting conditions and 300-400 ms during the application of an AP train (Takeshi Sakaba, 2008). Additionally, we have confirmed the emptying of the RRP by testing laser-evoked release 30 ms after the first high Ca^{2+} pulse (see methods); this time window is large enough to permit the diffusion of the calcium cage to the presynaptic terminal (Trigo et al., 2012) and short enough to permit the full replenishment of an empty docking site.

In this work we have assumed that the RRP reflects the number of vesicles in the docked state in a single active zone. This has been suggested by previous functional and electron microscopy studies of the Calyx of Held and neuromuscular junction (see introduction) and where the RRP has been interpreted

as the number of vesicles that are bound to a few docking sites (2-6) in the active zone (Neher and Sakaba, 2008; Ruiz et al., 2011; Sätzler et al., 2002; Nagwaney et al., 2009). However, recent findings suggest that not all but several (or many) of the vesicles in the docked state can contribute to the RRP, and that undocked vesicles can also be part of the RRP by rapid recruitment to activated ready-to-release docking sites (Kaeser and Regehr, 2017). In the same study it is also highlighted that estimates of RRP from Ca^{2+} photolysis, hypertonic sucrose application or prolonged presynaptic voltage steps often provide larger values than the ones based on evoking RRP release by AP trains (which as mentioned before, is thought to represent a physiological situation). The main difference between these techniques is that the Ca^{2+} rises evoked by the APs are both spatially an temporally constrained, creating what has been defined as Ca^{2+} micro or nanodomains, while Ca^{2+} rises produced by uncaging generate prolonged and unconstrained signals (Thanawala and Regehr, 2013). This is relevant if we consider that the distance between docking sites and the high Ca^{2+} microdomains (determined by individual or cluster of voltage-dependent Ca^{2+}channels) can limit the percentage of docked vesicles that fuse with the plasma membrane. Here we have generated a high and uniform Ca^{2+} transient; hence we propose that our estimate of the RRP includes all the vesicles in the docked state in the active zone

(independent of the distance to the VSCCs), although it is highly likely that this value also includes the contribution of vesicles that can be in an intermediate state, close to reaching the releasable-competent state of docking (priming state), and that perhaps can account for the average increase in the latency of all the events when comparing AP-evoked vs. laser-evoked responses (Fig 7-1). These delayed vesicles cannot be considered as a consequence of a full replenishment from the reserve pool, because it takes hundreds of milliseconds to seconds for this process to occur (Takeshi Sakaba, 2008). Instead, we think that they could reflect a semi-competent state of docking in the steps of the synaptic vesicle cycle.

One of the results of the present work confirms the previous observation that the RRP exhibits a high degree of fluctuation (Trigo et al., 2012). We interpreted this as reflecting spontaneous variations in the occupancy of docking sites. An alternative explanation could be that these fluctuations may reflect an incomplete recovery from the previous laser stimulation, nevertheless, this is highly unlikely considering that the inter-sweep interval for all the uncaging experiments was 1 minute, which is long enough to allow the full recovery from the previous laser stimulation.

8.2 Modulation of the RRP and docking site occupancy probability by subthreshold calcium levels and its impact on the features of the postsynaptic response

(i) PSC peak amplitude and synaptic charge: In this work we tested the hypothesis that subthreshold Ca^{2+} rises, in analogy to what has been reported during the phenomenon of analog-to-digital facilitation in MLIs, can effectively modulate GABA release by a mechanism that involves an increase in the occupancy probability of docking sites, which translates directly into an increase in the size of the RRP. We found that the application of a conditioning protocol consisting of a train of five low intensity laser pulses (10 Hz) produces an average increase in the peak amplitude and synaptic charge of the PSC. This was also accompanied by a decrease in the latency of the first fusion events (Fig 7-4). These results are in agreement with what had been previously showed in the calyx of Held, where an increase in the Ca^{2+} influx into the presynaptic terminal caused by changes in the external Ca^{2+} concentration produces and increase in the size of the excitatory postsynaptic current (EPSC) that cannot be explained merely by the Ca^{2+} cooperativity of the release process; instead, a Ca^{2+}-dependent increase of the RRP also contributes in one-third to the net effect (Thanawala and Regehr, 2013). Hence, our results suggest that the Ca^{2+}dependent modulation of the RRP size could be a general mechanism for modulation of the strength of central synapses.

The average increase in peak amplitude and synaptic charge observed in this work was relatively small (ratio test/control= 1.11 ± 0.04 vs. 1.18 ± 0.06, for peak amplitude and synaptic charge, respectively) in comparison with previous data from our laboratory showing an increase of around 42% when using a subthreshold somatic depolarization as the conditioning stimuli (Bouhours et al., 2011). We interpret that this difference might be due to the specific characteristics of the two protocols used. Bouhours et al, 2011 utilized a 10 s subthreshold somatic depolarization that generates a subthreshold Ca^{2+} rise that extends for several seconds, and which is likely to set the initial occupancy state of docking site to a higher level than what we have achieved here by the application of the train of conditioning pulses (occupancy levels change from 0.53 to 0.58; see Fig. 7-11). Additionally, because Bouhours et al., did not use a RRP-releasing suprathreshold stimuli (they used an AP), it is also highly probable that the effect on the peak amplitude resulted from changes in both release probability and RRP size; thus the net facilitating effect observed by Bouhours et al., would mainly reflect the release of a larger fraction of the RRP rather than an increase in the RRP.

From the results of Fig. 7-4, it is possible to observe that the effect on synaptic charge was larger than the effect on peak amplitude. This is in agreement with previous studies indicating that synaptic charge is a much better indicator of

neurotransmitter release (Pulido et al., 2015), because while peak amplitude reflects the maximum level of charges crossing the plasma membrane in a particular time, synaptic charge includes the contribution of individual fusion events occurring after the peak current level.

(ii) Synaptic latency: For the calyx of Held, it has been recently proposed that the large differences in strength and properties of short-term plasticity observed across glutamatergic synapses can be explained assuming that a fraction of vesicles in the active zone are in a "superprimed" state that confers them an enhanced release probability (Taschenberger, Woehlerb, and Neher, 2016). Furthermore, in the same study was suggested that the enhanced strength after post-tetanic potentiation or by the activation of the phospholipase-C–diacylglycerol (PLC-DAG) pathway result from an increase in the fraction of vesicles in the superprimed state. This effect is probably associated to the activation of the protein MUNC-13 which is an essential component of the release machinery that can control both forms of synaptic potentiation trough a regulation of the energy barrier for the fusion of synaptic vesicles (Schotten et al., 2015). In this thesis work we show that subthreshold Ca^{2+} rises can speed up GABA release and increase its temporal precision by decreasing both the average first latency values and its coefficient of variation CV (Fig.7-5), thus suggesting that the same mechanism that appears to modulate the primed state

of the RRP vesicles in the calyx of Held can be acting in GABAergic MLIs of the cerebellum. Furthermore, the fact that only the first latencies were affected by the conditioning stimuli suggests that a small fraction of the vesicles in the RRP adopt the superprimed state (in addition to the increase in the RRP size). Another possibility to explain our results is what has been suggested for the ribbon synapse, where the existence of an inverse relationship between the size of the RRP and the latency of the first fusion events has been proposed to mediate the fast vesicular release (Wittig and Parsons, 2008). It is possible that the same relationship could be valid for MLI synapses, in which case an increase in the RRP size could potentially increase the probability of any vesicle to undergo exocytosis, producing a decrease in the first latency values. Furthermore, it is also possible that this last effect and the superpriming effect could coexist within the same synapse.

(iii) RRP and docking site occupancy: In addition to the macroscopic analysis of PSC peak amplitude, charge and latency, we performed quantal analysis of the RRP at the level of single synaptic contacts. With this "microscopic" approach we measured the number of vesicles composing the RRP and the occupancy probability of docking sites before and after the conditioning treatment. Our results show that presynaptic terminals of MLIs possess a small number of docking sites, ranging from 1 to 5, with a modal value of 3. The average number of vesicles

composing the RRP was 1.70 and the average docking site occupancy probability was 0.53, which is slightly lower than previously reported values (1.9 and 0.7, respectively, Trigo et al., 2012). Overall, our data are consistent with the idea that each presynaptic terminal exhibits a small number of docking sites and whose occupancy level fluctuates from stimulus to stimulus. Under test condition the average values of RRP and docking site occupancy probability increased from 1.70 to 1.86 and 0.53 to 0.58, respectively. These results suggest that the conditioning treatment, while producing a facilitating effect, was unable to mediate the filling of the total number of available empty docking sites, suggesting the need for a longer preconditioning stimulation. It is also possible that other mechanisms that do not depend on subthreshold Ca^{2+} rises (thus, that are not activated here) can mediate at least to some extend the occupancy probability of dockings sites.

8.3 Differences in synaptic output (facilitation/depression) depend on both the number and occupancy of docking sites and the timing at which the effect is evaluated

(i) Uncaging experiments: Different synapses from the same neuron can express different forms of synaptic plasticity (Abbott and Regehr, 2004; Trommershauser et al., 2003; Reyes et al., 1998; Markram et al., 1998). It has been recently proposed that differences in the number of docking sites can account for differences in the properties of short-term synaptic plasticity in MLIs (Pulido et al., 2015; Pulido and Marty, 2017). Here we show that the strength of the facilitation effect evoked by subthreshold Ca^{2+} rises seems to exhibit an inverse relationship with both, the initial value of PSC peak amplitude and/or the synaptic charge ("macroscopic" view) and the initial value of RRP and docking site occupancy probability ("microscopic" view): synapses with larger values of peak amplitude and charge are less facilitated than those with lower values. Furthermore, many of them exhibited depression instead of facilitation. The same tendency was observed when looking at the averaged values of RRP and the initial docking site occupancy state: synapses exhibiting values of RRP larger than 2 vesicles and/or docking site occupancy probabilities larger than 0.5 tend to exhibit depression instead of facilitation (Fig.7-4, Fig. 7-5 and 7-11). This can be understood if we consider that synaptic facilitation and depression are the consequence of an increased and

decreased docking sites occupancy level, as recently discussed by Pulido and Marty, 2017. Assuming that this is true, the most likely explanation for the depression/facilitation observed here is that synapses expressing larger initial values of docking site occupancy are more sensitive to the effect of the conditioning treatment. This can be understood if we consider that an elevated number of vesicles available for immediate release will increase the probability that any of them to fuse with the plasma membrane and undergo exocytosis, hence these synapses tend to release (asynchronously) part of the RRP previous to its interrogation with a high Ca^{2+} pulse (this assumes that asynchronous and evoked release share the same vesicle pool). This means that while the conditioning stimuli increases the RRP it tends to be balanced by the accompanying increase in asynchronous release. Such a process will have a higher impact on the synapses exhibiting a high level of docking site occupancy or RRP size.

If this last suggestion is correct, it is logical to think that the net balancing effect will depend on the time window between the end of the conditioning stimuli and the suprathreshold pulse; in other words, the net effect will depend on how long is the interval before testing the RRP: the longer that interval, the higher the level of asynchronous release and the higher the probability of obtaining a small facilitating effect or even a depression. In fact, this is exactly what we observed here in the

experiments where the delay between the end of the conditioning train and the test pulse was increased from 200 ms to 2 seconds. In this case, instead of facilitation a small depression (although not significant) was evidenced when looking at both macroscopic (peak amplitude and charge) and microscopic (RRP and docking site occupancy probability) parameters. All together, these results suggest that variations in docking site occupancy account for differences in short-term plasticity (Pulido et al., 2015). Furthermore, they highlight the importance of the docking sites for synaptic plasticity.

(ii) Time dependency of the effect of subthreshold somatic depolarization in purely electrophysiological experiments: With the intention of testing our findings in a more physiological context, we performed electrophysiological experiments attempting to mimic the laser-evoked subthreshold Ca^{2+} rises of our uncaging experiments by applying subthreshold somatic depolarizations in pairs of synaptically connected neurons, according to what has been described before for MLIs (Bouhours et al., 2011; Christie et al., 2011). Our results show that under these experimental conditions the application of a 2 second subthreshold somatic depolarization to the presynaptic neuron can produce a facilitation of the PSC depending on the delay between the sub- and the suprathreshold stimuli: we only observed a significant effect when the delay between the end of the subthreshold

depolarization and the AP was equivalent to that used in experiments with Ca^{2+} uncaging (200 ms of delay). Furthermore, it appeared that there was a depression with 2 second delay (not statistically significant). These results confirm our previous findings and validate our main approach, where we supposed that the photorelease of Ca^{2+} can mimic the subthreshold Ca^{2+} levels reached during analog-to-digital facilitation. Nevertheless, the interpretation of these last results must be taken with caution because of the high free [Ca^{2+}] used in this set of experiments.

8.4 Possible mechanisms for the subthreshold calcium dependent modulation of the RRP and its relation to the analog-to-digital facilitation phenomenon in MLIs

Previous studies have proposed that subthreshold somatic depolarizations can modulate vesicular release in MLIs in a Ca^{2+} dependent way (Bouhours et al., 2011; Christie et al., 2011). From those studies it is clear that the application of subthreshold somatic depolarizations generates an influx of Ca^{2+} into the presynaptic terminal through voltage-dependent Ca^{2+} channels. However, different mechanisms were proposed. Bouhours et al., 2011 have suggested that the amount of Ca^{2+} entry associated to one action potential is not affected, while Christie et al., 2011 have suggested that subthreshold somatic depolarization facilitates AP-

evoked Ca^{2+} influx. Furthermore, more recently was proposed that subthreshold somatic depolarization modulates AP-evoked Ca^{2+} influx by increasing the width of the AP waveform (Rowan and Christie, 2017). From a functional point of view, the net effect of subthreshold somatic depolarization is always the same: it increases in the amount of GABA that is released by the arrival of an AP. Nevertheless, knowing the presynaptic parameters affected during this type of facilitation, it is fundamental to understand the processes governing synaptic plasticity. Unfortunately, none of those studies assessed the question of what specific parameters are modulated during analog-to-digital facilitation. Bouhours et al., 2011 suggested that the effect is mediated by a signaling pathway that involves local activation of PKC. However, Rowan and Christie, 2017 reported a facilitation of GABA release in PKC knock-out animals. Here we show that subthreshold somatic Ca^{2+} rises modulates GABA release by increasing the occupancy probability of docking sites, thereby producing an increase in the size of the RRP. We show that this effect is independent of the Ca^{2+} levels reached during the suprathreshold Ca^{2+} pulse (as long as the RRP is depleted); our Ca^{2+} imaging experiments show that the conditioning train of 5 low intensity laser pulses produces a subthreshold Ca^{2+} increase in the nanomolar range (lower than 170 nM). They additionally tend to suggest that the suprathreshold Ca^{2+} rise generated

by a single high energy laser pulse would exhibit a slow recovery phase that is well described by a double exponential function, like previously reported for juvenile MLIs (basket cells) in the mouse (Collin et al., 2015), nevertheless, there was no significant change in the kinetic parameters from the double exponential fit between control and test condition. More experiments are needed to confirm this because the observation relies in only three experiments.

From these experiments it is possible to observe that the Ca^{2+} levels reached during the conditioning treatment did not return to the basal level before interrogating the RRP, therefore it could be argued that the facilitating effect seen in our experiments was the result of the enhanced Ca^{2+} during the suprathreshold laser pulse, which in turn would generate the fusion of a larger faction of the RRP. This is unlikely to be the case because, as mentioned before, the intensity of the suprathreshold laser pulse in control condition was set to release the entire RRP.

Overall our results present the first evidence that subthreshold Ca^{2+} rises can modulate the RRP and its kinetics in presynaptic terminals of MLIs. The remaining obvious question concerns the molecular mechanism(s) underlying this effect. As mentioned in the introduction, the protein MUNC-18 is the most likely candidate to mediate the facilitating effect on GABA release. MUNC18-1 is an essential

component of the release machinery (Verhage et al., 2000; Zilly et al., 2006) that is phosphorylated by PKC under depolarization (Craig et al., 2003; de Vries et al., 2000) and has been implicated in the replenishment of vesicles under intense stimulation and in the control of the RRP in GABA and glutamatergic synapses (Nili et al., 2006; Toonen et al., 2006). On the other hand, the MUNC-13 protein (not related with MUNC-18), which is a component of the cytoskeletal matrix in the active zone and essential for all forms of vesicular release has been implicated in the superpriming phenomenon. As mentioned above, superpriming reflects the enhancement in the probability of NT release that is mediated by a decrease in the energy barrier for the fusion process to occur (Lee et al., 2013; Taschenberger et al., 2016). Like MUNC-18, MUNC-13 also presents C_1 and C_2 domains, possibly conferring to the protein modulation by Ca^{2+} ions, PKC and DAG. Additionally, it has been shown that two different and essential signaling pathways generating synaptic potentiation can exhibit an interplay between each other: one that depends on PKC activation by DAG or Ca^{2+} followed by phosphorylation of MUNC-18 (see introduction) and another that depends on the direct activation of MUNC-13 by DAG (Wierda et al., 2007). This interplay occurs because DAG potentiates the effects of residual Ca^{2+} on synaptic transmission (Lou et al., 2005; Wu and Wu, 2001), and residual Ca^{2+} can also stimulate the production of DAG (Micheva et al.,

2001). Here we propose that the subthreshold Ca^{2+} influx during analog-to-digital facilitation activates these two signaling pathways, which in turn produce an increase in the probability of docking site occupancy, enhancing the amount of GABA released by increasing the RRP size and producing a superpriming of the vesicles after their recruitment. The most straightforward way to probe the implication of these two signaling pathways acting on MUNC-18 and MUNC-13, respectively, would be to perform uncaging experiments in single synaptic contacts of genetically modified animals in which the sensitivity of MUNC-18 to PKC and the sensitivity of MUNC-13 to DAG is abolished (knock-out of any of these proteins results in the total arrest of spontaneous and evoked neurotransmitter release). In this way, we could test our hypothesis and even determine the relative contribution of these two pathways in single synaptic contacts. Such experiments also have the potential of providing important information to determine whether there are differences among individual presynaptic terminals in the same cell. Another option would be to disrupt or alter each signaling pathway by using specific inhibitors of PKC and PLC, such as the PKC inhibitor Go694 and/or the PLC inhibitor U73122.

9 Appendix

9.1 Tables

Table 1. Peak amplitude and synaptic latency values for AP-evoked and laser-evoked responses

	Peak amplitude (pA)					Synaptic latency (ms)				
Nb	AP-evoked	CV	Laser-evoked	CV	Ratio laser/AP	AP-evoked	CV	Laser-evoked	CV	Ratio laser/AP
1	121.22	0.28	216.00	0.20	1.78	2.21	0.44	1.76	0.78	0.80
2	149.95	0.45	302.50	0.25	2.02	1.49	0.26	3.74	0.58	2.51
3	59.39	0.88	143.00	0.21	2.41	1.54	0.46	3.23	0.73	2.10
4	137.54	0.21	186.46	0.16	1.36	1.21	0.20	2.27	0.71	1.88
5	252.85	0.31	206.57	0.25	0.82	1.17	0.29	2.20	0.69	1.88
6	31.15	0.53	162.22	0.20	5.21	1.18	0.50	2.90	0.79	2.45
7	97.10	0.24	100.67	0.35	1.04	2.60	0.53	2.00	0.37	0.77
8	274.93	0.38	49.20	0.24	0.18	1.51	0.16	2.30	0.47	1.53
9	108.93	0.63	101.57	0.24	0.93	1.80	0.29	1.96	0.41	1.09
10	157.29	0.38	156.81	0.41	1.00	1.51	0.44	2.36	0.52	1.57
11	114.26	0.46	158.20	0.17	1.38	1.31	0.21	2.43	0.50	1.85
12	225.53	0.39	622.78	0.18	2.76	1.34	0.12	2.70	0.51	2.01
13	532.93	0.31	273.90	0.19	0.51	2.20	0.11	1.11	0.28	0.50
14	203.13	0.43	335.88	0.18	1.65	1.02	0.25	2.65	0.54	2.59
15	58.62	0.50	82.16	0.36	1.40	2.85	0.14	4.86	0.56	1.70
16	136.53	0.33	124.74	0.19	0.91	1.38	0.14	2.57	0.68	1.87
Avg	166.33	0.42	201.42	0.24	1.59	1.65	0.28	2.56	0.57	1.69
SEM	29.91	0.04	34.39	0.02	0.29	0.14	0.04	0.21	0.04	0.16

Table 2. Peak amplitude and synaptic charge values for control and test condition

RRP Peak amplitude (pA)						RRP Synaptic charge (pC)					Failures (%)	
Nb	Ctl	CV	Tst	CV	Ratio Tst/Ctl	Ctl	CV	Tst	CV	Ratio Tst/Ctl	Ctl	Tst
1	216.00	0.20	226.70	0.15	1.05	6.81	0.31	7.18	0.21	1.06	0.00	0.00
2	220.00	0.71	267.70	0.57	1.22	4.20	0.73	4.77	0.58	1.14	0.27	0.18
3	110.00	0.62	110.00	0.49	1.00	1.26	0.64	1.23	0.52	0.97	0.23	0.15
4	161.60	0.44	154.10	0.43	0.95	5.44	0.50	5.45	0.49	1.00	0.13	0.13
5	145.80	0.73	156.90	0.67	1.08	4.88	0.69	5.54	0.70	1.14	0.29	0.29
6	97.33	0.88	127.30	0.65	1.31	1.90	1.01	2.93	0.72	1.54	0.40	0.27
7	69.69	0.81	94.37	0.41	1.35	5.17	0.88	6.92	0.53	1.34	0.31	0.08
8	35.14	0.72	33.32	0.79	0.95	0.55	0.76	0.61	0.80	1.12	0.29	0.36
9	81.25	0.58	64.98	0.86	0.80	1.66	0.73	1.36	0.88	0.82	0.20	0.40
10	148.60	0.48	175.80	0.63	1.18	2.94	0.59	3.73	0.78	1.27	0.05	0.16
11	103.20	0.78	110.20	0.70	1.07	3.25	0.88	3.54	0.77	1.09	0.35	0.30
12	622.80	0.18	571.70	0.49	0.92	10.76	0.30	9.72	0.63	0.90	0.00	0.11
13	273.90	0.19	269.50	0.19	0.98	9.64	0.26	9.71	0.22	1.01	0.00	0.00
14	206.70	0.85	326.50	0.34	1.58	4.66	0.94	9.13	0.41	1.96	0.38	0.08
15	41.08	1.14	52.38	1.13	1.28	0.70	1.19	1.21	1.32	1.73	0.50	0.44
16	72.77	0.91	89.00	0.75	1.22	1.32	0.99	1.62	0.79	1.23	0.45	0.36
17	149.20	0.37	159.40	0.28	1.07	3.25	0.45	3.77	0.24	1.16	0.08	0.00
18	566.50	0.31	566.00	0.26	1.00	15.72	0.31	15.17	0.23	0.97	0.00	0.00
19	536.80	0.35	493.80	0.35	0.92	10.24	0.48	9.06	0.60	0.89	0.00	0.00
20	300.60	0.18	291.50	0.16	0.97	10.72	0.23	9.56	0.18	0.89	0.00	0.00
21	226.60	0.77	307.10	0.40	1.36	7.60	0.83	11.19	0.47	1.47	0.33	0.08
Avg	208.84	0.58	221.35	0.51	1.11	5.36	0.65	5.88	0.57	1.18	0.20	0.16
SEM	37.14	0.06	34.98	0.06	0.04	0.89	0.06	0.87	0.06	0.06	0.04	0.03

Table 3. Temporal parameters of PSCs: All latency, first latency and time to peak values for control and test condition

	All latencies (ms)					First latencies (ms)					Time to peak (ms)				
Nb	Ctl	CV	Tst	CV	Ratio Tst/Ctl	Ctl	CV	Tst	CV	Ratio Tst/Ctl	Ctl	CV	Tst	CV	Ratio Tst/Ctl
1	1.76	0.78	1.69	1.14	0.96	1.09	0.31	0.97	0.30	0.89	2.90	0.48	2.23	0.19	0.77
2	3.74	0.58	1.94	0.78	0.52	1.89	0.48	1.49	0.32	0.79	3.10	0.61	2.42	0.41	0.78
3	3.23	0.73	3.43	0.80	1.06	2.10	0.67	1.80	0.48	0.86	3.12	0.36	2.85	0.96	0.91
4	2.27	0.71	2.39	1.10	1.05	1.26	0.67	1.13	0.55	0.90	1.77	0.63	1.18	0.58	0.67
5	2.20	0.69	2.36	0.78	1.07	1.79	0.52	1.57	0.40	0.88	1.17	0.60	1.16	0.52	0.99
6	2.90	0.79	2.22	0.51	0.76	1.92	0.87	1.79	0.34	0.93	1.63	0.28	1.93	0.55	1.19
7	2.00	0.37	2.18	0.62	1.09	2.00	0.37	1.83	0.27	0.91	4.21	0.48	5.34	0.34	1.27
8	2.30	0.47	2.60	0.60	1.13	2.32	0.48	2.17	0.37	0.93	1.44	0.23	1.93	0.26	1.34
9	1.96	0.41	1.88	0.62	0.96	1.86	0.44	1.39	0.28	0.75	1.43	0.30	1.58	0.58	1.11
10	2.36	0.52	2.27	0.69	0.96	1.82	0.47	1.55	0.54	0.85	2.40	0.41	2.85	0.41	1.18
11	2.43	0.50	2.59	0.62	1.07	2.43	0.50	2.09	0.60	0.86	1.19	0.34	1.54	0.42	1.29
12	2.70	0.51	2.68	0.66	0.99	1.85	0.44	1.68	0.29	0.91	2.39	0.42	2.25	0.51	0.94
13	1.11	0.28	1.49	1.13	1.35	1.11	0.28	0.98	0.17	0.89	1.98	0.30	2.00	0.24	1.01
14	2.65	0.54	3.20	0.73	1.21	2.12	0.55	1.92	0.55	0.91	1.67	0.20	2.20	0.38	1.32
15	4.86	0.56	5.14	0.52	1.06	2.91	0.44	2.98	0.28	1.02	2.04	1.13	3.36	0.80	1.65
16	2.57	0.68	2.42	0.95	0.94	2.01	0.40	1.69	0.44	0.84	0.96	0.20	0.95	0.28	0.99
17	1.72	0.64	2.30	0.75	1.34	1.14	0.28	1.33	0.40	1.17	1.84	0.44	2.13	0.58	1.15
18	2.01	0.93	3.24	0.75	1.61	1.40	0.29	1.17	0.18	0.83	4.58	0.39	4.64	0.34	1.01
19	2.13	0.94	1.86	1.19	0.88	1.26	0.45	0.96	0.25	0.76	1.95	0.30	1.66	0.24	0.85
20	3.50	0.69	2.59	0.41	0.74	1.82	0.31	2.07	0.38	1.14	4.16	0.58	2.05	0.42	0.49
21	2.74	0.58	3.17	0.55	1.16	1.87	0.44	1.98	0.18	1.05	2.23	0.60	3.44	0.79	1.54
Avg	2.53	0.61	2.55	0.76	1.04	1.81	0.46	1.64	0.36	0.91	2.29	0.44	2.37	0.47	1.07
SEM	0.18	0.04	0.17	0.05	0.05	0.10	0.03	0.11	0.03	0.02	0.23	0.05	0.24	0.04	0.06

Table 4. Peak amplitude and synaptic charge values for control and test condition for 2 second delay

RRP Peak amplitude (pA)						RRP Synaptic charge (pC) (0-150 ms)					Failures (%)	
Nb	Ctl	CV	Tst	CV	Ratio Tst/Ctl	Ctl	CV	Tst	CV	Ratio Tst/Ctl	Ctl	Tst
1	63.90	0.89	56.55	1.09	0.88	1.13	1.01	0.84	1.18	0.74	0.40	0.50
2	220.30	0.15	216.10	0.38	0.98	3.74	0.32	4.31	0.47	1.15	0.00	0.10
3	120.29	0.46	119.71	0.47	1.00	2.47	0.50	2.19	0.66	0.88	0.14	0.14
4	139.54	0.45	102.18	0.85	0.73	1.57	0.71	1.62	0.96	1.03	0.09	0.36
5	223.00	0.80	220.91	0.85	0.99	4.86	0.80	4.88	0.96	1.00	0.36	0.36
6	537.90	0.21	406.70	0.61	0.76	7.03	0.36	5.68	0.71	0.81	0.00	0.20
7	428.20	0.29	416.60	0.18	0.97	9.12	0.38	8.25	0.15	0.90	0.00	0.00
8	229.56	0.42	220.89	0.40	0.96	7.48	0.49	6.13	0.55	0.82	0.11	0.11
9	161.82	0.51	180.58	0.35	1.12	2.65	0.76	3.14	0.53	1.18	0.18	0.00
Avg	236.06	0.46	215.58	0.58	0.93	4.45	0.59	4.11	0.68	0.95	0.14	0.20
SEM	50.88	0.08	41.76	0.10	0.04	0.95	0.08	0.80	0.10	0.05	0.05	0.06

Table 5. Temporal parameters of PSCs for 2 second delay: All latency, first latency and time to peak values for control and test condition

	All latencies (ms)					First latencies (ms)					Time to peak (ms)				
Nb	Ctl	CV	Tst	CV	Ratio Tst/Ctl	Ctl	CV	Tst	CV	Ratio Tst/Ctl	Ctl	CV	Tst	CV	Ratio Tst/Ctl
1	2.59	0.17	2.03	0.26	0.78	2.59	0.17	2.03	0.26	0.78	0.79	0.29	1.00	0.23	1.26
2	2.52	0.57	2.35	0.57	0.93	1.82	0.54	1.37	0.53	0.75	2.13	0.77	2.88	0.57	1.35
3	1.99	0.34	2.50	0.71	1.26	1.71	0.33	1.56	0.32	0.91	1.51	0.46	1.75	0.43	1.16
4	1.24	0.50	1.27	0.53	1.03	1.24	0.50	1.21	0.58	0.98	0.90	0.28	1.20	0.50	1.33
5	2.38	0.72	1.91	0.36	0.80	1.62	0.40	1.52	0.22	0.94	2.30	0.61	2.31	0.40	1.00
6	2.08	0.54	2.72	0.59	1.31	1.78	0.52	2.21	0.57	1.24	1.61	0.62	1.91	0.82	1.19
7	1.91	0.70	2.31	0.75	1.21	1.05	0.22	1.14	0.24	1.09	1.93	0.28	2.13	0.53	1.10
8	3.41	0.54	3.07	0.53	0.90	2.14	0.38	2.31	0.28	1.08	3.30	0.52	2.16	0.30	0.65
9	2.83	0.43	2.98	0.51	1.06	2.47	0.48	2.30	0.44	0.93	1.94	0.65	2.11	0.49	1.09
Avg	2.33	0.50	2.35	0.53	1.03	1.82	0.39	1.74	0.38	0.97	1.82	0.50	1.94	0.47	1.13
SEM	0.21	0.06	0.19	0.05	0.07	0.17	0.04	0.16	0.05	0.05	0.25	0.06	0.19	0.06	0.07

Table 6. Distribution of docking sites among the synaptic terminals evaluated in this section.

Number of DS	% for 200 ms delay	% for 2 s delay	% for total n=30
1	0.0	11.1	3.3
2	19.0	11.1	16.7
3	52.4	44.4	50.0
4	23.8	33.3	26.7
5	4.8	0.0	3.3

Table 7. Number of docking sites, RRP_{avg} and docking site occupancy probability values for 200 ms delay

Nb	NDS	RRP avg		δ	
		Control RRP	Test RRP	Ctrl	Test
1	4	2.57	2.67	0.64	0.67
2	4	1.64	2.00	0.41	0.50
3	4	2.00	1.85	0.50	0.46
4	3	1.73	1.87	0.58	0.62
5	3	0.94	0.94	0.31	0.31
6	3	0.93	1.20	0.31	0.40
7	4	1.92	2.62	0.48	0.65
8	2	0.64	0.79	0.32	0.39
9	3	2.00	1.67	0.67	0.56
10	3	1.42	1.68	0.47	0.56
11	2	0.78	1.00	0.39	0.50
12	3	2.39	2.00	0.80	0.67
13	2	1.50	1.60	0.75	0.80
14	3	1.15	2.08	0.39	0.69
15	3	0.88	1.07	0.29	0.36
16	2	0.91	0.91	0.46	0.46
17	3	1.75	2.17	0.58	0.72
18	4	3.50	3.62	0.88	0.91
19	5	3.33	3.11	0.67	0.62
20	3	2.40	2.40	0.80	0.80
21	3	1.25	1.83	0.42	0.61
Avg	3.1	1.70	1.86	0.53	0.58
SEM	0.2	0.18	0.16	0.04	0.03

Table 8. Number of docking sites, RRP_{avg} and docking site occupancy probability values for 2 second delay

Nb	NDS	RRP avg		δ	
		Control RRP	Test RRP	Ctrl	Test
1	1	0.60	0.50	0.60	0.50
2	4	2.80	2.70	0.70	0.68
3	4	2.29	2.29	0.57	0.57
4	2	1.09	1.00	0.55	0.50
5	3	1.09	1.00	0.36	0.33
6	3	2.20	1.80	0.73	0.60
7	4	2.80	2.80	0.70	0.70
8	3	2.33	2.11	0.78	0.70
9	3	1.27	1.50	0.42	0.50
Avg	3.00	1.83	1.74	0.60	0.56
SEM	0.33	0.27	0.27	0.05	0.04

Table 9. PSC peak amplitude values for the 3 different delays tested

	Peak amplitude (pA)								
	No delay			200 ms delay			2 s delay		
Nb	Control	Test	Ratio Test/Control	Control	Test	Ratio Test/Control	Control	Test	Ratio Test/Control
1	47.19	50.77	1.08	38.58	44.67	1.16	55.80	60.40	1.08
2	214.00	265.00	1.24	174.00	264.00	1.52	181.00	230.00	1.27
3	79.00	128.00	1.62	83.00	81.00	0.98	103.00	74.00	0.72
4	170.00	161.00	0.95	161.00	140.00	0.87	149.00	161.00	1.08
5	56.00	46.00	0.82	46.00	44.00	0.96	70.00	66.00	0.94
6	70.50	66.00	0.94	48.00	77.50	1.61	75.00	61.00	0.81
7	47.50	81.00	1.71	39.50	98.30	2.49	63.50	44.30	0.70
8	-	-	-	199.00	264.00	1.33	229.00	247.00	1.08
Avg	97.7	114.0	1.2	98.6	126.7	1.4	115.8	118.0	1.0
SEM	25.2	29.8	0.1	24.0	31.8	0.2	22.5	29.2	0.1

Table 10. ARC peak amplitude values for the 3 different delays tested.

	ARC Peak amplitude (pA)								
	No delay			200 ms delay			2 s delay		
Nb	Control	Test	Ratio Test/Control	Control	Test	Ratio Test/Control	Control	Test	Ratio Test/Control
1	238.92	290.22	1.21	232.98	251.16	1.08	236.99	245.52	1.04
2	136.87	139.89	1.02	126.12	139.45	1.11	126.47	153.80	1.22
3	25.35	38.86	1.53	72.76	68.77	0.95	52.97	56.93	1.07
4	137.70	153.45	1.11	118.09	145.42	1.23	138.58	123.33	0.89
5	204.05	233.56	1.14	211.43	203.50	0.96	202.90	219.20	1.08
6	155.56	176.29	1.13	161.08	157.35	0.98	169.82	163.60	0.96
7	88.43	88.39	1.00	79.38	79.38	1.00	73.19	76.82	1.05
8	-	-	-	16.20	15.82	0.98	10.18	8.34	0.82
Avg	140.98	160.09	1.17	127.26	132.61	1.03	126.39	130.94	1.02
SEM	26.70	31.95	0.07	25.73	26.88	0.03	27.34	28.66	0.04

Table 11. Synaptic latency values for the 3 different delays tested

	PSC latency (ms)								
	No delay			200 ms delay			2 s delay		
Nb	Control	Test	Ratio Test/Control	Control	Test	Ratio Test/Control	Control	Test	Ratio Test/Control
1	1.3	1.41	1.08	1.42	1.49	1.05	1.18	1.44	1.22
2	1.49	1.55	1.04	1.61	1.45	0.90	1.61	1.45	0.90
3	2.26	2.42	1.07	2.19	2.07	0.95	2.14	2.5	1.17
4	1.38	1.86	1.35	1.66	1.82	1.10	1.76	1.86	1.06
5	2.02	2.1	1.04	1.56	1.59	1.02	1.6	1.56	0.98
6	1.56	1.58	1.01	1.525	1.52	1.00	1.47	1.495	1.02
7	1.82	2.04	1.12	1.88	1.84	0.98	1.84	1.98	1.08
8	-	-	-	2.07	2.07	1.00	2.16	2.05	0.95
Avg	1.69	1.85	1.10	1.74	1.73	1.00	1.72	1.79	1.05
SEM	0.13	0.14	0.04	0.10	0.09	0.02	0.12	0.13	0.04

10 Bibliography

1. Abbott LF, Regehr WG (2004) Synaptic computation. Nature 431:796–803.
2. Alle H, Geiger JR (2006) Combined analog and action potential coding in hippocampal mossy fibers. Science 311:1290–1293.
3. Alle H, Geiger JR (2008) Analog signalling in mammalian cortical axons. Curr Opin Neurobiol 18:314–320.
4. Alle, H. & Geiger, J.R. (2007) GABAergic spillover transmission onto hippocampal mossy fiber boutons. J. Neurosci., 27, 942–950.
5. Alle, H., Jonas, P., and Geiger, J.R. (2001). PTP and LTP at a hippocampal mossy fiber-interneuron synapse. Proc. Natl. Acad. Sci. USA98, 14708–14713.
6. Auger C, Marty A (2000) Quantal currents at single-site central synapses. J Physiol 526 (Pt 1):3–11.
7. Auger, C., and Marty, A. (1997). Heterogeneity of functional synaptic parameters among single release sites. Neuron 19, 139-150.
8. Auger, C., Kondo, S., and Marty, A. (1998). Multivesicular release at single functional synaptic sites in cerebellar stellate and basket cells. J. Neurosci 18, 4532-4547
9. Awatramani GB, Price GD, Trussell LO (2005) Modulation of transmitter release by presynaptic resting potential and background calcium levels. Neuron 48:109–121.
10. Barclay, J.W., Craig, T.J., Fisher, R.J., Ciufo, L.F., Evans, G.J., Morgan, A., and Burgoyne, R.D. (2003). Phosphorylation of Munc18 by protein kinase C regulates the kinetics of exocytosis. J. Biol. Chem. 278, 10538–10545.
11. Bouhours, B., Trigo, F.F., and Marty, A. (2011). Somatic depolarization enhances GABA release in cerebellar interneurons via a calcium/protein kinase C pathway. J. Neurosci. 31, 5804–5815.
12. Brager, D.H., Cai, X., and Thompson, S.M. (2003). Activity-dependent activation of presynaptic protein kinase C mediates post-tetanic potentiation. Nat. Neurosci. 6, 551–552.
13. Branco, T., and Staras, K. (2009). The probability of neurotransmitter release: variability and feedback control at single synapses. Nat. Rev. Neurosci. 10, 373–383.
14. Christie, J.M., Chiu, D.N., and Jahr, C.E. (2011). Ca^{2+}-dependent enhancement of release by subthreshold somatic depolarization. Nat. Neurosci. 14, 62–68.
15. Chu Y, Fioravante D, Leitges M, Regehr WG. (2014) Calcium-dependent PKC isoforms have specialized roles in short-term synaptic plasticity. Neuron 82:859–871.
16. Collin T, Chat M, Lucas MG, Moreno H, Racay P, Schwaller B, Marty A, Llano I. Developmental changes in parvalbumin regulate presynaptic Ca^{2+} signaling. J Neurosci. 2005;25:96–107.
17. Craig, T.J., Evans, G.J., and Morgan, A. (2003). Physiological regulation of Munc18/nSec1 phosphorylation on serine-313. J. Neurochem. 86, 1450–1457.
18. Crowley, J. J., Carter, A. G., and Regehr, W. G. (2007). Fast vesicle replenishment and rapid recovery from desensitization at a single synaptic release site. J. Neurosci 27, 5448-5460.

19. de Vries, K.J., Geijtenbeek, A., Brian, E.C., de Graan, P.N., Ghijsen, W.E., and Verhage, M. (2000). Dynamics of munc18-1 phosphorylation/dephosphorylation in rat brain nerve terminals. Eur. J. Neurosci. 12, 385–390.
20. Finley MF, Scheller RH, Madison DV (2003) SNAP-25 Ser187 does not mediate phorbol ester enhancement of hippocampal synaptic transmission. Neuropharmacology 45:857–862.
21. Fioravante, D., Chu, Y., Myoga, M.H., Leitges, M., and Regehr, W.G. (2011). Calcium-dependent isoforms of protein kinase C mediate posttetanic potentiation at the calyx of Held. Neuron 70, 1005–1019.
22. Forti, L., Bossi, M., Bergamaschi, A., Villa, A., and Malgaroli, A. (1997). Loose-patch recordings of single quanta at individual hippocampal synapses. Nature 388, 874-878.
23. Fortune, E. S. & Rose, G. J. Short-term synaptic plasticity as a temporal filter. *Trends Neurosci.* 24, 381–385 (2001).
24. Francis, H.W., J.C. Scott, and P.B. Manis. 2002. Protein kinase C mediates potentiation of synaptic transmission by phorbol ester at parallel fibers in the dorsal cochlear nucleus. Brain Res. 951:9–22.
25. Fujita, Y., Sasaki, T., Fukui, K., Kotani, H., Kimura, T., Hata, Y., Sudhof, T.C., Scheller, R.H., and Takai, Y. (1996). Phosphorylation of Munc-18/n-Sec1/ rbSec1 by protein kinase C: its implication in regulating the interaction of Munc-18/n-Sec1/rbSec1 with syntaxin. J. Biol. Chem. 271, 7265–7268.
26. Glitsch M, Marty A (1999) Presynaptic effects of NMDA in cerebellar Purkinje cells and interneurons. J Neurosci 19:511–519.
27. Gulyás, A. I., Miles, R., Sík, A., Tóth, K., Tamamaki, N., and Freund, T. F. (1993). Hippocampal pyramidal cells excite inhibitory neurons through a single release site. Nature 366, 683-687.
28. Harris, K.M., and Stevens, J.K. (1988). Dendritic spines of rat cerebellar Purkinje cells: serial electron microscopy with reference to their biophysical characteristics. J. Neurosci. 8, 4455–4469.
29. Hirokazu Hirai (2018). Protein Kinase C in the Cerebellum: Its Significance and Remaining Conundrums. Cerebellum. 2018 Feb;17(1):23-27.
30. Holderith, N., Lorincz, A., Katona, G., Rpózsa, B., Kulik, A., Watanabe, M., and Nusser, Z. (2012). Release probability of hippocampal glutamatergic terminals scales with the size of the active zone. Nat. Neurosci. 15, 988–997.
31. Hori T, Takahashi T (2009) Mechanisms underlying short-term modulation of transmitter release by presynaptic depolarization. J Physiol 587:2987–3000.
32. Hulo, S., Alberi, S., Laux, T., Muller, D., and Caroni, P. (2002). A point mutant of GAP-43 induces enhanced short-term and long-term hippocampal plasticity. Eur. J. Neurosci. 15, 1976–1982.
33. JH Wittig TD Parsons (2008). Synaptic ribbon enables temporal precision of hair cell afferent synapse by increasing the number of readily releasable vesicles: a modeling study. Journal of Neurophysiology 100:1724–1739.
34. Kaeser, P.S., and Regehr, W.G. (2017). The readily releasable pool of synaptic vesicles. Curr. Opin. Neurobiol. 43, 63–70.

35. Kandel, E. R., Schwartz, J. H. 1., & Jessell, T. M. (2000). *Principles of neural science* (4th ed.). New York: McGraw-Hill, Health Professions Division.
36. Kaplan JH, Ellis-Davies GC (1988) Photolabile chelators for the rapid photorelease of divalent cations. Proc Natl Acad Sci USA 85(17):6571–6575.
37. Klug, A., Borst, J.G., Carlson, B.A., Kopp-Scheinpflug, C., Klyachko, V.A., and Xu-Friedman, M.A. (2012). How do short-term changes at synapses fine-tune information processing? J. Neurosci. 32, 14058–14063.
38. Kondo S, Marty A (1998) Synaptic currents at individual connections among stellate cells in rat cerebellar slices. J Physiol 509:221–232.
39. Korogod, N., Lou, X., and Schneggenburger, R. (2005). Presynaptic Ca^{2+} requirements and developmental regulation of posttetanic potentiation at the calyx of Held. J. Neurosci. 25, 5127–5137.
40. Lee JS, Ho WK, Neher E, Lee SH (2013) Superpriming of synaptic vesicles after their recruitment to the readily releasable pool. Proc Natl Acad Sci USA 110(37):15079–15084.
41. Lee, J.S., Kim, M.H., Ho, W.K., and Lee, S.H. (2008). Presynaptic release probability and readily releasable pool size are regulated by two independent mechanisms during posttetanic potentiation at the calyx of Held synapse. J. Neurosci. 28, 7945–7953.
42. Liu, G., and Tsien, R. W. (1995). Properties of synaptic transmission at single hippocampal synaptic boutons. Nature 375, 404-408.
43. Llano, I., Marty, A., Armstrong, C. M., & Konnerth, A. (1991). Synaptic- and agonist induced excitatory currents of Purkinje cells in rat cerebellar slices. J. Physiol., 434(1), 183–213.
44. Lou, X., Scheuss, V., and Schneggenburger, R. (2005). Allosteric modulation of the presynaptic Ca^{2+} sensor for vesicle fusion. Nature 435, 497–501.
45. Majewski, H., and L. Iannazzo. 1998. Protein kinase C: a physiological mediator of enhanced transmitter output. Prog. Neurobiol. 55:463–475.
46. Markram, H., Wang, Y. & Tsodyks, M. Differential signaling via the same axon of neocortical pyramidal neurons. Proc. Natl Acad. Sci. USA 95, 5323–5328 (1998).
47. Micheva, K.D., Holz, R.W., and Smith, S.J. (2001). Regulation of presynaptic phosphatidylinositol 4,5-biphosphate by neuronal activity. J. Cell Biol. 154, 355–368.
48. Nagwaney S, et al. (2009) Macromolecular connections of active zone material to docked synaptic vesicles and presynaptic membrane at neuromuscular junctions of mouse. J Comp Neurol 513(5):457–468.
49. Nagy, G., Kim, J.H., Pang, Z.P., Matti, U., Rettig, J., Sudhof, T.C., and Sorensen, J.B. (2006). Different effects on fast exocytosis induced by synaptotagmin 1 and 2 isoforms and abundance but not by phosphorylation. J. Neurosci. 26, 632–643.
50. Neher E, Sakaba T (2008) Multiple roles of calcium ions in the regulation of neurotransmitter release. Neuron 59(6):861–872.
51. Nicholls J, Wallace BG (1978) Modulation of transmission at an inhibitory synapse in the central system of the leech. J Physiol 281:157–170.

52. Nili, U., de Wit, H., Gulyas-Kovacs, A., Toonen, R.F., Sørensen, J.B., Verhage, M., and Ashery, U. (2006). Munc18-1 phosphorylation by protein kinase C potentiates vesicle pool replenishment in bovine chromaffin cells. Neuroscience 143, 487–500.
53. Nusser Z, Cull-Candy S, Farrant M (1997) Differences in synaptic GABA(A) receptor number underlie variation in GABA mini amplitude. Neuron 19(3):697–709.
54. Oertner, T. G., Sabatini, B. L., Nimchinsky, E. A., and Svoboda, K. (2002). Facilitation at single synapses probed with optical quantal analysis. Nat. Neurosci 5, 657-664.
55. Pan, B., and Zucker, R.S. (2009). A general model of synaptic transmission and short-term plasticity. Neuron 62, 539–554.
56. Parfitt KD, Madison DV (1993) Phorbol esters enhance synaptic transmission by a presynaptic, calcium-dependent mechanism in rat hippocampus. J Physiol (Lond) 471:245–268.
57. Piccolino M (1998) Animal electricity and the birth of electrophysiology: the legacy of Luigi Galvani. Brain Res Bull 46:381–407
58. Pouzat, C. & Marty, A. (1999) Somatic recording of GABAergic autoreceptor current in cerebellar stellate and basket cells. J. Neurosci., 19, 1675–1690.
59. Pulido C, Trigo FF, Llano I, Marty A (2015) Vesicular release statistics and unitary postsynaptic current at single GABAergic synapses. Neuron 85: 159–172.
60. Rama, S., Zbili, M., and Debanne, D. (2015). Modulation of spike-evoked synaptic transmission: The role of presynaptic calcium and potassium channels. Biochim. Biophys. Acta 1853, 1933–1939.
61. Regehr WG (2012). Short-term presynaptic plasticity. Cold Spring Harb Perspect Biol 4, a005702.
62. Regehr, W.G., Carey, M.R., and Best, A.R. (2009). Activity-dependent regulation of synapses by retrograde messengers. Neuron 63, 154–170.
63. Reyes A, Lujan R, Rozov A, Burnashev N, Somogyi P, Sakmann B (1998). Target-cell-specific facilitation and depression in neocortical circuits. Nature Neurosci. 1, 279–285.
64. Rowan, M. J. M., and Christie, J. M. (2017). Rapid state-dependent alteration in Kv3 channel availability drives flexible synaptic signaling dependent on somatic subthreshold depolarization. *Cell Rep.* 18, 2018–2029.
65. Ruiz R, Cano R, Casañas JJ, Gaffield M.A, Betz WJ, Tabares L (2011) Active zones and the readily releasable pool of synaptic vesicles at the neuromuscular junction of the mouse. J Neurosci 31(6):2000–2008.
66. Ruiz, A., Fabian-Fine, R., Scott, R., Walker, M.C., Rusakov, D.A. & Kullmann, D.M. (2003) GABAA receptors at hippocampal mossy fibers. Neuron, 39, 961–973.
67. Ryan, T. A., Reuter, H., and Smith, S. J. (1997). Optical detection of a quantal presynaptic membrane turnover. Nature 388, 478-482.
68. Sakaba T (2008) Two $Ca^{(2+)}$-dependent steps controlling synaptic vesicle fusion and replenishment at the cerebellar basket cell terminal. Neuron 57(3):406–419.
69. Sätzler K, et al. (2002) Three-dimensional reconstruction of a calyx of Held and its postsynaptic principal neuron in the medial nucleus of the trapezoid body. J Neurosci 22(24):10567–10579.

70. Schikorski, T., and Stevens, C.F. (1997). Quantitative ultrastructural analysis of hippocampal excitatory synapses. J. Neurosci. 17, 5858–5867.
71. Schotten, S., Meijer, M., Walter, A.M., Huson, V., Mamer, L., Kalogreades, L., ter Veer, M., Ruiter, M., Brose, N., Rosenmund, C., et al. (2015). Additive effects on the energy barrier for synaptic vesicle fusion cause supralinear effects on the vesicle fusion rate. eLife 4, e05531.
72. Scott R, Ruiz A, Henneberger C, Kullmann DM, Rusakov DA (2008) Analog modulation of mossy fiber transmission is uncoupled from changes in presynaptic Ca^{2+}. J Neurosci 28:7765–7773.
73. Sheng, J., He, L., Zheng, H., Xue, L., Luo, F., Shin, W., Sun, T., Kuner, T., Yue, D.T., and Wu, L.-G. (2012). Calcium-channel number critically influences synaptic strength and plasticity at the active zone. Nat. Neurosci. 15, 998–1006.
74. Shimahara T, Tauc L (1975) Multiple interneuronal afferents to the giant cells in Aplysia. J Physiol 247:299–319.
75. Shu Y, Hasenstaub A, Duque A, Yu Y, McCormick DA (2006) Modulation of intracortical synaptic potentials by presynaptic somatic membrane potential. Nature 441:761–765.
76. Silva, A.J., Rosahl, T.W., Chapman, P.F., Marowitz, Z., Friedman, E., Frankland, P.W., Cestari, V., Cioffi, D., Su¨ dhof, T.C., and Bourtchuladze, R. (1996). Impaired learning in mice with abnormal short-lived plasticity. Curr. Biol. 6, 1509–1518.
77. Stevens, C. F., and Wang, Y. (1995). Facilitation and depression at single central synapses. Neuron 14, 795- 802.
78. Stevens, C.F., and J.M. Sullivan. 1998. Regulation of the readily releasable vesicle pool by protein kinase C. Neuron. 21:885–893.
79. Taschenberger, H., V. Scheuss, and E. Neher. 2005. Release kinetics, quantal parameters and their modulation during short-term depression at a developing synapse in the rat CNS. J. Physiol. 568:513–537.
80. Thanawala, M.S., and Regehr, W.G. (2013). Presynaptic calcium influx controls neurotransmitter release in part by regulating the effective size of the readily releasable pool. J. Neurosci. 33, 4625–4633.
81. Toonen, R.F., Wierda, K., Sons, M.S., de Wit, H., Cornelisse, L.N., Brussaard, A., Plomp, J.J., and Verhage, M. (2006). Munc18-1 expression levels control synapse recovery by regulating readily releasable pool size. Proc. Natl. Acad. Sci. USA 103, 18332–18337.
82. Trigo FF, Bouhours B, Rostaing P, Papageorgiou G, Corrie JE, Triller A, Ogden D, Marty A. (2010). Presynaptic miniature GABAergic currents in developing interneurons. Neuron 66, 235–247.
83. Trigo, F. F., Corrie, J. E. T., and Ogden, D. (2009). Laser photolysis of caged compounds at 405 nm: photochemical advantages, localisation, phototoxicity and methods for calibration. J. Neurosci. Methods 180, 9-21
84. Trigo, F. F., Papageorgiou, G., Corrie, J. E. T., and Ogden, D. (2009). Laser photolysis of DPNI-GABA, a tool for investigating the properties and distribution of GABA receptors and for silencing neurons in situ. J. Neurosci. Methods 181, 159-169.
85. Trigo, F.F., Chat, M. & Marty, A. (2007) Enhancement of GABA release through endogenous activation of axonal GABA(A) receptors in juvenile cerebellum. J. Neurosci., 27, 12452–12463.

86. Trigo, F.F., Marty, A., and Stell, B.M. (2008). Axonal GABAA receptors. Eur. J. Neurosci. 28, 841–848.
87. Trigo, F.F., T. Sakaba, D. Ogden, and A. Marty. 2012. Readily releasable pool of synaptic vesicles measured at single synaptic contacts. Proc. Natl. Acad. Sci. USA. 109:18138–18143.
88. Trommershauser, J., Schneggenburger, R., Zippelius, A. & Neher, E. Heterogeneous presynaptic release probabilities: functional relevance for short- term plasticity. Biophys. J. 84, 1563–1579 (2003).
89. Turecek, R. & Trussell, L.O. (2001) Presynaptic glycine receptors enhance transmitter release at a mammalian central synapse. Nature, 411, 587– 590.
90. Verhage, M., Maia, A.S., Plomp, J.J., Brussaard, A.B., Heeroma, J.H., Vermeer, H., Toonen, R.F., Hammer, R.E., van den Berg, T.K., Missler, M., et al. (2000). Synaptic assembly of the brain in the absence of neurotransmitter secretion. Science 287, 864–869.
91. Wierda, K.D., Toonen, R.F., de Wit, H., Brussaard, A.B., and Verhage, M. (2007). interdependence of PKC-dependent and PKC-independent pathways for presynaptic plasticity. Neuron 54, 275–290.
92. Wu, X.S., and Wu, L.G. (2001). Protein kinase c increases the apparent affinity of the release machinery to Ca^{2+} by enhancing the release machinery down- stream of the Ca^{2+} sensor. J. Neurosci. 21, 7928–7936.
93. Yuste, R., Majewska, A., Cash, S. S., Denk, W. (1999). Mechanisms of calcium influx into hippocampal spines: heterogeneity among spines, coincidence detection by NMDA receptors, and optical quantal analysis. J. Neurosci 19:1976-1987.
94. Zilly FE, Sorensen JB, Jahn R, Lang T. Munc18-bound syntaxin readily forms SNARE complexes with synaptobrevin in native plasma membranes. PLoS Biol 2006;4(10):e330.
95. Zorrilla de San Martin J, Jalil A, Trigo FF. Impact of single-site axonal GABAergic synaptic events on cerebellar interneuron activity. J Gen Physiol 146: 477–493, 2015.
96. Zucker, R.S., and Regehr, W.G. (2002). Short-term synaptic plasticity. Annu. Rev. Physiol. 64, 355–405.